

AN APPLICATION OF EQUIVALENCE CLASS TECHNIQUES
TO RADAR SIGNATURE ANALYSIS

By

GEORGE WARFIELD GRUVER

Bachelor of Science
Oklahoma State University
Stillwater, Oklahoma
1961

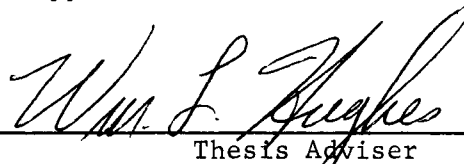
Master of Science
Oklahoma State University
Stillwater, Oklahoma
1962

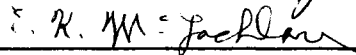
Submitted to the faculty of the Graduate College
of the Oklahoma State University
in partial fulfillment of the requirements
for the degree of
DOCTOR OF PHILOSOPHY
May, 1968

OCT 25 1968

AN APPLICATION OF EQUIVALENCE CLASS TECHNIQUES
TO RADAR SIGNATURE ANALYSIS

Thesis Approved:


Thesis Adviser









Dean of the Graduate College

688370

ACKNOWLEDGMENTS

I wish to express my gratitude to Professor W. L. Hughes, my thesis adviser and the Chairman of my committee. His guidance and encouragement have been invaluable during the course of my research and the preparation of this thesis. I am also indebted to him for his counsel and support during my undergraduate and graduate studies.

My special thanks are extended to Professor E. K. McLachlan for the many hours of instruction and the patient encouragement that I have received from him.

I also wish to thank the other members of my graduate committee, Professors B. L. Basore and R. L. Cummins for their advice and encouragement during my doctoral studies.

The Fort Worth Division of General Dynamics provided financial support and facilities for my research for which I am deeply grateful. I am especially indebted to my associate and friend, Dr. C. C. Freeny, for the encouragement and the gentle but firm pressure he exerted upon me during my research.

I also wish to acknowledge the kindness of Mr. D. M. Montana of the Rome Air Development Center in allowing information obtained under contract to his office to be presented in this thesis.

The patience and encouragement which I have received from my wife, Janice, means more to me than I can express in these few words. Her devotion and sacrifice have made this thesis a reality.

TABLE OF CONTENTS

Chapter	Page
I. RADAR SIGNATURE ANALYSIS	1
1.1 Introduction	1
1.2 State of the Art of Radar Signature Analysis	9
1.3 Scope of Research	12
II. THE EQUIVALENCE CLASS TECHNIQUE	15
2.1 General	15
2.1.1 The Source Space	16
2.1.2 The Signature Space	16
2.1.3 The Decision Space	19
2.2 Signature Information and Equivalence Classes	23
2.3 An ECT Formulation	32
2.4 Results	36
III. APPLICATION TO A MEASURE OF SIGNATURE-TYPE AMBIGUITY	39
3.1 General	39
3.2 Ambiguity Space Formulation	41
3.3 Description of Experiments	47
3.4 Analysis	50
3.4.1 Ambiguity of Complex Vehicles	52
3.4.2 Ambiguity of Generic Vehicles	69
3.5 Conclusions	75
IV. APPLICATION TO A MEASURE OF VEHICLE SIMILITUDE	79
4.1 General	79
4.2 The Dissimilar Ratio	80
4.3 Analysis	85
4.3.1 Complex Vehicles	85
4.3.2 Generic Vehicles	104
4.3.3 Composite Generic Vehicles	109
4.4 Conclusions	116
V. SUMMARY AND RECOMMENDATIONS	119
5.1 Summary	119
5.2 Recommendations for Further Research	121
BIBLIOGRAPHY	125

Chapter	Page
BIBLIOGRAPHY	125
APPENDIX A	128
APPENDIX B	147
APPENDIX C	156
APPENDIX D	171

LIST OF TABLES

Table	Page
I. Signature-Type Designation	18
II. Example of ECT Mapping	35
III. Reduction in Computer Storage Requirements Obtained Using the Equivalence Class Technique	37
IV. Effects of Cross Section and Phase Quantitization	56
V. Effects of Absolute Phase on Ambiguity	57
VI. Signature Elements Used for Computation of D/N	81
VII. Comparison of D/N and W/N	104
VIII. Comparison of Physical and Statistical Dissimilar Ratios .	110
IX. Scattering Matrix Measurement Procedure	141
X. Description of Models	157
XI. Construction of Models A1, A2, and A3	160

LIST OF FIGURES

Figure	Page
1. Bistatic Radar and Target Orientation	6
2. Space Representation of Radar Signature Analysis	15
3. Relationship Between Mapping and Inverse Mapping	21
4. Cross Section σ_{VV} Versus Aspect of a Right Circular Cylinder	24
5. Measured Phase and Differential Phase of Model C1	31
6. Representation of Ambiguity Space	45
7. STAP Computer Program Logic Diagram	48
8. Average Ambiguity of Complex Vehicles	53
9. Average Diameter of Equivalences Classes of Models 1, 2, and 3	65
10. STAP Output Listing Obtained for Model 2	66
11. Model 2 Cross Section σ_{VV}	68
12. Ambiguity of Generic Vehicles, $\epsilon_{\sigma} = 1$ dB	70
13. Ambiguity of Generic Vehicles, $\epsilon_{\sigma} = 3$ dB	72
14. Effects of Signature Set Size on Ambiguity	74
15. Differential Phase Exhibited by Models CY5, C1, and F5	76
16. Ambiguity Versus Vehicle Physical Classification	77
17. SSDP Computer Program Logic Diagram	84
18. Dissimilar Ratio Comparison of Models 1 and 2	87
19. Models 1 and 2 Cross Section σ_{VV}	89
20. Models 1 and 2 Cross Section σ_{HH}	90
21. Relationship Between Sets of Dissimilar Signatures	94

Figure	Page
22. Relationship Between $N_D(TP)$, $N_D(SPVV)$, $N_D(SPHH)$, and N_A of Models 1 and 2	95
23. Sets of Dissimilarities Between Models 1 and 2	97
24. Types of Backscatter Hypothesized for Models 1 and 2	100
25. Vehicle Similitude to Model C1 Established by Use of the Dissimilar Ratio	105
26. Dissimilar Ratio Relationships Between Models C1, F5, and CY5	107
27. Vehicle Similitude to Model A1 Established by use of the Dissimilar Ratio	111
28. Differential Phase Exhibited by Models CY5, C1, and F5	114
29. Differential Phase Exhibited by Models A1, A2, and A3	115
30. Coordinate System	129
31. The Ground Plane Radar	135
32. Radar Range at the Fort Worth Division of General Dynamics	148
33. Interior of Electronic Equipment Van	150
34. Block Diagram of the Electronic Measurement System	152
35. Construction of Composite Vehicles	158
36. Typical Generic Vehicles	159
37. Typical Composite Generic Vehicles	159
38. Model C1 Cross Section σ_{VV}	161
39. Model F5 Cross Section σ_{VV}	162
40. Model CY5 Cross Section σ_{VV}	163
41. Model C1CY1F3 Cross Section σ_{VV}	164
42. Model A1 Cross Section σ_{VV}	165
43. Model A2 Cross Section σ_{VV}	166
44. Model A3 Cross Section σ_{VV}	167
45. Model A1 Cross Section σ_{HH}	168

Figure		Page
46.	Model A2 Cross Section HH	169
47.	Model A3 Cross Section HH	170
48.	STAP Computer Program Flow Chart	172
49.	STAP Sample Problem Output Listing	178
50.	SSDP Computer Program Flow Chart	179
51.	SSDP Sample Problem Output Listing	187

CHAPTER I

RADAR SIGNATURE ANALYSIS

1.1 Introduction. The importance of information obtained by way of measuring electromagnetic scattering phenomena has been recognized for many years in the field of radar detection, direction finding, and tracking. However, until recently only a fraction of the information available from scattered energy has been exploited. In most radar systems, the information of primary importance has been that which is applicable in determining the location and the dynamics of motion of a target. The radar designer has been primarily interested in obtaining such information on a target as range, direction, relative motion, course, speed, and other pertinent data. All of these parameters are essentially independent of the scattering characteristics of a target. The only scattering characteristic of concern has been that of radar cross section, and radar cross section has only been incorporated in radar system design to the extent that this parameter affects some specified probability of detection. (1).

It has long been known that different types of targets exhibit different radar cross sections, and much literature has been devoted to determining the radar cross section of generic and complex shapes.¹

¹H. A. Corriher, Jr. and Berry O. Pyron, "A Bibliography of Articles on Radar Reflectivity and Related Subjects: 1957-1964," Proceedings of the IEEE, Vol. 53, No. 8, (1965), pp. 1025-1058.

However, the radar designer has only considered the radar cross section of an object in terms of specifying his system parameters to enhance the detection and tracking of that object.

Thus, historically, the classical radar scattering problem has been that of determining the radar parameters which will enable optimum detection of an object in terms of a given target geometry. In this sense, consideration had to be given to the fact that the radar cross section of an object generally varies as a function of the orientation of an object relative to the Radar Line of Sight (RLOS). This requirement had to be met in order to insert a meaningful value of cross section in the radar equation. (1). This value was also dependent on the requirements of other systems; consequently, various values have been used, including the average cross section and the peak cross section, all with the primary aim of increasing the minimum radar range at which a target is detectable.

Recently, the radar designer has turned his attention to the problems of target identification on the basis of radar measurements. (2,3,4,5). These problems represent the inverse of the problem of determining the radar cross section of a target since, in this case, the characteristics of the scattering target are to be determined from information extracted from the energy scattered from the target to the radar receiver.

"Signature" is a term which is commonly applied to a set of parameters that characterize an object. The signature of an object can consist of a finite (for example, a single number) or an infinite number of different characteristics which can be used to classify the object. For example, the spectral analysis of the electromagnetic or

acoustic emissions of an emitting body can be used to classify the emitter and hence the set of all (or only a few) Fourier coefficients could be called the emitter's signature. A physical signature of an object might be a set of dimensional relationships. In general, the dimension of a signature is limited only by the complexity desired in the classification system.

The origin of the term "Radar Signature Analysis" is unknown to the author. However, it has recently come into quite common usage in references to the general process or sequence of processes by which decisions, other than normal detection, location, and tracking decisions, are made on the basis of radar measurements. The term "Signature Analysis" has been used for a number of years by those interested in ascribing physical or personality traits to individuals on the basis of their signatures or handwriting. These investigators have been primarily interested in (1) identifying personal characteristics on the basis of particular signature features and (2) identifying individuals on the basis of comparisons of samples of their handwriting. The identification of personality traits from handwriting samples is at most a very nebulous art except, for example, in the case of such decisions as identifying a person as left- or right-handed. The matching of various samples of signatures or handwriting is generally approached by selecting a few distinguishing features for comparison. Such features as letter slant, method of dotting i's, method of crossing t's, etc., may prove to be suitable discriminants for use in this matching process. In an effort to maximize the confidence level that a match has been obtained, the handwriting analyst may consider additional features or large samples. The result is then a function of the

analyst's ability and the uniqueness of representation afforded by the signature.

A natural extension of signature analysis has been the pattern-recognition approach to written character identification taken by a number of authors. (6,7). In this approach, the recognition of letter features is used along with the probability of occurrence of particular letter combinations in the language being translated to determine the actual word to be translated. The recognition of each printed letter is fundamental to the success of this approach. A considerable amount of success has been demonstrated when the letters are printed to specified sizes and dimensions so that each letter can be uniquely recognized. However, if the letters are typewritten, hand printed, or written in long hand, the identification of each letter becomes increasingly more ambiguous unless the number of features or discriminants is increased, and/or the recognition process is made more sophisticated. The concept of ambiguous signatures carries over into the field of radar signature analysis, and it will be discussed in detail in a later portion of this thesis.

A radar signature (more correctly a radar target signature) can be defined by use of a set of one or more radar measurements made at some common time on a radar scattering target. A variety of different measurements can be obtained by the use of a radar; however, the most fundamental consists of the measurement of the scattered power received by the radar receiver and the phase of the received wave relative to some reference phase. Generally, the received power is calibrated so that it is representative of the radar cross section of the target. The radar cross section of a target is defined as the area intercepting

that amount of power which, if it were scattered equally in all directions, would produce an echo at the radar equal to that from the target. (1,8). Skolnik (1) provides a thorough discussion of radar measurements and of the fundamentals of radar cross section. Kerr (8) provides more detail in a discussion of the relevance of this definition of radar cross section with respect to radar polarization.

The radar cross section of an object is solely a function of the scattering properties of the object. However, the amount of coupling which exists between a radar transmitter and receiver via energy scattered from an object is determined by the polarization of the radar transmitter and receiver. Propagation path effects which alter the polarization of the incident and/or scattered waves will produce erroneous cross section measurements unless their effects can be removed.

The radar cross section of an object measured by use of a typical pulsed radar is a function of the following parameters:

1. Object orientation (θ, ζ) relative to the radar line-of-sight
2. Angle (bistatic angle or α) between the line-of-sight from target to transmitter and the line-of-sight from target to receiver
3. Wavelength (λ)
4. Polarization (γ)
5. Pulse Width (τ)

A typical bistatic radar system is shown in Figure 1. The target orientation relative to the line-of-sight from the target to the transmitter is described on the basis of the spherical angle coordinates θ and ζ which relate a reference line on the target to the line-of-sight.

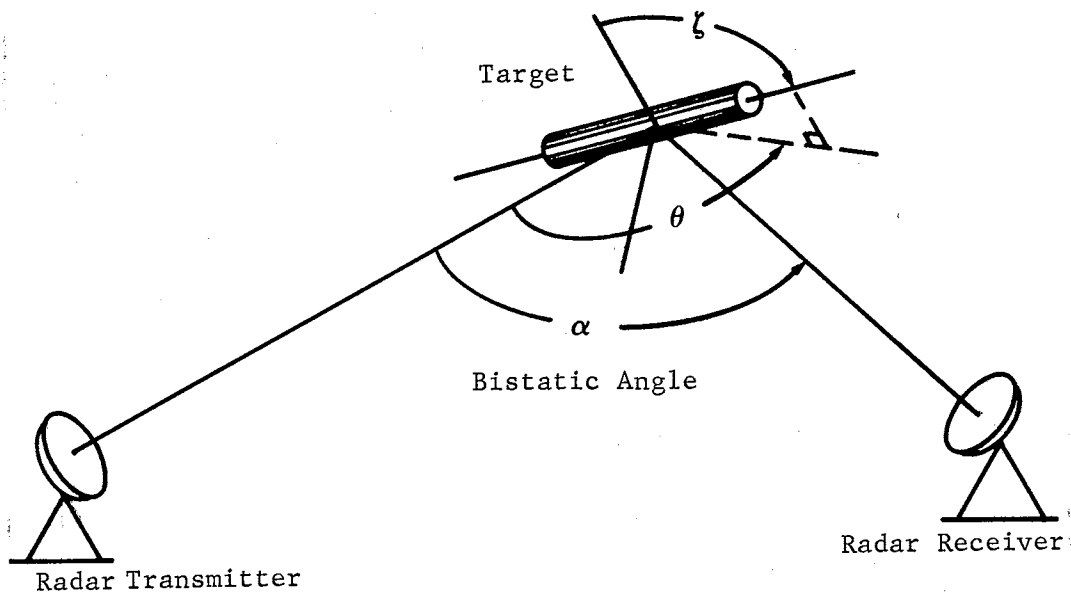


Figure 1. Bistatic Radar and Target Orientation

If the radar transmitting and receiving antennas are located so that the bistatic angle is very small, the radar is called a monostatic radar. The signatures used in this research were obtained by use of a monostatic radar. In addition, the targets used in this research were constrained to rotate in a horizontal plane defined by $\zeta = 0$ degree.

The energy scattered from any structural region of a target is sensitive to frequency as a result of the frequency dependence of the radiating currents which are induced along the surface of the target by the incident field. Additional wavelength sensitivity results from the fact that the total scattered field is equal to the vector addition of the fields scattered from all the individual scattering regions on the target.

In order to describe the polarization dependence of radar cross section, two characteristics relating scattered and incident waves must be considered. The first of these is related to dependence upon the polarization of the incident wave, and the second to the fact that the polarization of the scattered wave is not necessarily the same as that of the incident wave. A long thin dipole target provides an example of the first of these characteristics for it is well known that an incident field, linearly polarized parallel to the dipole, will produce more scattered energy than any other linear polarization. Also, the scattered field polarization will be identical to that of the incident field provided that the dipole is very thin with respect to wavelength.

The second characteristic, called depolarization, is exemplified by the fact that large flat targets will completely depolarize an incident circularly polarized wave. Thus, if circular polarization is to be used for detecting specular-type targets, the radar receiving and transmitting antennas must be polarized in opposite senses.

Most radar targets display both of these characteristics; the more complex the structure of the target, the more sensitive it is to the polarization of the radar. As a result of this polarization dependence, measured radar signatures should always be related to the polarization of the transmitting and receiving antennas. In this thesis, a pair of subscripts will be used to denote the polarization of the radar transmitter and receiver, for example σ_{LR} or ϕ_{LR} . Here the first subscript denotes the transmitter polarization (left circular in both cases) and the second subscript denotes the receiver polarization (right circular in both cases).

The pulse width of most conventional radars is long compared to

the size of targets of interest. Consequently, the entire target is illuminated by the radar at the same time, and the scattered field is composed of contributions from the entire target. A considerable amount of interest is presently being placed on short-pulse radars in which use is made of pulse widths that are only a fraction of the size of the target. These radars are able to determine radar cross section on the basis of measuring energy scattered from discrete regions of the target as a function of the location of these discrete regions along the radar line-of-sight.

The resulting variations in σ produced by changes in any of these five variables or parameters provide a powerful diagnostic tool for the identification of a target. Of these parameters, only λ , θ , and γ are readily varied, and only θ varies as a result of target motion. For this reason, the relationship between cross section and aspect orientation has long been of considerable interest to both radar system designers and radar target designers.

The phase center associated with electromagnetic scattering represents the apparent position in space where the scattered signal is originated. The target phase center is also a function of wavelength, aspect orientation, etc., and in most radar measurements the measurement of this center is complicated as a result of the large number of cycles traveled along the radar line-of-sight by the transmitted and received waves. Techniques for removing the range term from measured phase include range measurement, doppler frequency techniques, and the use of multiple frequencies and/or polarizations.

In this dissertation it will be assumed that the values of σ and ϕ vary only as a function of θ and γ since α , λ , and τ are fixed. The

use of multiple frequency and multiple site radars to provide multidimensional radar signatures is presently being investigated. The feasibility of utilizing extremely short radar pulses (of less than 10^{-9} second in duration) is currently being investigated by a number of researchers whose recent activities were described at the Second Ground Identification of Satellites (GISAT) Symposium in October, 1967; however, formal publication of this material has not been completed. Many of the techniques discussed in this dissertation are directly applicable to these multidimensional signatures.

1.2 State of the Art of Radar Signature Analysis. The rapid development of radar technology was initiated during World War II, primarily under the stimulating influence of the Radiation Laboratories in the United States and the Telecommunications Research Establishment in Great Britain. During this early period, primary emphasis was placed on improving radar target detection and tracking capabilities. These capabilities have been further expanded in the past decade as a result of rapid advances in radar component designs, the application of new concepts in modulation, detection, and processing, and the integration of digital computers with the radar. Much of the recent interest in radar has resulted from the desire to detect and track missiles and satellites. The small size, high speed, and long ranges associated with these types of targets have forced the radar designer to utilize larger antennas, higher power sources, better receivers, and faster computational techniques. The satisfaction of these requirements has resulted in stimulating the growth of many supporting subtechnologies.

The improvements in detection, resolution, and tracking capabilities has also led to the realization that additional information is

available from the electromagnetic radiation scattered by radar targets.

Skolnik (1) has reviewed the information available in the various time, frequency, and position derivatives of scattering amplitude and phase measurements. He notes that, in addition to the normal range, range rate (velocity), and angular position information which are essentially obtained from phase derivatives, information on target size, shape, and change of shape is available in the amplitude derivatives.

Skolnik does not explicitly discuss the role of polarization as a source of information. However, the change of scattered amplitude and/or phase with changes in polarization has been shown to be a useful discriminant for determining vehicle physical properties. (4,9).

A major problem presently confronting the radar system designer is the desirability of classifying or identifying radar targets on the basis of radar measurements. This problem is of concern both in the case of ground targets which might be illuminated by an aircraft radar and targets such as aircraft and/or space targets which might be illuminated by a ground based radar.

Renewed interest has been taken in the solution of the Space Object Identification (SOI) problem as a result of the development of satellites for military applications. The primary interest of the radar designer who is interested in SOI is directed to providing a radar which can be used to classify an unknown satellite on the basis as to whether it is a scientific or nonscientific type and to determine whether the satellite constitutes a threat or not. Additional levels of classification such as the determination of the size and shape of the object are also certainly of interest. (10,11).

The research reported in this thesis is primarily restricted to

the SOI problem; however, this restriction has only been imposed as a result of the types of scattering models which can be conveniently investigated. The techniques developed as a result of this research may be applicable to many other areas of radar identification. The availability of other target models and additional signature measurements would facilitate investigations into these other areas.

The feasibility of using radar signatures to identify or classify objects is inherently limited by the ability of the associated decision making process (human and/or mechanical) to assimilate and make efficient use of the large amounts of data which a radar system is capable of obtaining. This limitation, coupled with the tactical necessity of making decisions in virtually real time, are sufficient to establish a need for developing a real-time technique which can be used to compress a large amount of measured data into a useful set of identification discriminants.

One technique of obtaining an interpretable set of discriminants is to limit the amount of raw data obtained. For example, the amount of data can be limited by using a simple signature, such as the time variation of cross section obtained at a single polarization, frequency, and bistatic angle. Under these circumstances, an experienced cross section analyst may be able to identify objects on the basis of these signatures; however, the attendant confidence level associated with this identification may be extremely poor. Experience has shown that more radar information is required if a high degree of confidence is to be placed on the resulting decision. The analysis of more complex signatures is limited by analyst saturation and the resultant time delay imposed by the required examination and correlation of multi-

dimensional signatures. The need for more sophisticated decision-making techniques is established by the fact that complex signatures do indeed provide desirable discriminants.

The state-of-the-art of radar measurements is at present commensurate with obtaining both cross section and phase signature elements under various conditions of polarization, frequency, and bistatic angle. (12,13). Additionally, the concept of using an extremely wide band radar to accommodate nanosecond pulse widths has recently added a new dimension to radar measurements. (14,15). The short-pulse concept is providing new insight into scattering phenomena by providing signature data as a function of depth (along the RLOS) into the target. As previously stated, in the operation of conventional long-pulse radars, the pulse width is considerably greater than the target dimensions.

While it is desirable to utilize as much information about the object as possible, the feasibility of using additional information in approximately real time is ultimately limited by the implementation of computerized techniques of compressing the measured data and extracting only those features which contribute most to the decision of interest.

1.3 Scope of Research. This thesis contains a description of a technique based on the use of equivalence classes to map a multi-dimensional signature space into a space of much smaller dimension and to retain some (or all) of the signature features which contribute to object identification. The development of this Equivalence Class Technique (ECT) is presented in Chapter II. The flexibility of the ECT for use in making various types of decisions is emphasized in Chapter III in a detailed investigation of the information content of

different signature types. In order to attain the objectives set for this investigation, the target Scattering Matrix (SM) and its various subsets are investigated by using measured SM signatures obtained for a variety of different vehicle configurations on a radar scattering range. (16).

Chapter IV contains a discussion of the use of an ECT to form a particular measure of the similitude between pairs of vehicles. Computed similitude data based on measured radar signatures on a number of vehicles are presented in this chapter. An investigation of the relationship between vehicle similitude and signature type is also described.

Chapter V contains conclusions and recommendations for further study as well as a discussion of the feasibility of extrapolating the results obtained from the static measurements to the dynamic case.

The reader who is familiar with the fundamentals of radar cross section measurements should have no difficulty in understanding the research results presented in Chapters II, III, and IV. However, a set of appendices is provided in order to establish a basic understanding of such phenomena as the ground plane radar range, radar cross section and phase measurement techniques, and some of the fundamental characteristics of the scattering matrix.

Appendix A contains an analysis directed to demonstrating the validity of measurements made on a ground plane radar scattering range and to establishing certain criteria which must be satisfied in order to produce accurate measurements. Appendix B contains a description of the radar scattering range used to obtain the measured data on which this research is based and a detailed description of the measurement

procedures. Appendix C contains a description of the vehicle models used in this research and the rectilinear analog plots of the cross section signatures which are used in Chapters III and IV. Appendix D contains a detailed documentation on the two computer programs, STAP and SSDP, which are discussed in Chapters III and IV.

CHAPTER II

THE EQUIVALENCE CLASS TECHNIQUE (ECT)

2.1 General. The general process of radar signature analysis can be conveniently represented as a series of transformations between a set of geometrical spaces, as shown in Figure 2. A similar space representation is profitably used by Sebestyen (17) to represent membership in classes. In Sebestyen's scheme, each dimension of a space expresses a property, and different classes are defined on the basis of the numerical values which correspond to the amount of each property related to an event or observation. In Figure 2, the three spaces (source, signature, and decision) represent a general categorization of all types or processes of interest in radar signature analysis.

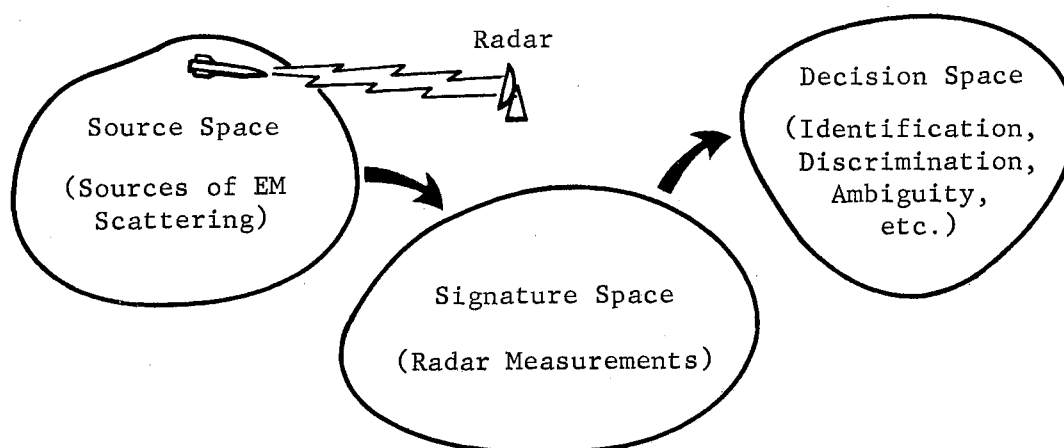


Figure 2. Space Representation of Radar Signature Analysis

2.1.1 The Source Space. The source space provides a representation of all possible object configurations of interest in a particular type of investigation. This representation may possibly be quite definitive in the case of simple shapes, such as cylinders and cones, or it may be quite abstract and reflect only the fact that different objects occupy different positions in the space, without providing a definitive index of the position of each object. The latter concept will be used in this research since the determination of object shape and dimension is not an objective.

2.1.2 The Signature Space. The signature space contains sets of signatures representing the objects belonging to the source space. The radar system is used to transform or map an object in the source space into a set of signature measurements. These signatures may consist of radar measurements obtained at one or more bistatic angles, multiple frequencies, and/or polarizations, and either long- or short-pulse radars may be used. Whatever the type of signature, it will consist of a set of measurements obtained at some time reference or vehicle position reference. A precise definition of a radar signature is given in D2-1, i.e., the first definition in Chapter II:

D2-1: Let the signature element s_{ij} represent a radar measurement of either cross section of phase or a combination of cross section and/or phase measurements obtained at vehicle position i by using a radar parameter condition indexed as j . Then the i^{th} radar signature, S_i , is defined as the ordered n -tuple of signature elements

$$S_i = (s_{i1}, s_{i2}, \dots, s_{ij}, \dots, s_{in})$$

where $j = 1, 2, \dots, n$ represents the particular conditions

of polarization, frequency, bistatic angle, etc., used in obtaining the j^{th} signature element.

As used in definition D2-1, the position index i relates all the signature elements obtained at a common time or a common vehicle aspect orientation (if signature elements obtained at different times are to be utilized). The inclusion of combinations of cross section and/or phase measurements enables ratios, averages, etc., to be used or signature elements.

For the sake of brevity, different types of signatures, i.e., the signature types considered in this research will be referred to in terms of descriptive acronyms. Table I contains a list of the signature types to which a repeated reference is made. The parameters T and R which occur as subscripts of the signature elements and in the parenthesis of the PHASE and TP acronyms refer to the polarization of the transmitter and receive antennas respectively. The letters V, H, L, and R refer to vertical, horizontal, left circular, and right circular polarizations respectively. As an example, the signature type TP (VV,HH) designates the two-polarization signature (two-dimensional signature) composed of σ_{VV} and σ_{HH} , where σ_{VV} is the cross section obtained with both the transmitter and receiver vertically polarized and σ_{HH} is the cross section with both horizontally polarized. Appendix A contains a general discussion on antenna polarization and a description of the polarizations utilized in this investigation.

TABLE I
Signature-Type Designation

Acronym	Signature Element Description
SPVV	Single-Polarization Cross Section (σ_{VV})
SPVH	Single-Polarization Cross Section (σ_{VH})
SPHH	Single-Polarization Cross Section (σ_{HH})
PHASE (TR)	Single-Polarization (ϕ_{TR})
TP(T_1R_1 , T_2R_2)	Two-Polarization Cross Sections ($\sigma_{T_1R_1}$, $\sigma_{T_2R_2}$)
3P	Three-Polarization Cross Section (σ_{VV} , σ_{VH} , σ_{HH})
SPP	Single-Polarization Cross Section and Phase (σ_{VV} , ϕ_{HH})
TPP	Two-Polarization Cross Section and Single-Phase (σ_{VV} , σ_{HH} , ϕ_{HH})
SM	Scattering Matrix (σ_{VV} , σ_{VH} , σ_{HH} , ϕ_{VH} , ϕ_{HH})

All of the signatures exhibited by a scattering source will be called a signature set:

D2-2: A Signature Set S consists of a set of signatures S_i for $i = 1, 2, \dots, N$ obtained by using a particular scattering source.

Reference to D2-1 therefore indicates that the signature space is an $n + 1$ dimensional Euclidian Space where n is the dimension of the radar signatures being measured. In this analysis, it will be assumed that

all of the information available on a particular object is contained in its associated signature set.

2.1.3 The Decision Space. The end results of every process of radar signature analysis is manifested by a decision. Examples of decisions of interest are the identification of vehicle type, cone, cylinder, complex aerospace vehicle; the determination of object dimensions, length, volume; or such decision pairs as threat-no threat or similar vehicles-dissimilar vehicles. Additional decisions might be classified in the area of signature diagnostics, such as the investigation of the relative ambiguity of signature-type representation presented in Chapter II. A decision space can only be realistically defined in terms of the particular decision of interest. The dimension of a decision space is determined by the number of discriminants or parameters which result from the analysis process. The decision itself is obtained by applying a decision rule to the decision space. An example of a mapping between a signature space and a decision space and the subsequent application of a particular decision rule will help to clarify these processes.

First, assume that a transformation T is applied to signature sets S_A and S_B corresponding to vehicles A and B. Then, let the result of this transformation be a single discriminant, in this example a number X between 0 and 1 which is a measure of the physical similarity between vehicles A and B. In this example, the decision space is unidimensional: it consists of the real line between 0 and 1. Various decision rules could be used in this example to divide the decision space into such categories as similar, dissimilar, etc. The decision rule used in this case might result from the analysis of a set of signatures corresponding

to known vehicles; these signatures would be used to establish a degree of confidence in the transformation process.

Although an investigation of the types of decisions possible is not the subject of this thesis, they are mentioned because they do enter into the criteria required for defining mappings from the signature space to the decision space. The following criteria should be considered in the definition of a specific mapping technique:

1. The physical significance of the parameters of each space
2. The utility of the mapping in terms of the desired decision
3. The ability to "invert" the mapping or to effect an inverse mapping from the decision space to the signature space and/or the source space.

Throughout this thesis, stress will be placed on the idea of applying discriminants which have physical meaning to the decision problem of interest. This approach is a departure from the use of purely statistical discriminants such as the mean, variance, etc., of the various signature element distributions. It can be shown that many complex scatterers exhibiting quite different structural characteristics may also exhibit virtually identical distributions of cross section and phase over rather large frequency ranges. The cross section patterns of two such scatterers may be quite different; however, the inherent loss of order, which arises when only distributions are considered, results in the consequent loss of an extremely powerful discriminant. The use of the order properties of signatures will receive a great deal of attention in the remainder of this thesis.

The utility of a mapping encompasses the entire spectrum of feasibility, economy, and reliability. For example, it might be

feasible to obtain an accurate measurement of the scattering matrix of a satellite. However, the cost of a processing system in which the scattering matrix data could reliably be used might force the radar designer to measure fewer signatures in order to obtain a total decision-making system. Similarly, decision-making techniques upon which high confidence can be placed may have to be discarded if the required accuracies of signature measurements are not presently possible within the state-of-the-art of feasible and/or economical measurement systems.

The concept of inversion generally denotes the idea of determining an inverse mapping by which a region of one space is mapped back into a region of another space so that, if T maps R_i into S_i , then T' maps S_i back into R_i , as illustrated in Figure 3.

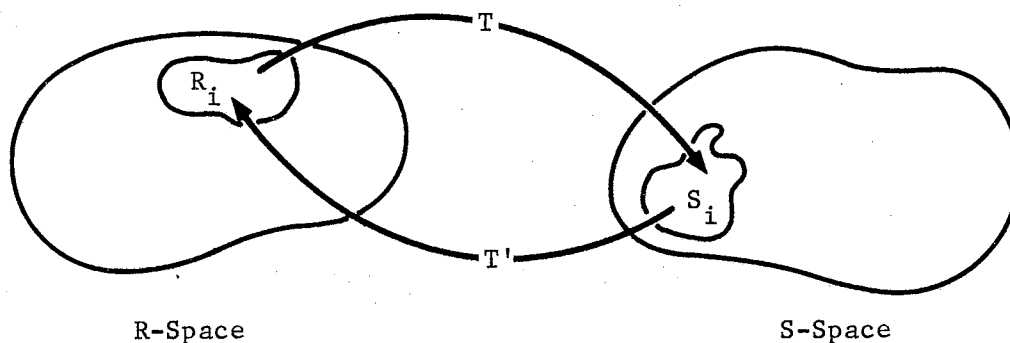


Figure 3. Relationship Between Mapping and Inverse Mapping

In general, an inverse mapping T will not exist if any information which was necessary in forming the mapping T is lost during the mapping process. For example, let T be the mapping used to transform the signature set S into a single signature whose elements are the mean values of the measured signature elements.

$$T: S \rightarrow \mu_s$$

In this mapping process, the individual value of the elements of each signature and the order of occurrence of each signature are lost; consequently, confident identification of the source vehicle from the resulting data cannot be explained. Only in such special cases as those in which the type of target is known but its size is unknown would data of this type be expected to contain useful identification information.

An ideal SOI identification system might be, for example, one in which (1) all cylinders (members of the source space) are mapped by use of a particular signature type (member of the signature space) into a unique region of the decision space and (2) all points in this unique region represent mappings of cylinders.

The Equivalence Class Technique (ECT) represents a mapping or transformation between the signature space and the decision space. The motivation for developing this mapping is based on a desire to achieve some measure of the following characteristics:

1. Real-time analysis and decision capability.
2. Reduced computer storage requirements.
3. Contraction mapping.

In addition to these characteristics, in order to relate the information available in different signature types, it is desirable to obtain a mapping whose formulation is independent of the type of signature representation. This independence is necessary if the information content of different types of signatures is to be objectively compared on the basis of information contained in the decision space.

The storage of a signature set, S , in a digital computer involves the allotment of an $N \times n$ array of storage locations. However, the

mapping of S into a fundamental set of equivalence classes can result in considerable reduction of the amount of storage necessary and the preservation of all or most of the information contained in S. This concept of data contraction (without significant loss of information) will be discussed in more detail with regard to the specific ECT's discussed in the remainder of this chapter.

2.2 Signature Information and Equivalence Classes. Most conventional radars are capable of measuring only the single-polarization cross section return from a target in addition to generating the normal ranging and tracking information. This SP data is usually presented in the form of rectilinear plots of cross section in dBsm as a function of the aspect orientations of the target vehicle or time. A typical analog plot of an SP signature set of a right circular cylinder is shown in Figure 4. As indicated in the legend on this figure, the abscissa of the plot represents the variation of aspect angle, θ , as the cylinder is rotated in a plane formed by the cylinder axis and the Radar Line of Sight (RLOS). This plot of σ_{VV} versus θ provides an example of the type of information in a signature set that is generally utilized. This information basically consists of the relationship between amplitude and order since the amplitude of each measurement and the order of the measurement are sufficient to allow the pattern to be completely reconstructed. The trained cross section analyst consciously or subconsciously utilizes amplitude and order as he considers the location and amplitude of specular reflections, lobe widths, etc.¹

¹A specular reflection occurs whenever adjacent scatterers tend to reinforce each other, such as when a radius of curvature of a surface approaches infinity in the direction of the RLOS.

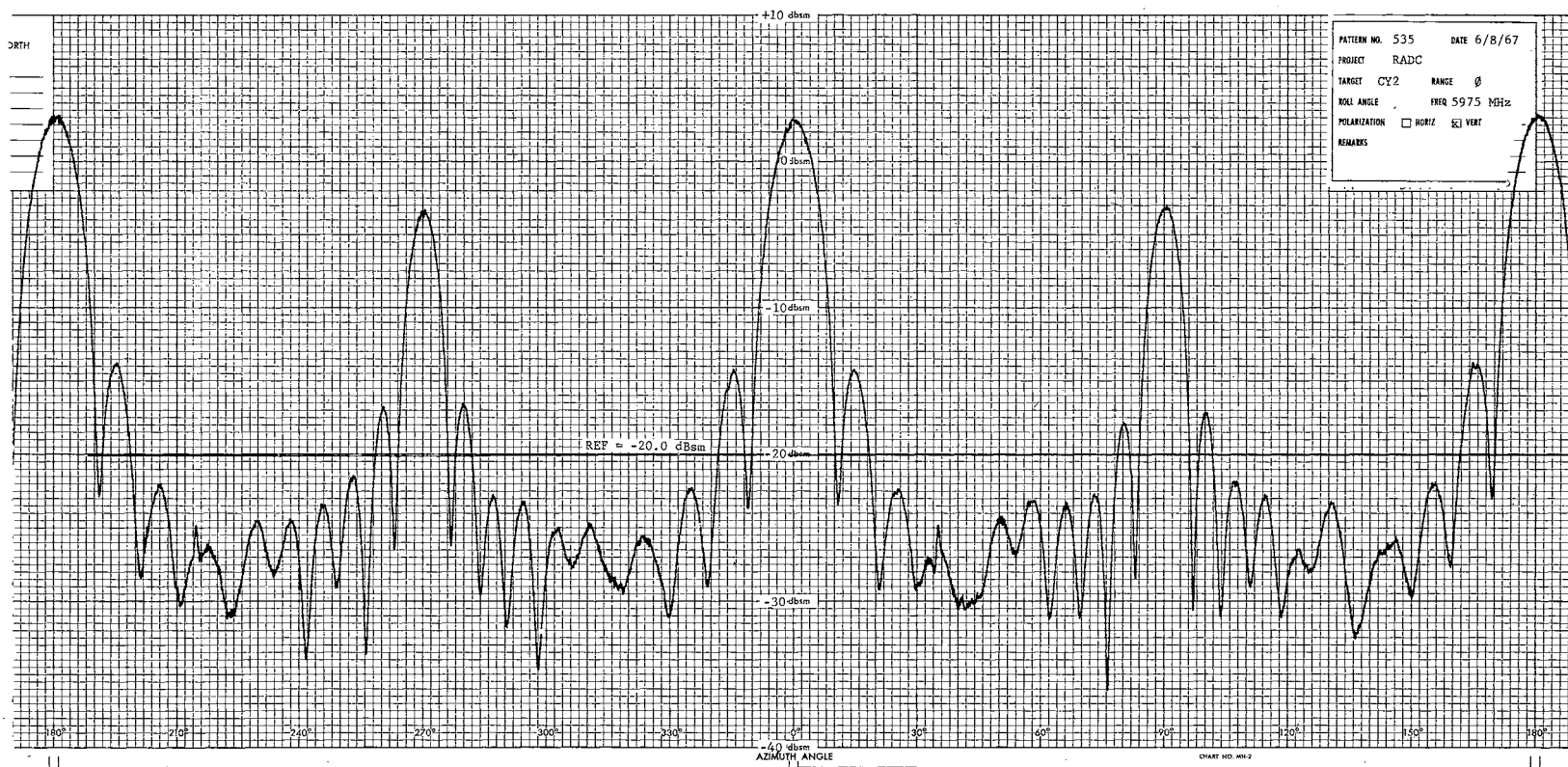


Figure 4. Cross Section σ_{VV} Versus Aspect of a Right Circular Cylinder

As in any measurement process, there is always some error associated with each measurement, and the experienced analyst takes this error into account in his analysis. A typical amplitude error may be as high as 3 to 4 dB in the case of a conventional radar system. As a result of these amplitude errors and the limited dynamic range of the radar, there will generally be a number of values of θ exhibiting the same value of σ_{VV} . If there are, for example, eight values of θ which are such that $\sigma_{VV}(\theta) = -12$ dBsm, this information can be stored in only nine storage locations rather than 16 since only the number -12 and the eight values of θ must be stored. This reduction in storage requirements can be achieved with no loss of information whatsoever.

The above described technique for obtaining a contraction mapping of the data of interest was based on the premise that signatures exhibiting equal elements are indeed equal and may be grouped into ordered sets without loss of information. This concept can be easily extended; in fact, it can be made more physically significant by grouping signatures into a class or group where all the signatures in the classes are, for example, equal within 3 dB of each other.

The ECT is based on a generalization of the preceding mapping. The desired contraction mapping consists of mapping the signature set S into a set of Equivalence Classes (EC's).

D2-3: A signature S_i belongs to equivalence class E_k , $S_i \in E_k$, if and only if S_i exhibits property P_k . All signatures belonging to E_k are said to be equivalent relative to the criteria set forth in P_k .

Property P_k is simply the specification of a relationship or set of relationships which exist between all the signatures belonging to E_k .

The definition of a set of properties $P_1, P_2, \dots, P_k, \dots, P_m$, allows the entire signature set of N signatures to be mapped into a set of K nonempty equivalence classes. It is a trivial exercise to show that $K \leq N$. In the case in which the number of nonempty equivalence classes, K , equals the number of signatures, N , it can be implied that there are not two signatures in S which are equivalent in terms of the set of properties P_1, P_2, \dots, P_m .

The nature of the set of P_k 's determines the amount of contraction obtained during the mapping process, as well as the amount and kind of information retained after mapping. A desirable mapping technique would be one where all of the pertinent decision information available in the signature space is retained while a significant contraction of the data is achieved. In fact, a mapping which results in the retention of most of the measured information can be realized; the amount of contraction achieved in such a process is a function of the vehicle type, the type of signature representation, and the system measurement resolution associated with the determination of S .

A mapping based on the presumption of retaining all information in S may be achieved by forming equivalence classes in the following manner. First, all the signatures in S exhibiting property P_1 are classified as belonging to the first equivalence class E_1 . Second, assume that a total of k_1 signatures belong to E_1 . From the remaining $N - k_1$ signatures in S , the signatures exhibiting property P_2 are then selected and classified as belonging in E_2 . This process is continued until all N signatures in S are mapped into a set of K equivalence classes so that E_p contains k_p signatures where

$$\sum_{p=1}^K k_p = N$$

The properties P_1, P_2, \dots, P_m must be mutually exclusive, i.e., no signature can exhibit the properties of more than one equivalence class (this restriction is naturally imposed if order is used in defining P_k). Additionally, the set of equivalence classes must span the signature space to assure that every signature in S belongs to an equivalence class. The contraction achieved by using an ECT can be observed in the following analysis.

Consider equivalence class E_p containing k_p signatures, each composed of n elements as defined in D2-1. All of these k_p signatures are equivalent in the sense that they all exhibit the common property P_p . However, all the signature elements of each of these signatures need not be stored since knowledge of the n elements of one signature and the k_p index numbers for this and the remaining $k_p - 1$ signatures is equivalent, under P_p , to knowledge of each signature in E_p . Thus, instead of storing a $k_p \times n$ array of numbers, only $k_p + n$ need be stored. The total storage requirement for the transformed signature set is obtained by summing $k_p + n$ over the K equivalence classes. This summation gives

$$\sum_{p=1}^K (k_p + n) = \sum_{p=1}^K k_p + \sum_{p=1}^K n = N + n \times K$$

as opposed to the $N + n \times N$ storage locations required to store S .

Consequently, a reduction of $n \times (N - K)$ storage locations is achieved without loss of information, in the equivalence class sense. Strictly speaking, only the information relating to the confidence with which a signature is placed in an equivalence class is discarded.

In the ECT, the meaningful order of the signatures in S is preserved. If meaningful decisions can be made without the knowledge of order, a greater reduction in storage can be achieved. For example, if only the number of signatures in each equivalence class is retained, then only $n + 1$ storage locations will be required for each equivalence class. The total storage requirement in this case would be

$$\sum_{p=1}^K (n + 1) = K + (n \times K)$$

locations, a reduction of $n \times (N - K) - K$ storage locations in comparison to those required to store the entire signature set.

Basically, the mapping of S from a signature space into a set of equivalence classes represents an intermediate mapping between the signature space and the decision space since the characteristics or features of the equivalence class representation constitute the final information on which decisions are based. An example of the significance of equivalence class features is especially evident in the analysis presented in the next chapter.

The properties used to define an equivalence class mapping should have some physical meaning in terms of the decisions of interest if decisions based on the equivalence class formulation are to be physically meaningful. A number of physical properties of measured signatures might be incorporated, including the following:

1. Values of signature elements (cross section, phase)
2. Order properties (time, aspect orientation)
3. Separation properties (e.g., ratios of measurements)
4. Rates of change of signature elements.

Each of these properties represent discriminants which are utilized to some degree by any analyst in making decisions on the basis of measured signatures. All of these properties are evident in the examination of a typical cross section or phase plot although they are not necessarily independent. The choice of the property or properties to be used is inseparable from the concept of utility discussed earlier in this chapter. Also, the use of multidimensional signatures whose parameters include frequency and polarization tends to expand the number of properties that may be potentially useful and further complicates the analyst's job since a great deal of correlation must be established between properties of different signature elements.

The ECT under primary consideration in this thesis is based on properties relating the measured values of cross section and phase measurements and on order properties. However, the nature of these phase measurements should be explained to avoid confusion. The phase measured by use of a coherent radar system is ambiguous in the sense that it contains an additive term which appears as a result of the range separating the radar and the target. In order to remove this range dependency and thus provide a phase measurement which is only a function of the scattering properties of the target vehicles, the general procedure is to measure the phase at two different polarization conditions and use the difference or differential phase as the phase signature element. If the range to the target does not change

significantly with respect to a wavelength during the time period between the two phase measurements, the differential phase will be a true target signature. Nevertheless, the differential phase may be ambiguous (modulo 2π) if the target phase centers at the two polarizations are separated by more than one half wavelength.² In order to measure the actual phase characteristics of a space object, one must in general be able to remove the rapidly changing component of phase which is produced by the component of the motion of the object along the RLOS. At microwave frequencies, the rate of change of phase produced by vehicle motion in the RLOS will be much greater than the rate of change produced by changes in vehicle orientation relative to the RLOS. The removal of the effects of range-rate and those anomalies introduced by propagation through the ionosphere are discussed in Chapter V in relation to the manner in which they affect the extrapolation of results obtained by use of range-radar signatures to those which would be obtained under operational conditions.

An example of measured and differential phase signatures is shown in Figure 5. Whenever the target exhibits an axis of symmetry along the RLOS, the differential phase should be zero along this axis and at all other points where the two polarization phase centers lie in a common plane perpendicular to the RLOS. In the remainder of this thesis, the word phase will be used in reference to differential phase. When reference is made to the actually measured phase, the phrase measured phase will be used.

²A one half wavelength separation on the target transforms into a 2π separation at the phase center as a result of the two way radar path.

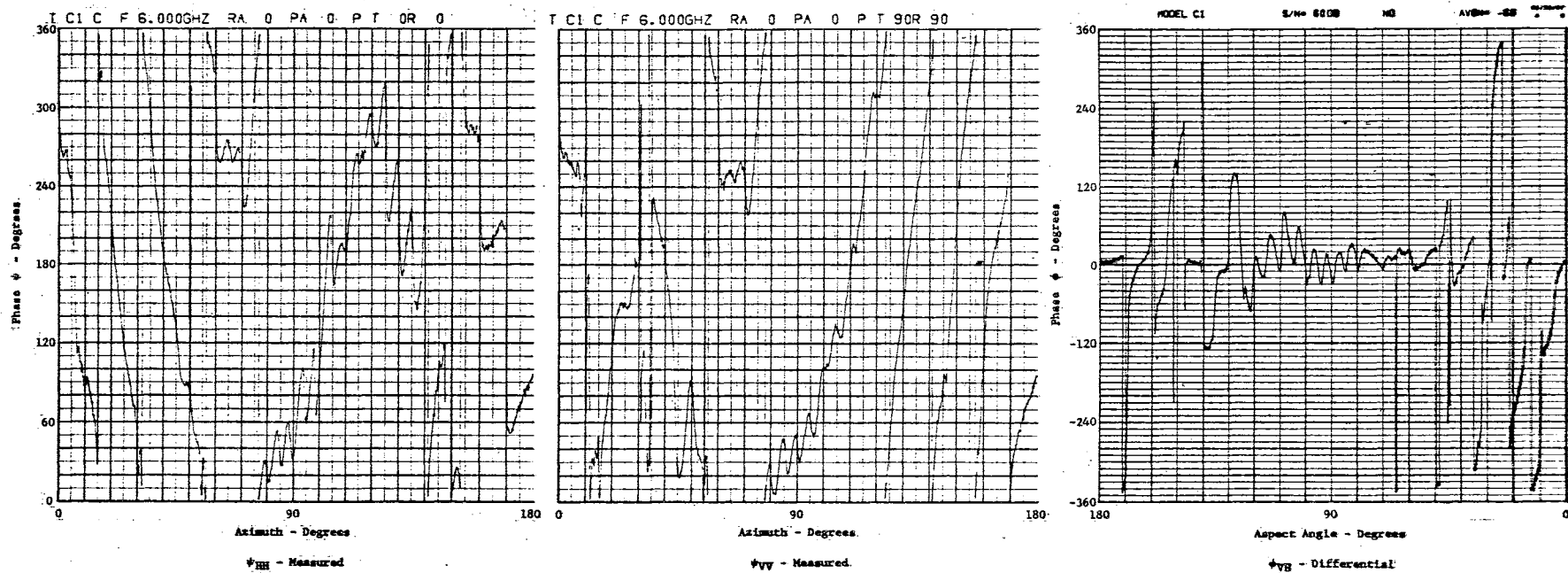


Figure 5. Measured Phase and Differential Phase of Model C1

2.3 An ECT Formulation. The ECT used as the basis of the analyses presented in Chapters III and IV is formulated as a result of satisfying the property defined below:

D2-4: Two signatures, S_i and S_k , are equivalent if the values of each of their respective elements s_{ij} and s_{kj} are within some ϵ_j of each other, or

$$s_{ij} - \epsilon_j \leq s_{kj} \leq s_{ij} + \epsilon_j \quad \forall \quad j = 1, 2, \dots, n$$

implies that

$$S_i \approx S_k$$

otherwise,

$$S_i \not\approx S_k$$

The physical meaning of this property is dependent on the physical meaning of the ϵ_j 's. If the ϵ_j 's are indeed representative of physical error phenomena, then the property defined in D2-4 represents a meaningful relationship between two signatures.

This relationship can be incorporated into an ECT in the following manner.

D2-5: Let $S_1^b, S_2^b, \dots, S_k^b, \dots, S_K^b$ be a set of basis signatures spanning S and let

$$S_i^b \neq S_k^b \quad i, k = 1, 2, \dots, K$$

Definition D2-5 is constructed so as to assure that no two basis signatures in S will satisfy D2-4. The number of basis signatures K must be such that the basis signatures span the signature space. This require-

ment is expressed in D2-6.

D2-6: Let S^b , the set of basis signatures, be such that

$\forall S_i \in S$ and $\forall \epsilon_j, j = 1, 2, \dots, n$, there exist $S_k^b \in S^b$ so that

$$S_i \approx S_k^b$$

S^b is then said to span S .

The fundamental formulation of the equivalence classes can now be defined as

D2-7: $S \rightarrow S^b$ if and only if $\forall S_i \in S, i = 1, 2, \dots, N$ and $\forall \epsilon_j, j = 1, 2, \dots, n$ there exist an $S_k^b \in S^b, k = 1, 2, \dots, K$ so that

$$s_{kj}^b - \epsilon_j \leq s_{ij} \leq s_{kj}^b + \epsilon_j \quad j = 1, 2, \dots, n$$

The notation $S \rightarrow S^b$ denotes that the signature set S is mapped into the set of basis signatures or into the set of equivalence classes.

In the sense of D2-3, the property P_k represents the case in which a signature is equivalent to the respective basis signature S_k^b .

The actual process of mapping a signature set S into a set of equivalence classes is facilitated by selecting the basis signatures from S . This selection may be accomplished in the following manner.

First, a basis signature for the first equivalence class, E_1 , is arbitrarily selected from S . For convenience, let this signature be S_1 , i.e., $S_1^b = S_1$. Next, all of the remaining signatures in S which exhibit property, P_1 , as defined in D2-3, are classified as belonging to E_1 . Assume that k_1 signatures (including S_1) belong to E_1 . From the remaining $N - k_1$ signatures in S , a basis signature for E_2 is then

selected, for example, S_6 , and the set of k_2 signatures exhibiting property P_2 are classified in E_2 . This process is continued until all N signatures are classified into K equivalence classes and the equivalence class mapping is complete.

An example of an ECT mapping is shown in Table II. In this example, a signature set consisting of 29 measured cross section signatures is mapped into a set of four equivalence classes by use of an error limit of 0.2 dB on cross section. The four basis signatures are the four signatures which exhibit aspect angle values of 180.2, 178.7, 178.1, and 177.5 degrees, respectively. These basis signatures were selected from the signature set in the manner described in the preceding paragraph.

It is significant to note that the number of equivalence classes obtained by use of the formulation described above is dependent upon both the signature set S and the values of the ϵ_j 's. A small value of K probably indicates that (1) the vehicle is a very small vehicle (relative to wavelength) or simple in shape, (2) a simple signature type is being used, (3) the aspect orientation of the vehicle changed insignificantly during the measurement sequence, or (4) the set of properties (ϵ_j 's) are such that many signatures belong to each equivalence class. Conversely, a large value of K probably indicates that the vehicle is (1) a complex vehicle, (2) one measured with a complex signature type, (3) one whose aspect orientation changes considerably, or (4) one measured under conditions of measurement resolution where only a few signatures belong to each equivalence class.

TABLE II
EXAMPLE OF ECT MAPPING

Error Limit on Signature Element $\epsilon_{\sigma} = 0.2$ dB			
Signature Index (i)	Aspect Angle θ (Degrees)	Signature Element (dBsm)	Equivalence Class Number
1	180.2	3.7	1
2	180.1	3.7	1
3	180.0	3.7	1
4	179.9	3.7	1
5	179.8	3.7	1
6	179.7	3.7	1
7	179.6	3.7	1
8	179.5	3.8	1
9	179.4	3.8	1
10	179.3	3.8	1
11	179.2	3.7	1
12	179.9	3.7	1
13	179.0	3.7	1
14	178.9	3.6	1
15	178.8	3.6	1
16	178.7	3.4	2
17	178.6	3.3	2
18	178.5	3.3	2
19	178.4	3.3	2
20	178.3	3.2	2
21	178.2	3.2	2
22	178.1	3.2	2
23	178.0	3.0	3
24	177.9	3.0	3
25	177.8	3.0	3
26	177.7	2.9	3
27	177.6	2.8	3
28	177.5	2.7	4
29	177.4	2.6	4

The analysis in the following two chapters reveals that K , as well as other equivalence class features, may provide information which is significant for use as identification aids as well as for use in obtaining a measure of the information contained in different signature-type representations.

2.4 Results. A large number of measured signature sets were mapped into equivalence classes by use of the ECT described above. The signature sets were obtained by using the ground plane radar scattering range described in Appendix B to measure a variety of different vehicle models which range from very complex to very simple geometrical configurations. An investigation was made of signature types which included the SM and various subsets of the SM in order to enable the comparison of conventional, coherent, and SM radars.

Examination of the data in Table III will indicate the reduction in storage requirements obtained by using the ECT described above in comparison to requirements for storage of the entire signature set. Variations in the percent reduction obtained as a function of signature type, vehicle complexity, and measurement resolution (signified by the ϵ_j 's) are revealed in this data. This data was compiled by using the STAP computer program to compute the data on the ambiguity of signature-type representation described in Chapter III. The data in Table III was obtained by using Model 3, one of the complex vehicles. The data contraction achieved by use of most of the other vehicles described in Appendix D was even greater than that obtained from Model 3.

TABLE III

REDUCTION IN COMPUTER STORAGE REQUIREMENTS OBTAINED
USING THE EQUIVALENCE CLASS TECHNIQUE

Signature Type	Error Limits		N n K Nxn + N				ECT With Order		ECT Without Order	
	ϵ_{σ}	ϵ_{ϕ}					Kxn + N	Percent Reduction	Kxn + K	Percent Reduction
SM	1	10	1426	5	1039	8556	6621	22.6	6234	27.2
SM	2	10	1426	5	910	8556	5976	30.2	5460	36.2
SM	3	10	1426	5	845	8556	5651	33.9	5070	40.7
SM	4	10	1426	5	814	8556	5496	35.7	4884	42.8
SM	5	10	1426	5	787	8556	5361	37.3	4722	44.8
SPVV	1	--	1426	1	32	2852	1458	48.9	64	97.8
SPVV	2	--	1426	1	18	2852	1444	49.3	36	98.6
SPVV	3	--	1426	1	12	2852	1438	49.6	24	99.2
SPVV	4	--	1426	1	10	2852	1436	49.6	20	99.4
SPVV	5	--	1426	1	8	2852	1434	49.6	16	99.5

The motivation for developing the ECT is primarily a desire to provide as much information as possible in the form of as few separate discriminants as possible for use in conjunction with automatic decision-making processes. The fact that a great deal of measured signature data can be compressed into a much smaller number of data points in the formulation of an equivalence class is evident from the discussion and the data presented in this chapter. The fact that a given ECT will transform different source vehicles (i.e., their signature sets) into sets of equivalence classes which exhibit characteristics peculiar to that vehicle will be brought out in the next two chapters and will be utilized to form a basis for two distinct automatic decision-making processes. It is the properties of the equivalence class formulation of a signature set which appear to provide a useful basis upon which to concentrate computerized decision processes.

CHAPTER III

APPLICATION TO A MEASURE OF SIGNATURE-TYPE AMBIGUITY

3.1 General. A question which has concerned the radar designer since the earliest beginnings of radar has been that of which polarization to utilize for particular radar measurements. Usually, the answer to this question has been primarily based on a desire (1) to receive the largest possible radar return, (2) to maximize the probability of detecting a target, or (3) to optimize detection and/ or tracking of an object in an environment such as clutter, rain, etc. In each case, the scattering properties and the dynamics of typical targets must be considered. In order to receive the largest possible return, the radar designer would probably choose that polarization to which the scattering object presented the greatest radar cross section. However, if the target orientation were arbitrary, it might not be detected because the orientation might be insensitive to that particular radar polarization. If the radar transmitted a high-power signal and the target was large, one might prefer to use a circularly polarized wave. In this way a target which was preferentially sensitive to a linear polarization (e.g., a dipole) would still be detected although a sacrifice of 3 dB of power would be incurred.

Sinclair (18), Ridenoir (19), and Kennaugh (3) have performed extensive investigations of the polarization most desirable for

extracting a target from clutter, notably rain and snow. Clutter of this type becomes a problem at high microwave frequencies as a result of the resonant effect of the small particles at the short wavelengths. These investigators found that the use of circular polarization provides a great deal of clutter rejection as a result of the different backscatter characteristics of large complex and asymmetrical objects, such as aircraft and small, symmetrical rain drops. Kennaugh actually went considerably further in his investigations by showing that various targets exhibit "null polarizations", i.e., that there exist certain polarization conditions of the transmitter and receiver to which a target will couple no energy.

Kennaugh (3) and a number of later investigators based their polarization analyses on the properties of the target scattering matrix. (20,21). The scattering matrix proves to be an extremely useful tool in polarization analysis since, at a single frequency and aspect orientation, knowledge of the scattering matrix provides all of the polarization properties of vehicles at that frequency and aspect. This rather classical development is summarized in Appendix A for the interested reader; however, it is not necessary for understanding the analyses presented in this thesis. It is interesting to note that knowledge of the scattering matrix at a single frequency and aspect angle provides information which can be used for simulating the complete rotation of the target about the RLOS.

As radar designers have more recently turned their thoughts to the identification of radar targets rather than the detection of targets, the question of what signature should be measured has become important. It is well known that the various elements of the SM signature are not

necessarily independent, a fact that can be demonstrated by the high degree of correlation between σ_{VV} and σ_{HH} over some aspect regions in the case of many different targets.

To the author's knowledge, no investigation of the degree of independence of the elements of the SM has been performed, nor has the question of how much information can be obtained by utilizing, for example, σ_{VV} and σ_{HH} as opposed to σ_{VV} alone, been sufficiently answered.

The amount of information contained in a particular signature type is closely related to how effectively a particular signature type can be used to represent a target unambiguously. A spherical scatterer, for example, represents a completely ambiguous target even when it is represented by the SM; i.e., it is ambiguous in the sense that the orientation of the sphere cannot be determined from one, two, or any number of signature measurements. On the other hand, the orientation of a more complex target may be much less ambiguously determined as the complexity of the signature-type representation is increased. It will be shown that every SM signature is unique in the case of some complex targets through a complete rotation of the target.

D3-1: A signature $S_i \in S$ is unique if there exists no $S_k \in S$ which satisfies the equation

$$s_{ij} = s_{kj} \text{ for every } j = 1, 2, \dots, n$$

3.2 Ambiguity Space Formulation. The equivalence class formulation (or the equivalence class space) provides a convenient set of parameters or features which are related to the idea of ambiguity presented above. One of these features, K , the number of equivalence classes, was discussed in Chapter II in terms of its relationship to

vehicle complexity, signature complexity, and measurement resolution. In the case of a given vehicle, a given measurement resolution, and a given orientation, K is related to the probability that the vehicle can be unambiguously represented by a particular signature type. One would expect the value of K to increase monotonically as a function of an increase in the dimension or complexity of the signature-type representation; however, the rate of increase of K would be difficult to predict without extensive empirical analysis.

The value of K could be used by itself to form a measure of signature-type ambiguity; however, the fact that one equivalence class may contain many signatures while another contains only one signature indicates that a few signatures could heavily bias the results by producing a large value of K , even though a large percentage of the signatures belonged to a small number of equivalence classes.

The number of signatures in an equivalence class is also related to orientation ambiguity, for as the number of signatures per equivalence class increases, the ambiguity must necessarily increase.

A third equivalence class feature which reveals the ambiguous nature of a particular signature representation is provided by the spread of the aspect orientation of the signatures belonging to an equivalence class. For example, if all of the signatures in a particular equivalence class result from a very small angular region of the vehicle orientation parameter, then the probability of unambiguously determining the vehicle orientation from the orientation of the basis signature of that equivalence class would be large. On the contrary, if a large spread of orientation angles were represented in the equivalence class, the probability of error in unambiguously

determining the orientation of the vehicles from the orientation of the basis signature would be small.

In order to utilize each of these parameters without regard to the size of the signature set, it is desirable to normalize each parameter. In the case of large signature sets, the use of this normalization appears to be reasonable. The three normalized parameters used to form a measure of ambiguity are defined in D3-2, 3, and 4.

D3-2: C_p is defined as the size (normalized) of the p^{th} equivalence class E_p , so that

$$C_p = \frac{k_p - 1}{N}$$

The value of $k_p - 1$ is used so that an equivalence class will be considered empty if it contains only a basis signature ($k_p = 1$). This restriction is necessary if $C_p = 0$ is to provide an implication of uniqueness.

D3-3: D_p will represent the diameter (normalized) of E_p so that

$$D_p = \frac{\text{Maximum aspect separation (modulo 180 degrees) of signatures in } E_p}{180}$$

D3-4: The ratio K/N is the number (normalized) of equivalence classes in S .

These three parameters can now be used to formulate a measure of the ambiguity of signature-type representation. However, prior to such a formulation, the relationships between these parameters and ambiguity should be noted.

C_p is related to the probability that a signature belonging to E_p will be observed for a given vehicle, signature type, and set of error

limits. D_p is related to the probability that, for a given vehicle, a given set of error limits, and a given signature type, the aspect angle orientation of the vehicle will be ambiguous if it is determined by observing a signature belonging to E_p . $1 - K/N$ behaves, in a real sense like, one minus the probability that a given vehicle can be unambiguously identified by using a particular signature type and a given set of error limits.

On the basis of these probability relationships, the three parameters may be incorporated to form an ambiguity vector, \bar{A}_p , defined in D3-5.

$$D3-5: \bar{A}_p = (C_p, D_p, 1 - K/N)$$

Each of the three components of \bar{A}_p may now be used to form an axis of a three-dimensional ambiguity space in which an ambiguity vector can be represented as a point. The ambiguity space representation of a signature set is then a set of points, each point representing an ambiguity vector (or equivalence class). This representation is a function of vehicle geometry, signature type, and system measurement resolution.

An ambiguity space is illustrated in Figure 6. Representative points are indicated in this figure for two limiting cases: (1) that of a highly ambiguous representation corresponding to a sphere, a case of very poor measurement resolution, or a very ambiguous signature type, and (2) that of a highly unique representation corresponding to a very complex vehicle, a case of extremely fine measurement resolution, or a highly unique signature type.

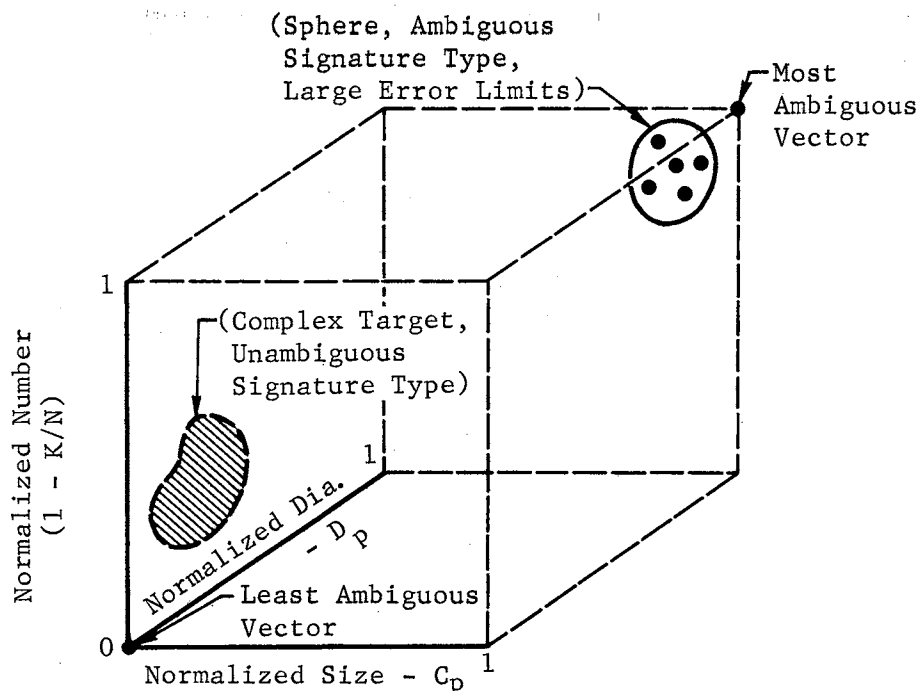


Figure 6. Representation of Ambiguity Space

It should be pointed out that, when $K = N$, there are no two equivalent signatures in S , and $\bar{A}_p = (0, 0, 0)$ for all values of $p = 1, 2, \dots, N$. This situation results from the fact that an equivalence class is considered empty if it contains only a basis vector. When $K = 1$, all of the signatures in S are equivalent, and there will be only one ambiguity vector whose value will be

$$\bar{A}_1 = (1 - 1/N, 1, 1 - 1/N)$$

Thus, the ambiguity vector $(1, 1, 1)$ can never be realized; however, when the values of N are large, the difference between $1 - 1/N$ and unity will be negligible.

In general, each signature set will be mapped into a set of K points in ambiguity space. These points may or may not cluster,

depending on the values of C_p and D_p for each equivalence class.

In the case of a given vehicle, the average location of these points is indicative of the average ambiguity of the representation. The expected value of the magnitude of the ambiguity vector provides a similar indication of ambiguity. In this analysis, the sample mean of the magnitude of \bar{A}_p is used to approximate the expected value. Thus,

$$D3-6: \quad AVGA = \frac{1}{3 \cdot K} \sum_{p=1}^K |\bar{A}_p|$$

The value of average ambiguity, AVGA, ranges from a lower limit of 0, corresponding to $K = N$ (completely unambiguous representation), to an upper limit of approximately unity, corresponding to $K = 1$ (completely ambiguous representation). Note that, of $N = 1000$, the error in the computation of AVGA, for the case where $K = 1$, is less than 0.03 percent.

The computation of the average ambiguity represents a mapping of N distinct signature measurements in a multi dimensional signature space, via the ECT, onto an interval of the real line from 0 to 1. This mapping process is independent of the value of N (N is assumed to be large) and of the type and dimension of the signature used. It has also been shown that the mapping is based on the use of properties which are physically related to the basic ambiguity of signature representation.

It should be pointed out that the mapping from ambiguity space to a value of average ambiguity does not represent a one-to-one mapping since a single value of AVGA can result from more than one equivalence class formulation.

3.3 Description of Experiments. A number of measured signature sets were processed by using a digital computer in order to establish the usefulness of AVGA as a measure of signature-type ambiguity. Library data in the form of signature sets recorded on magnetic tape were used as input to the computer program. A logic diagram of Signature Type Ambiguity Program (STAP) is shown in Figure 7, and flow charts and a Fortran IV listing of the STAP are included in Appendix D for the interested reader.

In order to make the investigation of signature-type ambiguity as flexible and as thorough as possible, a number of options were included in STAP. These options are designated and defined as follows:

1. Reduced Signature Set - This option is used for periodically skipping as many signatures as desired and/or considering signatures over aspect angle intervals less than 360 degrees.
2. Synthesize Additive Noise - This subroutine is used for synthesizing the effects of additive noise on the cross section elements of a signature set. (21).
3. Noise Subtraction - This subroutine is used for estimating the true target cross section by subtraction of the average noise level from the measured cross section. (21).
4. Error Limits - This option is used for examination of the effects of system measurement errors through the application of variable error limits to each signature element.
5. Signature-Type - This option is used for the selection of any subset of the SM signature or any subset of the signature type recorded on the library tape.

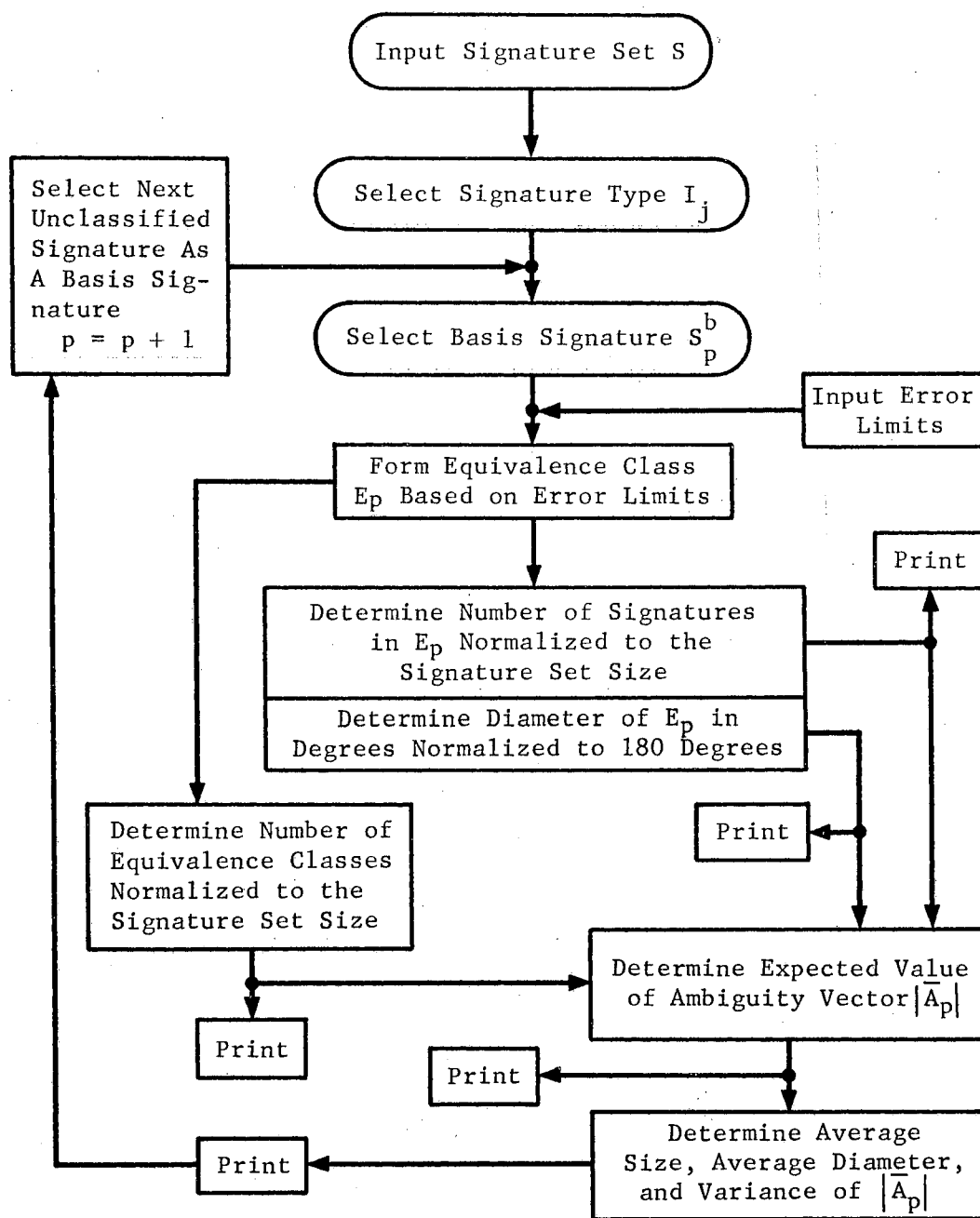


Figure 7. STAP Computer Program Logic Diagram

Option 1 constitutes a means of investigating the sensitivity of AVGA to the size of S and to vehicle-symmetry properties. Options 2 and 3 are used to investigate the effects of noise on ambiguity. Option 4 is used to provide data on desirable design trade-offs between system measurement resolution and signature complexity. Option 5 provides the basic flexibility needed to compare different signature-type representations of a selected vehicle.

Signature data on a number of vehicle models were processed by using the STAP program. The measurement system described in Appendix B was used to obtain these signature measurements. Table IX in Appendix C contains a detailed description of all models utilized to provide experimental data for this thesis. The models cover a broad spectrum of degrees of geometrical complexity and a range in ka from 12 to 170.¹

Signature sets from 10 different vehicles were used to provide data on the ambiguity of signature-type representation. The SM signature was recorded on magnetic tape so that each record contained a signature in the following order:

$$(\theta, \sigma_{VV}(\theta), \sigma_{VH}(\theta), \sigma_{HH}(\theta), \phi_{VH}(\theta), \phi_{HH}(\theta))$$

The values of $\phi_{VH}(\theta)$ and $\phi_{HH}(\theta)$ represent differential phase terms and are formed as

$$\phi_{VH}(\theta) = \psi_{VH}(\theta) - \psi_{VV}(\theta)$$

and

$$\phi_{HH}(\theta) = \psi_{HH}(\theta) - \psi_{VV}(\theta)$$

¹ k is the wave number and a is the largest characteristic dimension of the model.

where the $\psi(\theta)$ terms represent actual measured phase and include a range term. It should also be pointed out that the cross section values on tape were recorded in units of dBsm since actual recordings are made in log space rather than in square meter space.

In the case of the generic vehicles (e.g., cones, cylinder, frustrums, etc.), the scattering matrix is a diagonal matrix since $\sigma_{VH} = \sigma_{HV} = 0$. This phenomenon is a result of the axial symmetry of the generic shapes; it is explained in Appendix A. The designation TPP represents the scattering matrix of the generic models. The scattering matrix signature of the generic models should be more ambiguous than that of the asymmetrical models. This fact is evident since all σ_{VH} signatures would be zero at all orientations whenever the axis of revolution was co-planar with the horizontal polarization vector and the RLOS. On the basis of these relations, it can be shown that increased physical symmetry leads to increased ambiguity of signature representation; this physical relationship has been incorporated in forming the ambiguity vector.

3.4 Analysis. The results of the ambiguity analysis are presented in Figures 8 through 14. In order to emphasize the natural distinction between the physical characteristics of the vehicles investigated, the analyses of these results are grouped according to the types of vehicles under consideration. Two rather distinct vehicle types were investigated in order to provide signature sets composed of five-element SM signatures and three-element SM signatures. The five-element signatures provided the SM for Models 1, 2, and 3 which are respectively a toroid, toroid-dipole, and a typical aerospace vehicle. These vehicles are described in detail in Appendix C; however, the

reason for choosing these particular geometrical designs should be mentioned. The toroid portion of Models 1 and 2 was constructed of a loosely woven wire mesh (chicken wire) in order provided a number of highly resonant scattering regions in the S-band frequency (3.0 gigahertz) at which Models 1, 2, and 3 were measured. The orientation of these resonant regions and the mutual coupling between them provided a large amount of depolarization of the incident wave and assured a high cross polarization return.

The dipole utilized in conjunction with the toroid to form Model 2 was designed to exhibit a value of cross section approximately equal to that of the toroid. This design, coupled with the spatial separation between the toroid and the dipole, provided a much larger spatial movement of the vehicle phase center as the vehicle was rotated than that observed on the toroid alone. Observation of the analog plots of Models 1 and 2, contained in Appendix C, will indicate the differences between the corresponding signature elements of these models. However, a discussion of the significance of these differences will be deferred until Chapter IV where the physical similitude of the vehicles is discussed in terms of the similarities in their signatures.

Model 3 was a model of a typical aerospace vehicle. This model provided regions of specular scattering, a large spatial movement of the scattering phase center, and a fairly high cross polarization return as a result of illuminating a highly asymmetrical rocket engine.

The remaining models considered during this investigation represented vehicles which were bodies of revolution, such as combinations of the generic bodies selected for study. As a result of the symmetry of these models and the fact that sample measurements of their cross

polarization returns were in accordance with the radar antenna rejection, their cross polarization signatures were not recorded.² Thus, the SM representation of these vehicles was the diagonal form, i.e.,

$$SM = \begin{bmatrix} \sqrt{\sigma_{VV}} & 0 \\ 0 & \sqrt{\sigma_{HH}} e^{i\phi_{HH}} \end{bmatrix}$$

where $\phi_{HH} = \psi_{HH} - \psi_{VV}$. The corresponding TPP signature representation was recorded on magnetic tape in the following form,

$$S_i = [\theta, \sqrt{\sigma_{VV}}(\theta_i), \sqrt{\sigma_{HH}}(\theta_i), \phi_{HH}(\theta_i)]$$

while that of the general scattering matrix was given by

$$S_i = [\theta, \sqrt{\sigma_{VV}}(\theta_i), \sqrt{\sigma_{VH}}(\theta_i), \sqrt{\sigma_{HV}}(\theta_i), \phi_{VH}(\theta_i), \phi_{HH}(\theta_i)]$$

3.4 Ambiguity of Complex Vehicles. The ambiguity data presented in Figure 8 was computed by using signature sets of Models 1, 2, and 3; these sets consisted of alternate recorded signatures of a 360-degree rotation of the vehicle model.³ Each of these models is considered a complex vehicle in the sense that it is not a body of revolution; on the contrary, each exhibits a fairly high cross polarization return. In order to provide a clear presentation of the effects of signature type and error limits on ambiguity, the error limits placed on all phase elements used to obtain the data in Figure 8 were constant

²Antenna rejection is a measure of the coupling between cross polarized antennas when a nondepolarizing target is illuminated. Better than 35 dB of isolation was achieved with the antenna system used in this measurement program.

³The SM measurements for Models 1, 2, and 3 were obtained by Dr. C. C. Freeny of the Fort Worth Division of General Dynamics and are reported in Experimental and Analytical Investigation of Target Scattering Matrices, Technical Report No. RADC-TR-65-298, December 1965, Rome Air Development Center. (21).

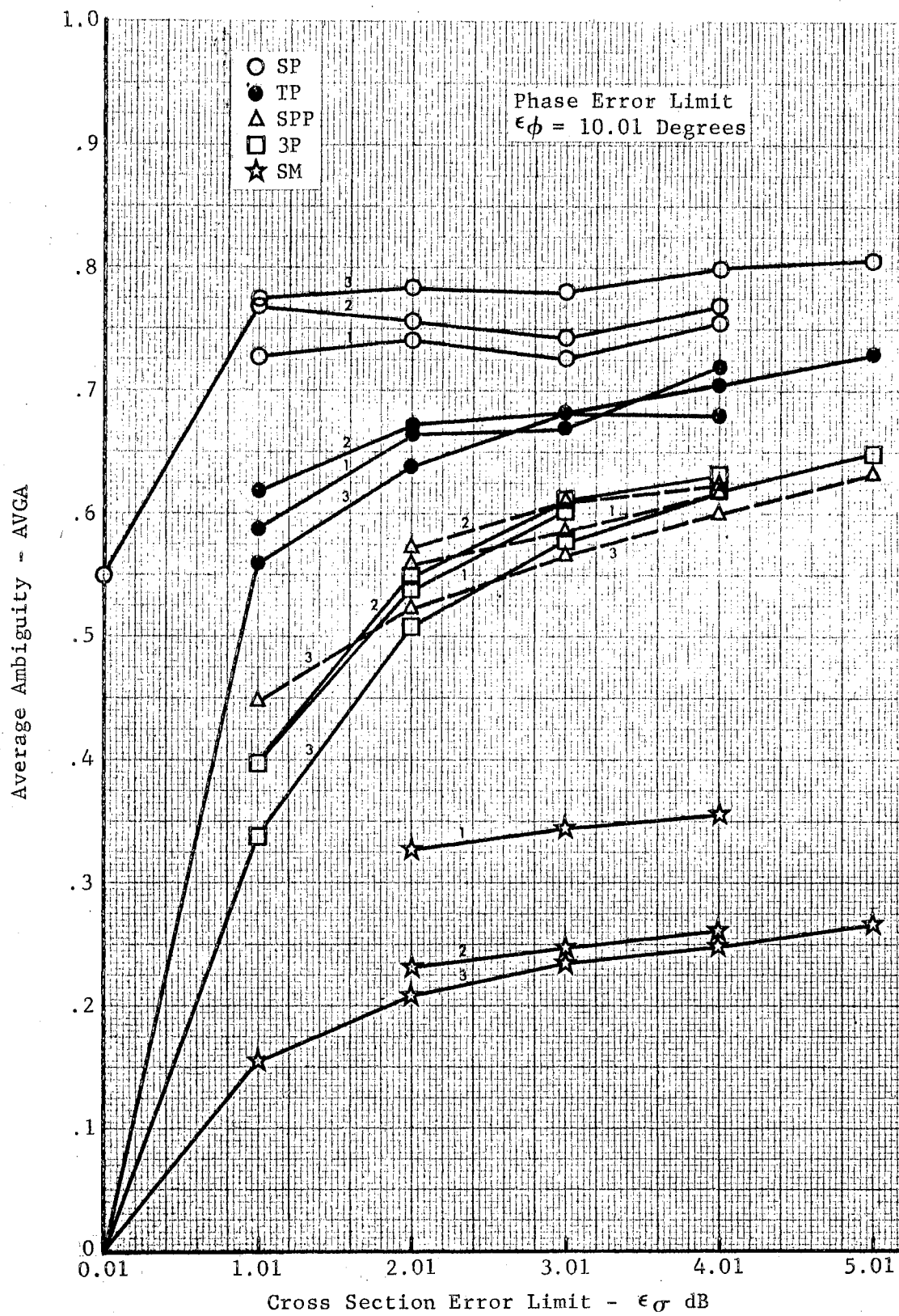


Figure 8. Average Ambiguity of Complex Vehicles

($\epsilon_\phi = 10$ degrees). The only exception was the case where the SM signature was used with all error limits set at zero in order to provide a lower bound on ambiguity for Model 3. Actually, real numbers, such as 10.01 degrees and 2.01 dB, were used as error limits rather than integers so that the effects of computer round-off could be eliminated. These fractional values have no effect on the formulation of equivalence classes since the radar system was able to resolve cross section within 0.1 dB, phase within 1.0 degree, and aspect angle within 0.1 degree. Thus, the use of error limits of 0.01 dB on cross section is actually in keeping with the measurement resolution of the radar measurement system. In the process of developing the ECT used to define ambiguity, error limits were so applied that measurement systems could be simulated to provide cross section and phase measurement resolution worse than that actually used. For example, when reference is made to an error limit of 5 dB, it will be understood that a value of 5.01 dB will be used in the STAP computations. Computer round-off is handled in a similar manner in the program discussed in Chapter IV.

The use of the Model 3 signature set composed of SPVV signatures resulted in an average ambiguity of 0.55 when an error limit of $\epsilon_\sigma = 0$ dB was used (refer to the data in Figure 8). The addition of only one signature element to form the TP signature resulted in an average ambiguity of 0.02. When the complete SM signature was used with $\epsilon_\sigma = 0$ dB and $\epsilon_\phi = 0$ degrees, a value of 0.0000 was obtained for AVGA, in other words; the SM provided a unique representation of Model 3, i.e., there were no two SM signatures in S which were identical element for element. These results indicate, at least in the case of Model 3, that the TP signature provides an essentially unambiguous

representation of a signature set obtained by using a high-resolution ($\epsilon_\sigma = 0.1$ dB and $\epsilon_\phi = 10$ degrees) radar system.

When the error limits on cross section were increased to 1 dB, the value of AVGA increased considerably in the case of all signatures (note that $\epsilon_\phi = 10$ degrees whenever $\epsilon_\sigma = 0$ dB). Further increases in ϵ_σ produced a much smaller increase in AVGA. Of particular interest are the values of AVGA obtained by using values of ϵ_σ between 2 and 4 dB. These values correspond to the resolution capabilities of many operational radar systems. The change in ambiguity associated with this range of ϵ_σ is generally quite small, the greatest change being about 20 percent in the case of 3P and SM signatures. A decrease in ϵ_σ from 4 dB to 1 dB (doubling the resolution of the radar in terms of cross section) produces a change of less than five percent in ambiguity.

On the other hand, the SM signature is about twice as unique as the SPP signature and at least three times as unique as the SPVV signature for all values of ϵ_σ except those very near to 0 dB.

On the average, in the range of ϵ_σ between 2 dB and 4 dB, the use of an additional cross section signature element produced approximately a 7- to 15-percent decrease in ambiguity. The addition of a single phase element (based on a phase error limit of $\epsilon_\phi = 10$ degrees) produced a 20- to 30-percent decrease in ambiguity - about twice the change obtained from a cross section element. This difference is discussed in the following paragraph.

In the first place, the phase data utilized in computing the data in Figure 8 exhibited a dynamic range of 720 degrees. This range resulted from the fact that ψ_{VV} , ψ_{VH} , and ψ_{HH} were measured over a range from 0 to 360 degrees. Therefore, the differential phase terms,

such as $\phi_{VH} = \psi_{VH} - \psi_{VV}$, covered a range from -360 to +360 degrees. The use of a 10-degree error limit corresponded to a quantitization of this 720-degree dynamic range into, at most, 72 distinct intervals (i.e., 72 distinct basis signatures) on the basis of assuming that the signature element encompassed the full dynamic range. On the other hand, the maximum dynamic range of a cross section element is 50 dB, and a 2-dB error limit would quantitize this range into a maximum of 25 distinct intervals corresponding to 25 basis signatures.

The significance of this approximately 3-to-1 ratio between the number of quantitization levels of phase and cross section signature elements (approximately 6-to-1 in the case of cross section error limits of 4 dB) is discussed in the following analysis.

The data in Table IV was obtained by using the SPP signatures of Model 3 and of three combinations of ϵ_{σ} and ϵ_{ϕ} . This data was taken to obtain information on the relative significance of changes in quantitization levels determined by ϵ_{σ} and ϵ_{ϕ} .

TABLE IV
EFFECTS OF CROSS SECTION AND PHASE QUANTITIZATION

Signature-Type SPP				
Case No.	dB	ϕ Degrees	K	AVGA
1	1.0	5.0	637	.3676
2	1.0	10.0	470	.4466
3	2.0	10.0	324	.5265

Examination of the three cases presented in Table IV will indicate that, when constant error limits are placed on phase, doubling the error limits on cross section (Cases 2 and 3) produced a 31-percent decrease in the number of equivalence classes and a 13.5-percent increase in the value of AVGA. Similarly, doubling the error limits placed on phase (Cases 1 and 2) and maintaining ϵ_{σ} constant produced a 26-percent decrease in the number of equivalence classes and a 21.5-percent increase in the value of AVGA. Doubling the value of ϵ_{σ} or ϵ_{ϕ} is equivalent to reducing the number of quantization levels of the corresponding signature element by one-half.

In order to obtain further insight into the role of phase quantization, the computational technique in the STAP was modified so that the absolute value of ϕ could be used. This change effectively reduced the dynamic range of phase signature elements to the interval from 0 to 360 degrees. The ambiguity of SPP and SM signature representations of Model 3 were then computed by using absolute phase without changing any other input data. The results of this computation are listed in Table V.

TABLE V
EFFECT OF ABSOLUTE PHASE ON AMBIGUITY

Model 3 Signature Type	$\epsilon_{\sigma} = -3$ dB	$\epsilon_{\phi} = 10$ degrees
	AVGA	AVGA Absolute Phase
SM	.2374	.3915
SPP	.5673	.6349

The increase in ambiguity produced by halving the number of phase quantization levels is observed to be about the same, in terms of percentage, as that obtained by doubling the phase error limits used in Case 1 (refer to Case 2, Table IV). Absolute phase was used in computing the ambiguity of all the generic vehicles.

At this point, some additional effects of phase data on ambiguity should be discussed since comparisons between the results obtained by using signatures which contain phase elements and those that do not may be misleading. In the limit, as the error limits on phase are increased toward 180 degrees, the ambiguity obtained by using the SM approaches that obtained by using the 3P signature. Thus, the values of ambiguity indicated by the three curves representing SM signatures could not exceed the values of ambiguity obtained for the 3P signatures, if constant cross section error limits are assumed. This result establishes the 3P ambiguity data as an upper bound on the ambiguity obtained by use of the SM and a prescribed cross section measurement accuracy.

Examination of the data in Figure 8 indicates that, in some instances (notably in the case of Model 3 SPVV signature data), the average ambiguity may decrease as a function of an increase in error limits. Intuitively, one would expect the ambiguity to increase as the error limits are increased, especially when one draws an analogy between an increase in error limits and poorer system measurement resolution. The phenomenon described above results from the discontinuous nature of the equivalence class diameter.

The values of ambiguity presented in Figure 8 represent the expected value of the magnitude of the ambiguity vector obtained by

computing the sample mean of all the ambiguity vectors for a particular signature set. Each individual ambiguity vector is determined on the basis of the value of its components. One of these components, the normalized number of equivalence classes, $1 - K/N$, is the same for each vector, and this number increases monotonically as a function of increasing error limits. However, the other two components of a particular ambiguity vector, equivalence class size, C_p , and equivalence class diameter, D_p , can decrease when error limits are increased. The apparent anomalies which appear as a result of the decrease of either or both C_p and D_p (as a function of increasing ϵ_σ or ϵ_ϕ) are discussed in the following analysis.

Any change in AVGA must be accompanied by a change in either (1) the number of equivalence classes and/ or (2) the size of at least two equivalence classes. In the first case, the number of equivalence classes decreases if the increase in error limits causes an equivalence class to be eliminated, causing the value of $1 - K/N$ to increase. For example, an equivalence class containing no signatures other than a basis signature may be eliminated as a result of an increase in error limits since increasing the error limits may cause that signature to be included in another equivalence class. The inclusion of this signature in an established equivalence class may cause the diameter of that equivalence class to remain unchanged or to increase in compliance with the definition of the equivalence class diameters specified in D3-3. However, the diameter would not be decreased in any event since the controlling parameters would not be changed.

A change in the size of an equivalence class must be accompanied by a change in size of at least one other equivalence class since

$$\sum_{p=1}^K C_p = 1 - K/N$$

remains constant independent of the values of the individual C_p 's (it is assumed that K remains constant).

In the case in which an increase in error limits produces no change in K , a decrease in ambiguity can only be produced by a decrease in the diameter of one or more equivalence classes. The proof of this hypothesis is set forth in Theorem T3-1.

T3-1: Let ϵ_1 and ϵ_2 denote error limits where $\epsilon_2 > \epsilon_1$. Assume that $K_2 = K_1 = K < N$. Further assume that $AVGA_2 < AVGA_1$; then there exists $m \leq K$ so that $D_{m2} < D_{m1}$ where D_{m2} and D_{m1} are the diameters of the m^{th} equivalence class obtained with error limits ϵ_2 and ϵ_1 , respectively.

PROOF:

1. In the relationship $AVGA_2 < AVGA_1$, it can be shown that

$$\sum_{p=1}^K \sqrt{1 + B_{p2}^2} < \sum_{p=1}^K \sqrt{1 + B_{p1}^2}$$

where $B_p^2 = (C_p^2 + D_p^2)/(1 - K/N)^2$.

2. Since $B_p^2 \geq 0$ for all $p = 1, 2, \dots, k$

$$\sum_{p=1}^K B_{p2}^2 < \sum_{p=1}^K B_{p1}^2$$

3. Thus,

$$\sum_{p=1}^K (C_{p2}^2 + D_{p2}^2) < \sum_{p=1}^K (C_{p1}^2 + D_{p1}^2)$$

4. As a result of the linearity of summation and the fact that $K_2 = K_1$,

$$\sum_{p=1}^K D_{p2}^2 < \sum_{p=1}^K D_{p1}^2$$

5. Assume $D_{p2} = D_{p1}$ for all $p = 1, 2, \dots, K$; therefore,

$$\sum_{p=1}^K D_{p2}^2 = \sum_{p=1}^K D_{p1}^2$$

This equality is a direct contradiction of the inequality in (4).

6. Hence, there exists at least one value of $p = m$ which is such that

$$D_{m2} \leq D_{m1}$$

The case where $K_1 = K_2 = N$ is trivial since the formulation of the equivalence classes is unchanged.

The case in which a decrease in ambiguity is accompanied by a decrease in K can be quite easily described by using specific cases.

Consider the signature set containing only the three SP signatures

described below in the form $S_i = (\theta_i, \sigma(\theta_i))$:

$$S_1 = (180.0, -11.0)$$

$$S_2 = (179.0, -13.0)$$

$$S_3 = (139.0, -14.0)$$

Assume that an error limit of 1 dB results in two equivalence classes, E_1 and E_2 , where

$$E_1 \supset S_1$$

$$E_2 \supset S_2, S_3$$

The respective diameters and sizes of these equivalence classes are

$$k_1 = 1, D_1 = 0 \text{ degree}$$

and

$$k_2 = 2, D_2 = 40 \text{ degrees}$$

where, for convenience, the values are not normalized. Increasing the error limit to 2 dB would still result in obtaining two equivalence classes; however, the values of k_i and D_i would then be

$$k_1 = 2, D_1 = 1 \text{ degree}$$

and

$$k_2 = 1, D_2 = 0 \text{ degree}$$

In the case of the 2-dB error limit, the relative ambiguity would be less than in the case of the 1-dB error limit simply as a result of the large change in the diameter component of the second ambiguity vector. In this example, the number of equivalence classes remained the same, a phenomenon which would only be expected when a small number

of signatures were considered or when the error limits were large relative to the dynamic range of the signature element.

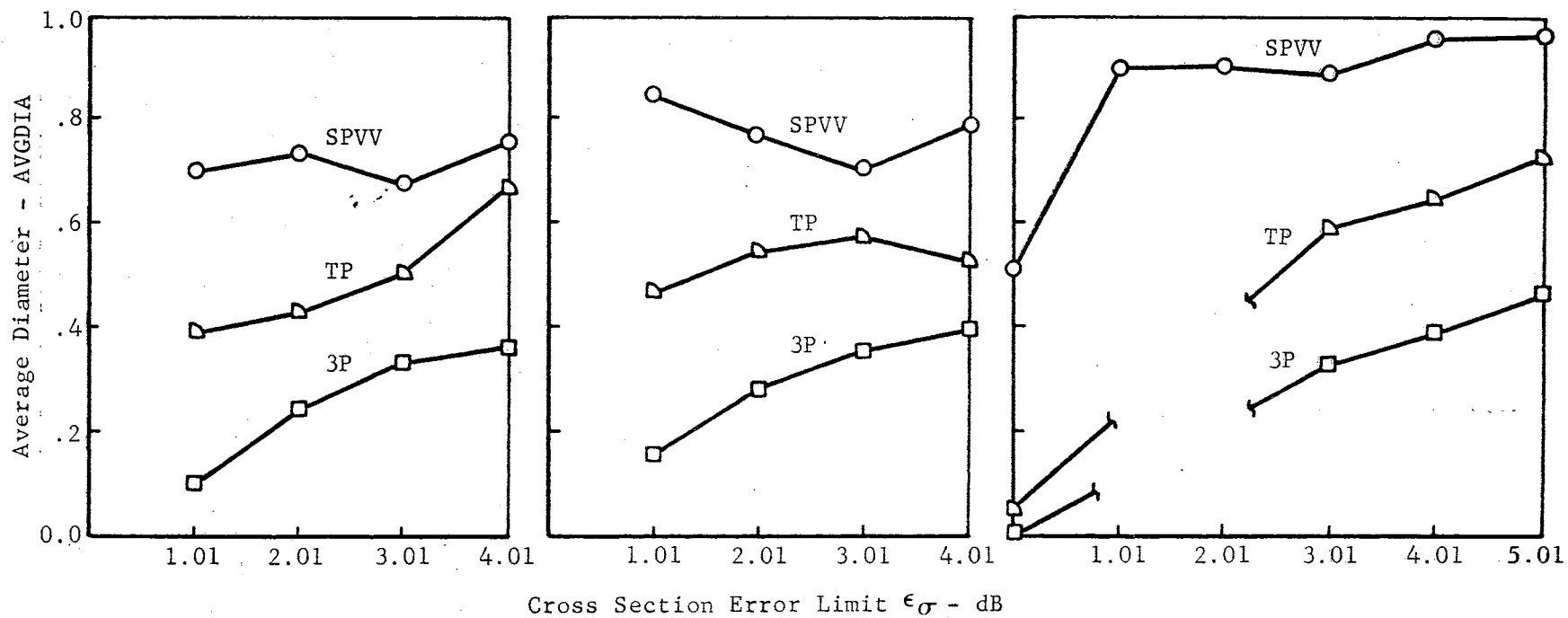
If the signature S_2 had been used as the basis signature for E_1 , an identical value of ambiguity would be obtained by using an error limit of 1 dB. However, the use of an error limit of 2 dB would cause all three signatures to be placed in a single equivalence class whose diameter would be 41.0 degrees. This latter illustration is indicative of the fact that the result obtained in the formulation of an equivalence class is somewhat dependent upon choice of the starting point used in the signature set. In addition, this illustration can be used to demonstrate the large changes in equivalence class diameter that may result from changes in error limits.

In contrast to the above results, it is highly probable that increasing the error limits will produce an increase in the diameter of some equivalence classes since the probability of a signature belonging to any given equivalence class must increase when the error limits are increased. Therefore, in the case of a large number of signatures, it is unlikely that an increase in error limits will cause a significant decrease in the diameter of a large number of equivalence classes. The average diameter of all the equivalence classes may be indicative of how the effects of error limits are propagated through changes in the diameter of equivalence classes. Nevertheless, the characteristics of particular vehicles are reflected in their signature set descriptions, and such reflections may cause unique effects in terms of the formulation of a signature set into equivalence classes. The insignificance of these anomalies in this investigation is demonstrated by the fact that (1) the few times AVGA is observed to decrease when the error

limits are increased, the decrease is small and (2) a general trend has been established on the basis that AVGA usually increases when the error limits are increased, and this trend has been maintained in the case of all vehicles and signature types investigated in this thesis.

The values of the average diameter of Models 1, 2, and 3 are shown in Figure 9 (a, b, and c). Some of the ambiguity data related to Model 3 was computed prior to the inclusion of a procedure for computing the average diameter and is not shown in Figure 9 (c). The Model 2 data shown in Figure 9 (b) indicates a decrease in equivalence class diameter resulted from an increase in ϵ_{σ} (the SPVV signature was being used) from 1 dB to 2 dB. That this decrease in diameter is primarily responsible for the accompanying decrease in AVGA (see Figure 8) can be deduced by examining the output listing of the computer program. Figure 10 contains the output listing for these two problem runs ($\epsilon_{\sigma} = 1$ dB and $\epsilon_{\sigma} = 2$ dB). The number of equivalence classes decreased from 17 to 11. However, equivalence classes 3, 16, and 17 (in the 1-dB case) are evidently identical to equivalence classes 3, 10, and 11 (in the 2-dB case). These three equivalence classes represent the greater fraction of the total number of equivalence classes in the case of the larger error limits; they are therefore given greater weight in the computation of AVGA. These results indicate that the decrease in AVGA is closely related to the decrease in average diameter.

This phenomenon is apparently indicative of an object whose signature elements in general take on the same values (or more explicitly, equivalent values) at many widely spaced points which are separated by a few signatures that are unique in the sense of the peaks and nulls encountered in a cross section pattern. Increasing the error limits



(a) Average Diameter
for Model 1

(b) Average Diameter
for Model 2

(c) Average Diameter
for Model 3

Figure 9. Average Diameter of Equivalence Classes of Complex Models 1, 2, and 3

GENERAL DYNAMICS 7090 PROCEDURE H65
FORT WORTH DIVISION PROBLEM 054846-004

SMUS - STATISTICAL SIGNATURE AMBIGUITY

SIGNATURE TYPE SP

SM TAPE NUMBER 61D01 MODEL NUMBER 2

S/N = 70 DB

SAN = NO AVGN = -77 DBSM

NOISE SUBTRACTION = NO CCNS = NO

ERROR LIMITS ARE

E(1) = 2.010 E(2) = 0. E(3) = 0. E(4) = 0. E(5) = 0.

ACUT1= 183.1 ACUT2= 0. ACUT3= 360.0 ACUT4= 183.2

ISMVAR = 1

C(S 1)= 0.0368	D(S 1)= 0.9689
C(S 2)= 0.0206	D(S 2)= 0.9650
C(S 3)= 0.0009	D(S 3)= 0.0000
C(S 4)= 0.0494	D(S 4)= 0.9994
C(S 5)= 0.1580	D(S 5)= 1.0000
C(S 6)= 0.3294	D(S 6)= 1.0000
C(S 7)= 0.2926	D(S 7)= 1.0000
C(S 8)= 0.0197	D(S 8)= 0.9517
C(S 9)= 0.0835	D(S 9)= 0.7478
C(S 10)= 0.0018	D(S 10)= 0.8556
C(S 11)= 0.0072	D(S 11)= 0.0122

NORMALIZED AMBIGUITY VECTOR

0.8000	0.7983	0.5716	0.8127	0.8175
0.8344	0.8298	0.7969	0.7179	0.7554
0.5716				

AVGA = 0.7551 VARA = 0.0922 1-K/N = 0.9900
AVGSIZ = 0.0909 AVGDIA = 0.7737 DNUMM = 1100.

GENERAL DYNAMICS 7090 PROCEDURE H65
FORT WORTH DIVISION PROBLEM 054846-003

SMUS - STATISTICAL SIGNATURE AMBIGUITY

SIGNATURE TYPE SP

SM TAPE NUMBER 61D01 MODEL NUMBER 2

S/N = 70 DB

SAN = NO AVGN = -77 DBSM

NOISE SUBTRACTION = NO CCNS = NO

ERROR LIMITS ARE

E(1) = 1.010 E(2) = 0. E(3) = 0. E(4) = 0. E(5) = 0.

ACUT1= 183.1 ACUT2= 0. ACUT3= 360.0 ACUT4= 183.2

ISMVAR = 1

C(S 1)= 0.0233	D(S 1)= 0.9417
C(S 2)= 0.0108	D(S 2)= 0.9594
C(S 3)= 0.0009	D(S 3)= 0.0000
C(S 4)= 0.0395	D(S 4)= 0.9994
C(S 5)= 0.0709	D(S 5)= 1.0000
C(S 6)= 0.1059	D(S 6)= 0.9983
C(S 7)= 0.1526	D(S 7)= 1.0000
C(S 8)= 0.1957	D(S 8)= 1.0000
C(S 9)= 0.1831	D(S 9)= 1.0000
C(S 10)= 0.0790	D(S 10)= 0.9994
C(S 11)= 0.0260	D(S 11)= 0.9967
C(S 12)= 0.0054	D(S 12)= 0.9650
C(S 13)= 0.0072	D(S 13)= 0.9278
C(S 14)= 0.0359	D(S 14)= 0.9617
C(S 15)= 0.0548	D(S 15)= 0.7411
C(S 16)= 0.0018	D(S 16)= 0.8556
C(S 17)= 0.0072	D(S 17)= 0.0122

NORMALIZED AMBIGUITY VECTOR

0.7857	0.7937	0.5684	0.8103	0.8112
0.8118	0.8150	0.8181	0.8171	0.8113
0.8090	0.7959	0.7811	0.7949	0.7122
0.7531	0.5685			

AVGA = 0.7681 VARA = 0.0774 1-K/N = 0.9845
AVGSIZ = 0.0588 AVGDIA = 0.8446 DNUMM = 1100.

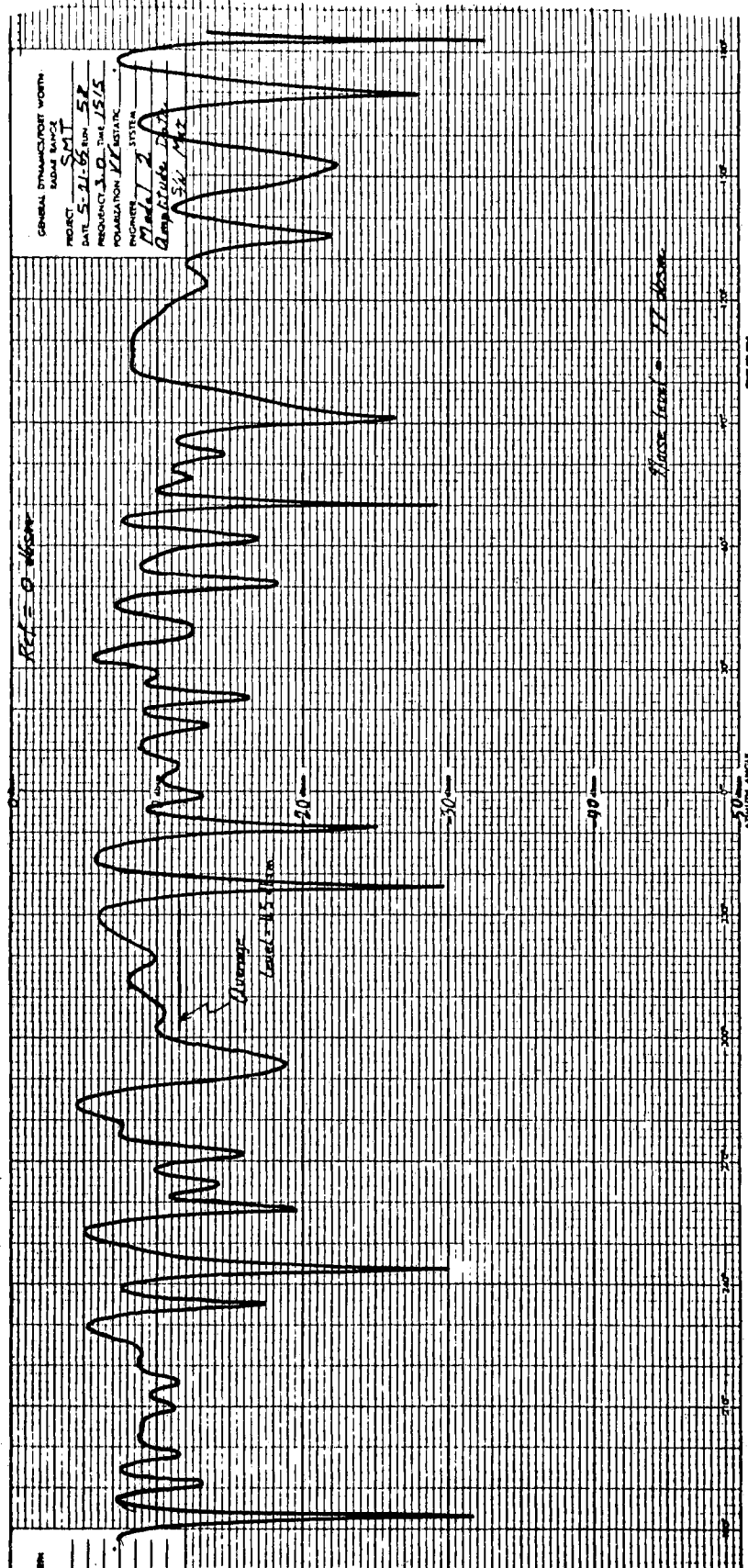
Figure 10. STAP Output Listing Obtained for Model 2

could then have a considerable effect on the formulation of an equivalence class of these signatures.

Model 2 cross section data related to the transmit vertical-receive vertical, SPVV signature fits this signature model very well, as indicated in the cross section pattern shown in Figure 11. For any signature whose cross section falls between -5.0 dBsm and -20.0 dBsm, there exists at least one other signature which is widely separated in aspect. On the contrary, the peak at 283.5 degrees and the null at 183.5 degrees are unique and their equivalence class formulations may not change as a result of a change in error limits. This fact can be demonstrated in the case of an increase in ϵ_{σ} from 1 to 2 dB.

The output listings shown in Figure 10 are typical samples of the output of the ambiguity computer program. The data used as problem input are identified in the heading. Output data consists of (1) the normalized size and diameter of each individual equivalence class given as $C(S_i)$ and $D(S_i)$, respectively, for $i = 1, K$ and (2) the magnitude of the ambiguity vector associated with each equivalence class. Also listed are the values of $1 - K/N$, the normalized number of equivalence classes; AVGA, the expected value of the magnitude; AVGSIZ, the average equivalence class size; AVGDIA, the average equivalence class diameter; and DNUMM = N, the number of signatures in the signature set.

The most important result of the ambiguity study is the fact that low values of average ambiguity were obtained for each of the three vehicles when the scattering matrix was utilized. This result indicates that the use of the scattering matrix signature for representing vehicles of quite different physical configurations results in

Figure 11. Model 2 Cross Section σ_{VV}

considerably less ambiguity than use of other signatures derived from the scattering matrix. Of course, these signatures were obtained while a fairly high signal-to-noise ratio was being maintained, and it is obvious that use of a very low signal-to-noise ratio will cause an increase in ambiguity, at least in terms of the cross section elements of the signature. At very low signal-to-noise ratios, the distribution of the noise cross section and phase will dominate the resulting ambiguity. For example, the measured variation of phase which is obtained from a spherical target whose cross section is less than the average noise level may be quite large if the variance of the noise phase is large. The occurrence of this condition would result in a value of ambiguity less than unity (unity is the value of ambiguity expected from the measurement of a perfect sphere by use of a perfect measurement system).

3.4.2 Ambiguity of Generic Vehicles. Figures 12 through 14 contain the results of computing the average ambiguity of a set of vehicles which are bodies of revolution. These vehicles include cones, cylinders, frustrums, and composite vehicles formed from these generic shapes. The interest in such vehicles results from the fact that many space and ballistic objects are constructed by using similar generic shapes. The vehicle designer may also be interested in synthesizing signature sets of complex vehicles composed of such shapes as paraboloids of revolution, ogives, etc., by using more easily machined shapes, such as cones, cylinders, and hemispheres. Appendix C contains a photograph of various generic shapes used in this research.

Figure 12 contains values of AVGA computed for four generic vehicles on the basis of their SPVV and TP signature sets. These four

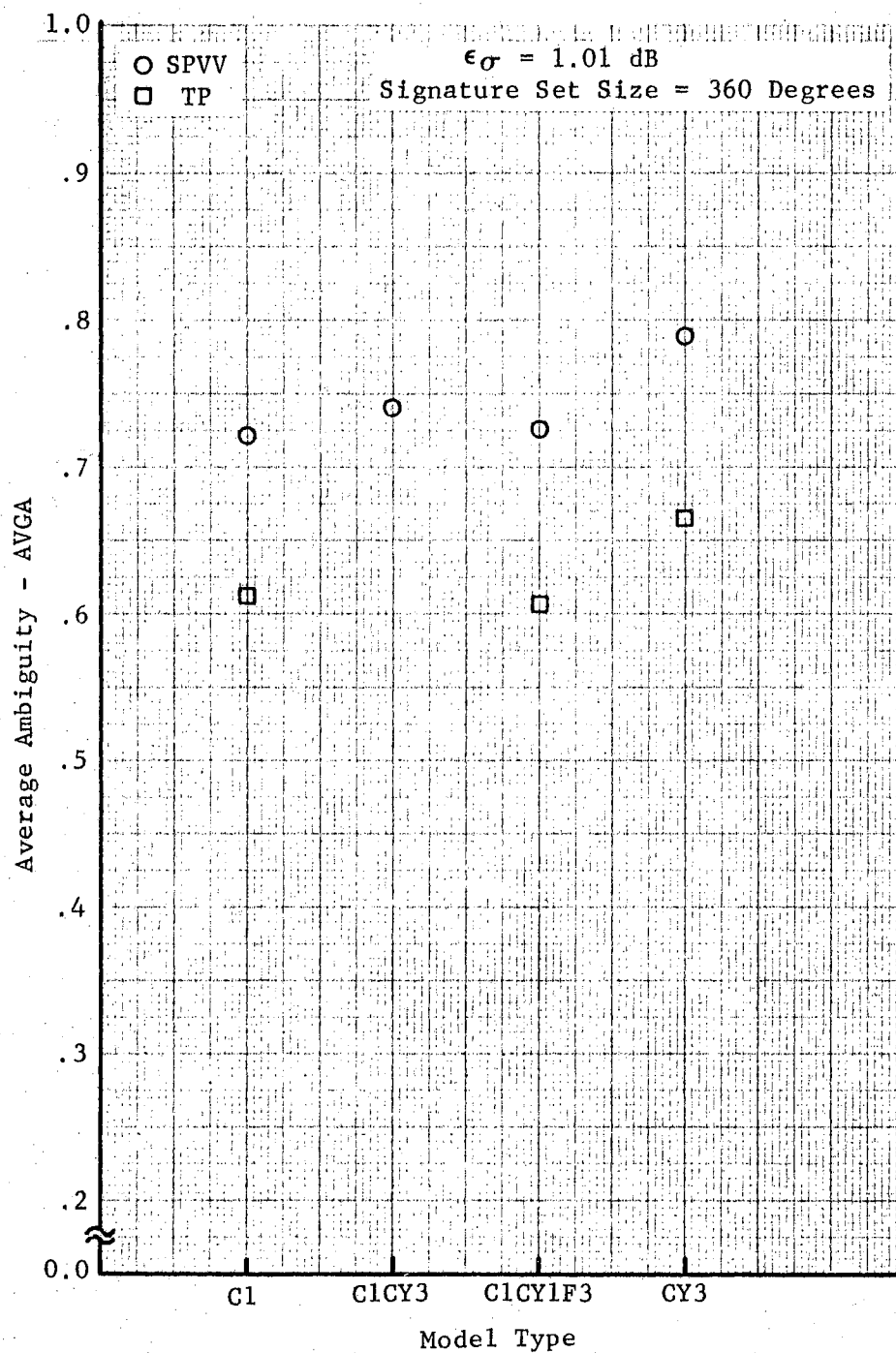


Figure 12. Ambiguity of Generic Vehicles, $\epsilon_{\sigma} = 1$ dB

vehicles are Cone C1, Cylinder CY3, Cone-Cylinder ClCY3, and Cone-Cylinder-Frustrum ClCY3F3. The error limits on cross section were 1 dB in each case, and the signature sets consisted of every other signature obtained during a 360-degree rotation of the target vehicle. An examination of these data indicates that (1) in general the TP signature type provides an approximately 15 percent less ambiguous representation of each of the four vehicles than the SPVV signature and (2) the cylinder representation is noticeably more ambiguous than that of the other three models.

The first of the above mentioned observations agrees with the results obtained by using the complex vehicles with regard to the relative ambiguity of the SPVV and TP signatures. The second observation provides an indication of the increase in ambiguity obtained as a result of the greater symmetry of the cylinder. Ideally, a 360-degree rotation of a cylinder would result in a signature set consisting of four identical 90-degree intervals. The other three vehicles exhibit only rotational symmetry; consequently, their 360-degree signature sets would ideally consist of only two identical 180-degree intervals. An examination of the cross section and phase patterns of these four vehicles confirms these observations. Data presented in Figure 14 provides additional information regarding the effects of body symmetry on ambiguity.

Figure 13 contains computed ambiguity data on a selected set of rotationally symmetric vehicles represented by SPVV, TP, SPP and TPP signatures. The error limits used in the equivalence class formulation were 3 dB on cross section and 20 degrees on phase. In contrast to the data shown in Figure 12, the signature sets of these vehicles were

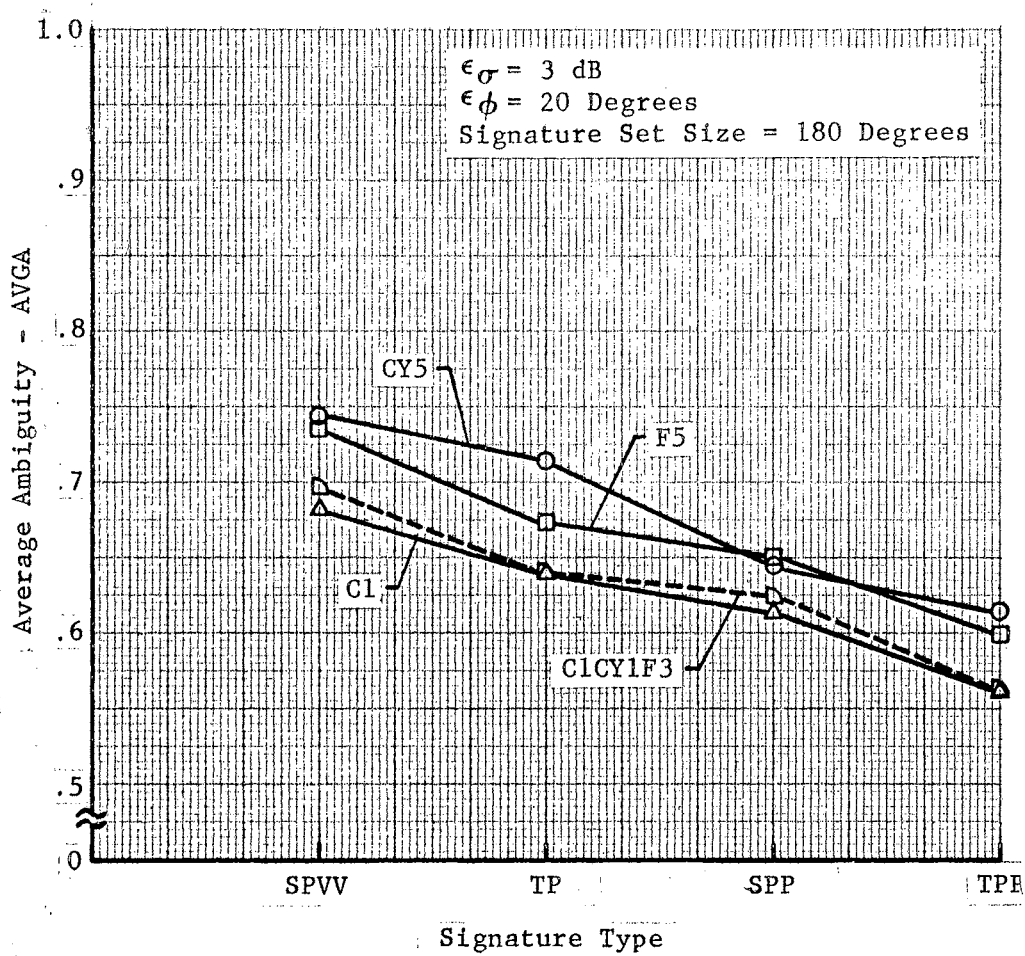


Figure 13. Ambiguity of Generic Vehicles, $\epsilon_{\sigma} = 3 \text{ dB}$

formed by using every signature over a 180-degree interval from 180 degrees to 0 degree (0 degree represents the end-on aspect, i.e., the tip of the cones and the small end of the frustrum). Thus, except in the case of the cylinder, these signature sets contain sets of signatures which are unique in the sense that they are produced from unique scattering surfaces. The additional symmetry property of the cylinder results in some redundancy in its signature sets; however, the resulting ambiguity of the cylinder was only slightly greater than that of the other vehicles.

The data in Figure 13 clearly show the decrease in AVGA which results as the dimension of the radar signature is increased. Nevertheless, the difference in AVGA between the SPVV and the SM (TPP in this case) signatures representations is significantly less than that obtained when complex models 1, 2, and 3 were used. The following paragraphs contain a discussion of the role of signature dimension in relation to this difference.

In the case of SPVV, TP, and SPP signatures, the dimension of the signatures remains the same for both complex and generic vehicles. Consequently, any differences between the symmetrical and assymetrical cases must be a result of the way in which body symmetry affects the formation of equivalence classes although the use of the absolute value of differential phase also contributes a slight increase in ambiguity.

The data contained in Figure 14 is useful for investigating the effects of body symmetry on ambiguity. It is observed that the SPVV signature of both of these rotationally symmetric objects is more ambiguous in the case of using a 360-degree signature set than that of

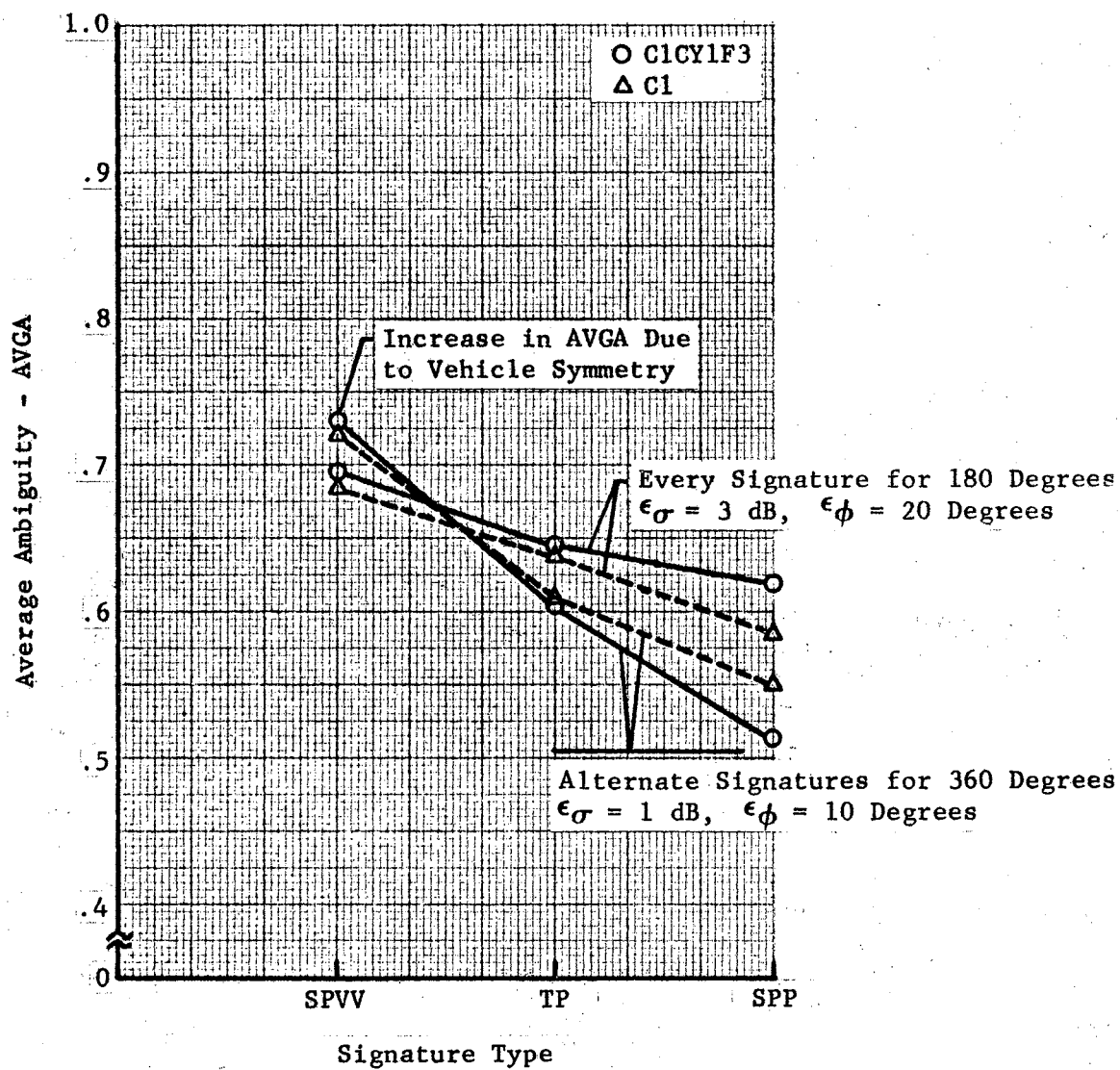


Figure 14. Effects of Signature Set Size on Ambiguity

using a 180-degree signature set in which the error limits are increased. The effects of the error limits tends to offset the effect of symmetry as the signature dimension is increased via use of the TP and SPP signatures.

Figure 15 contains plots of the differential phase signatures of Models CY5, C1, and F5. These plots demonstrate that differential phase signatures of generic shapes are fairly constant over a large set of aspect angles; in other words, the data show that (TV, RV) and (TH, RH) phase centers appear to track each other. However, fairly large changes in \emptyset are to be observed near the end-on regions of vehicles which contain discontinuities as a result of the different location of the polarization phase centers.

3.5 Conclusions. The discussion presented in this chapter has been oriented to fulfilling two primary objectives. First, the definition of a measure of ambiguity in terms of an equivalence class formulation has provided (1) a direct application of the general ECT to a problem of interest and (2) an example of a complete mapping from a signature space to a decision space. Second, the results of the ambiguity investigation stand alone as a contribution to the state-of-the-art of radar signature analysis.

The fact that a degree of dependence exists between the various elements of the scattering matrix as a function of vehicle complexity is evident from the results of this research. In fact, a measure of this dependence (for example, a comparison of the values of AVGA computed for the SP and TP signatures) appears to provide a considerable amount of information on vehicle complexity. The data in Figure 16 portrays the relationship between the ambiguity measure and the physical

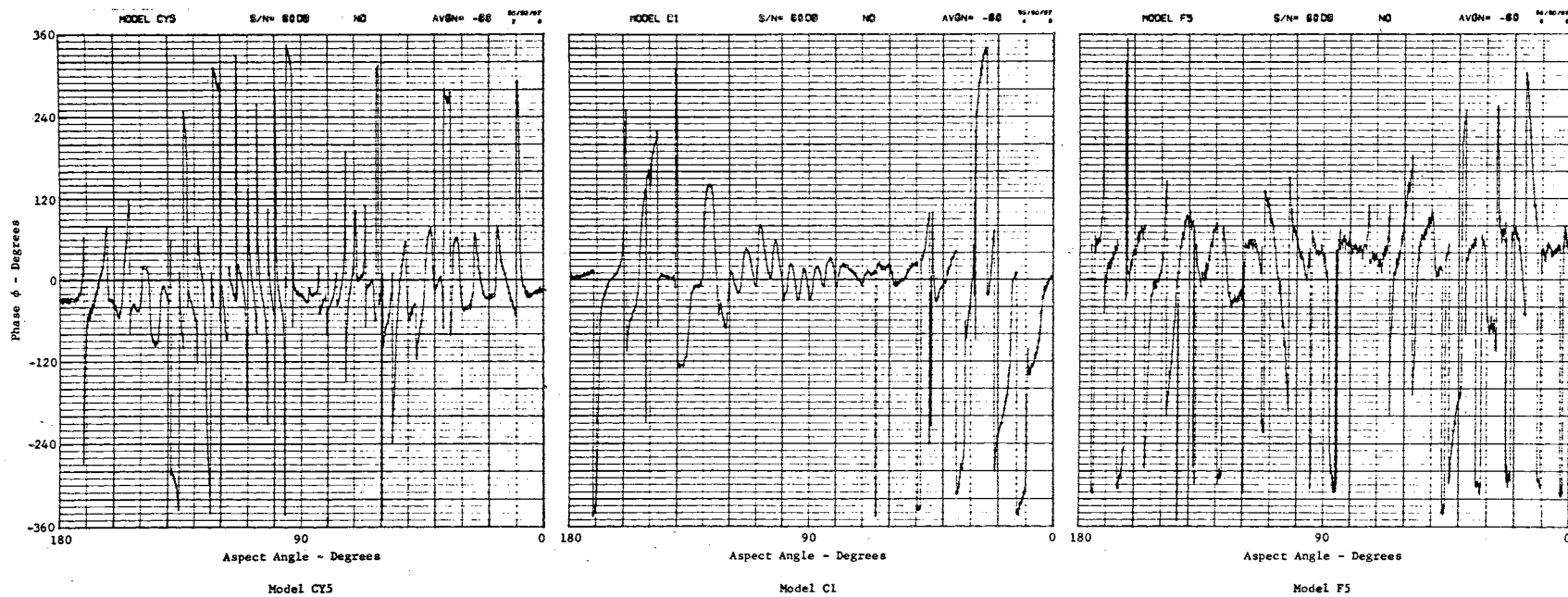


Figure 15. Differential Phase Exhibited by Models CY5, C1, and F5

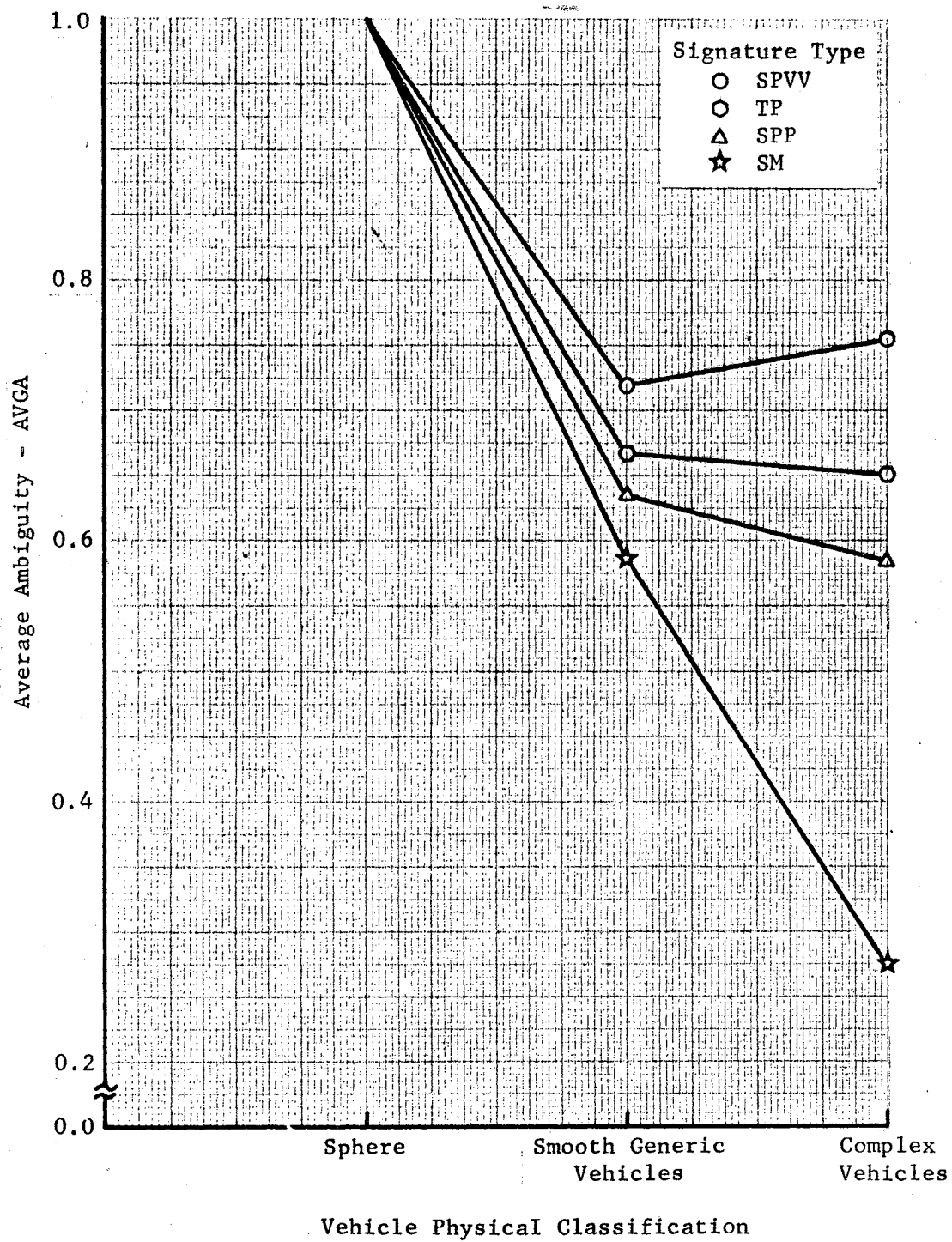


Figure 16. Ambiguity Versus Vehicle Physical Classification

complexity of the vehicle. This data was obtained from the data on the complex and generic vehicles presented in this chapter.

The large spread in the values of AVGA of the complex vehicles reveals the fact that the signature elements of the SM are not highly correlated in the case of these vehicles. The compacting of the values of AVGA of the generic vehicles places emphasis on the correlation which exists between the elements of the SM of symmetrical targets that are basically constructed of smooth optical surfaces. The values of ambiguity in Figure 16 are referred to that of a sphere in order to emphasize the influence of vehicle physical characteristics on ambiguity. The desirability of utilizing the SM to represent complex vehicles is evident from these data. On the other hand, the signature type is of less concern when very simple shapes are considered since the variation in AVGA is small for different signature representations.

CHAPTER IV

THE EQUIVALENCE CLASS TECHNIQUE AND VEHICLE SIMILITUDE

4.1 General. In the preceding chapter, the ECT was utilized to provide a contraction mapping of a multi-dimensional signature space into a one-dimensional decision space. The decision of interest in that particular investigation was primarily directed toward the signature space rather than the source space. Different sources (vehicles) of radar signatures were considered solely in an effort to broaden the spectrum of application of the basic ambiguity study. That investigation also provided basic information on the utility of the general ECT in terms of (1) the degree of data contraction achievable commensurate with meaningful measurement resolution parameters, types of radar signatures, and classes of vehicle complexity and (2) the extraction of physically meaningful features directly from the equivalence class formulation.

This chapter contains a description of an application of an ECT which forms a measure of the physical similitude between two vehicles on the basis of their signature similarities. The principal objectives set for this investigation are (1) to present and evaluate a measure of vehicle similitude on the basis of an ECT mapping and (2) to provide additional information on signature-type ambiguity to complement the analysis presented in Chapter III.

4.2 The Dissimilar Ratio. The measure of vehicle similitude being investigated in this chapter is called the "dissimilar" ratio and is based on the formation of an equivalence class between two signature sets which represent a pair of vehicles. The dissimilar ratio is defined as the normalized number of signatures belonging to signature set S^A which are not equivalent to any signatures belonging to signature set S^B . This measure is intuitively meaningful in the sense that it is reasonable to assume that physically similar vehicles would exhibit a large number of "equivalent" signatures. This hypothesis is predicated on the fact that the signature representation of the vehicles have physical meaning. Conversely, for example, a highly ambiguous signature representation would cause vehicles which exhibit quite dissimilar physical properties to produce a large number of equivalent signatures.

In the equivalence class sense, the dissimilar ratio is simply the number of equivalence classes, D , which contain a single signature (the basis signature) from signature set S^A and no signatures from signature set S^B . Thus, D represents the number of empty (except for a basis signature) equivalence classes, and the dissimilar ratio is the ratio, D/N , where N is the number of signatures in S^A .

In accordance with the general definition of an ECT, two signatures are called equivalent if and only if they satisfy a common set of properties. The properties which must be satisfied in this case are similar to those used to establish equivalence classes in the investigation of ambiguity. However, in order to incorporate additional physical significance in the measure, an "order" property has been included for optional use.

The denumeration of dissimilar signatures is initiated by selecting

a basis signature, A_i , from S^A and then interrogating S^B to determine if there exists at least one signature, B_k , belonging to S^B which is equivalent to A_i . If there is no such B_k belonging to S^B , the dissimilar number, D , is indexed by one and another basis signature A_{i+1} is selected. If signature B_k is equivalent to A_i , B_k is destroyed, and the next basis signature is selected. This process is continued until all N_A signatures belonging to S^A have been utilized as basis signatures.

In this particular application, the signature representations are as follows:

$$A_i = (a_{i1}, a_{i2}, \dots, a_{ij}, \dots, a_{i6}) \text{ for } i = 1, 2, \dots, N_A$$

and

$$B_i = (b_{i1}, b_{i2}, \dots, b_{ij}, \dots, b_{i6}) \text{ for } i = 1, 2, \dots, N_B$$

where the signature elements are indexed on j .

Table VI contains a list of the signature elements used in this analysis and their respective indices.

TABLE VI
SIGNATURE ELEMENTS USED FOR
COMPUTATION OF D/N

Signature Element Index	Signature Element
1	θ
2	σ_{VV}
3	σ_{VH}
4	σ_{HH}
5	ϕ_{VH}
6	ϕ_{HH}

Definition D4-1 denotes the relationship which must be satisfied in order for a signature dissimilarity to exist.

D4-1: Let I_j be the signature element index set defining a signature type; then signatures A_i and B_k are similar if and only if

$$a_{ij} - \epsilon_j \leq b_{kj} \leq a_{ij} + \epsilon_j \quad \text{for every } j \in I_j$$

otherwise, signatures A_i and B_k are dissimilar.

In this context, ϵ_1 represents a tolerance on aspect angle and is representative of the degree of aspect angle correlation between the two vehicles. Thus, $\epsilon_1 = 180$ degrees represents the case in which the relative orientations of the two vehicles are completely unknown. A value of $\epsilon_1 = 0$ degree represents the case of perfect correlation. Similarly, ϵ_2 represents an error limit on σ_{VV} , ϵ_3 represents an error limit on σ_{VH} , etc.

It should be noted that other multidimensional signature types could be represented by the signature type index set. The analysis of the dissimilar ratio can be directly extended to other signature types simply by redefining the elements of A_i and B_k .

A value of $D/N = 1.0$ would be obtained if, for every signature in S^A , there exists at least one equivalent signature in S^B . A value of $D/N = 0.0$ would be obtained if there were no signatures in S^B which were equivalent to any signatures in S^A .

The definition of signature similarity presented in D4-1 was intentionally formulated in order to bias the dissimilar ratio towards dissimilarity. This bias results from the stipulation that all corresponding signature elements must be equivalent for two signatures

to be called similar. Other measures could be formulated on the basis of the degree of dissimilarity between signatures. For example, the degree of dissimilarity between two signatures could be defined in terms of the fraction of the signature elements which are not equivalent. This technique would produce a weighted dissimilar ratio in the sense that the number of n-dimensional signatures having k dissimilar signature elements would be weighted by the fraction k/n . A weighted measure of dissimilarity is briefly discussed and compared with the unweighted measure in the investigation presented in this chapter.

A digital computer program was written and utilized to compute the dissimilar ratio of selected pairs of vehicles on the basis of their measured radar signatures. This computer program will be referred to as SSDP, i.e., Statistical Signature Dissimilarity Program. Figure 17 contains a logic diagram of the SSDP showing the general implementation of the program and the various options which may be used to provide additional flexibility in the analysis. The SSDP includes all of those options listed in Section 3.3 with regard to STAP; it also contains the following capabilities:

1. Aspect Angle Correlation - This option can be used for incorporating any degree of correlation between the aspect angles of a pair of vehicles.
2. Adjustment of Mean Values - This subroutine can be used for computing the mean values of each signature element of a signature set and adjusting the element values of the signature sets S^A and S^B so that their mean values are equal.

A complete documentation of the SSDP is contained in Appendix D,

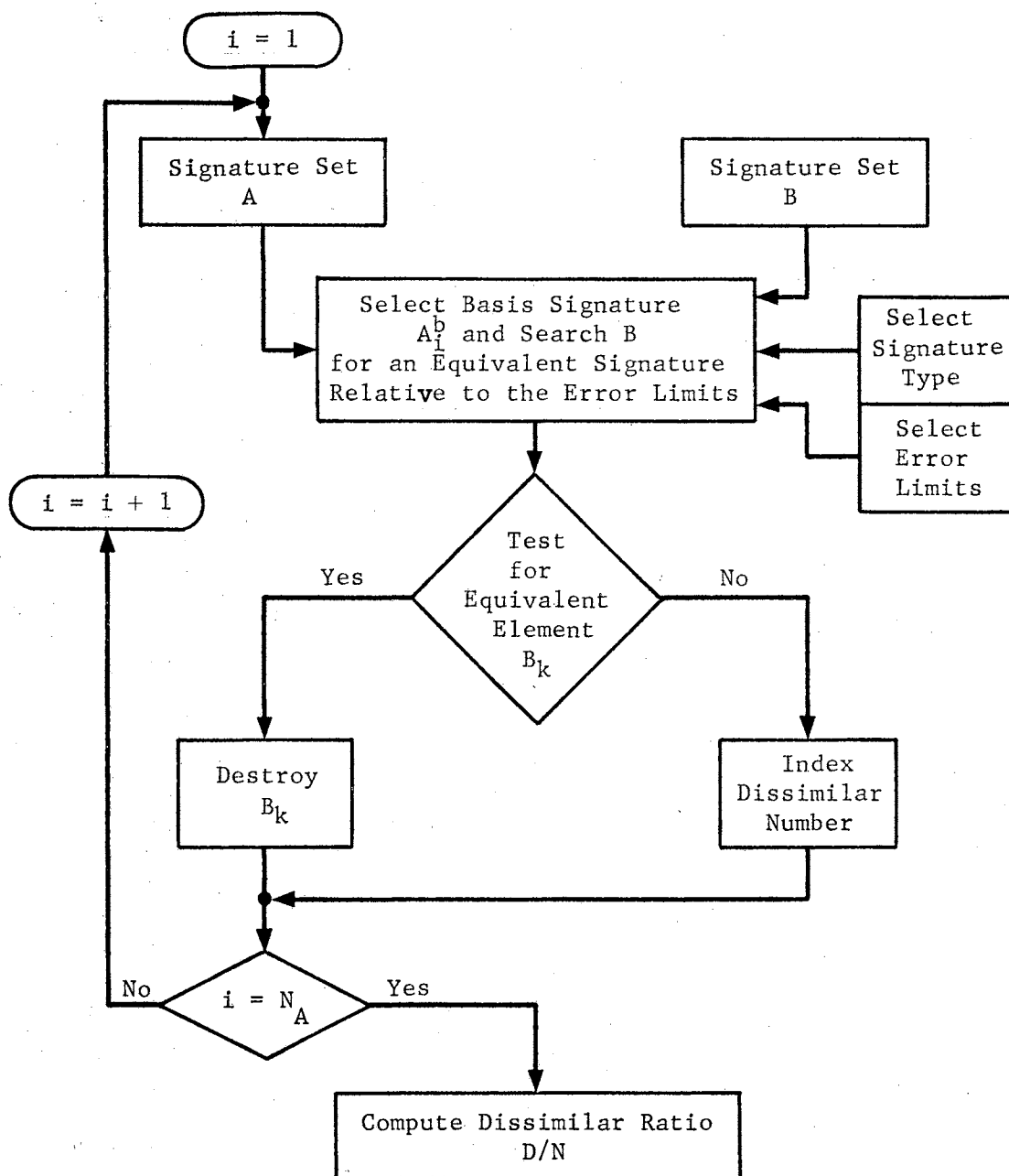


Figure 17. SSDP Computer Program Logic Diagram

including a flow chart, a Fortran IV listing, and a sample problem.

Two types of information can be obtained from the dissimilar ratio: (1) a measure of the physical similitude of vehicles based on a statistical analysis of the signature sets of the vehicle and (2) a second measure of the relative amount of information contained in various subsets of the SM signature. In addition, an analysis of the sets of dissimilar signatures obtained as a function of signature type is seen to provide information on the structural differences between two vehicles. An analysis of the relationship between sets of signature and some particular structural differences between Models 1 and 2 is presented in the next section.

4.3 Analysis. The results obtained by using the dissimilar ratio as a measure of vehicle similitude are presented in the following three subsections which are distinguished on the basis of the general physical classification of the vehicles which are being compared. These classifications are (1) complex vehicles, (2) generic vehicles and (3) composite generic vehicles.

4.3.1 Complex Vehicles. Two vehicles in this category were compared, Models 1 and 2. The S-band SM signature sets of these two vehicles obtained over 360 degrees of vehicle rotation were utilized as a basis for the analysis. It will be recalled that these two vehicles represent highly resonant scattering bodies as a result of their wire mesh construction. In addition, the dipole structure of Model 2 was designed to exhibit approximately the same level of cross section as the toroid so that the variation of the phase center of Model 2 would be considerably greater than that observed for Model 1, (at least in the case of a linear radar polarization which is parallel to the dipole

axis). These two vehicles thus constitute an ideal pair of physical structures for comparison.

Presented in Figure 18 are the computed values of D/N obtained by using signature sets composed of signatures separated by approximately 0.3 degree in azimuth. A number of signature types were utilized, all being subsets of the SM. The values of ϵ_θ , ϵ_σ , and ϵ_ϕ were 180 degrees, 2 dB, and 20 degrees, respectively; the value of ϵ_θ indicated that the two signature sets were completely uncorrelated.¹

Three fairly distinct regions of the D/N space are represented in Figure 18 by the signature types used. Both the SPVH and SPHH signature representations resulted in a fairly low value of the dissimilar ratio. On the other hand, the SPVV representation resulted in approximately twice the number of signature dissimilarities (the normalizing constant N was the same in each case). The data obtained by using PHA(HH) and TP(VV,HH) signatures also fall in the same region as the SPVV data. Use of 3P and SPP(VV,HH) signatures resulted in values of D/N near 0.5, a result which indicates that about half of the 3P and SPP signatures contain at least one dissimilar element. Finally, the SM signature indicates that the two vehicles are quite dissimilar on the basis of this measure. The latter results are to be expected since it has been demonstrated that the SM provides a very unique representation of these two vehicles, and the biased nature of the unweighted dissimilar ratio adds emphasis to this uniqueness (refer to subsection 3.4.1). It is rather interesting to note that even 5 percent

¹No effort was made to align Models 1 and 2 when the measurements in Reference 22 were performed, and a 60-degree shift in their aspects resulted.

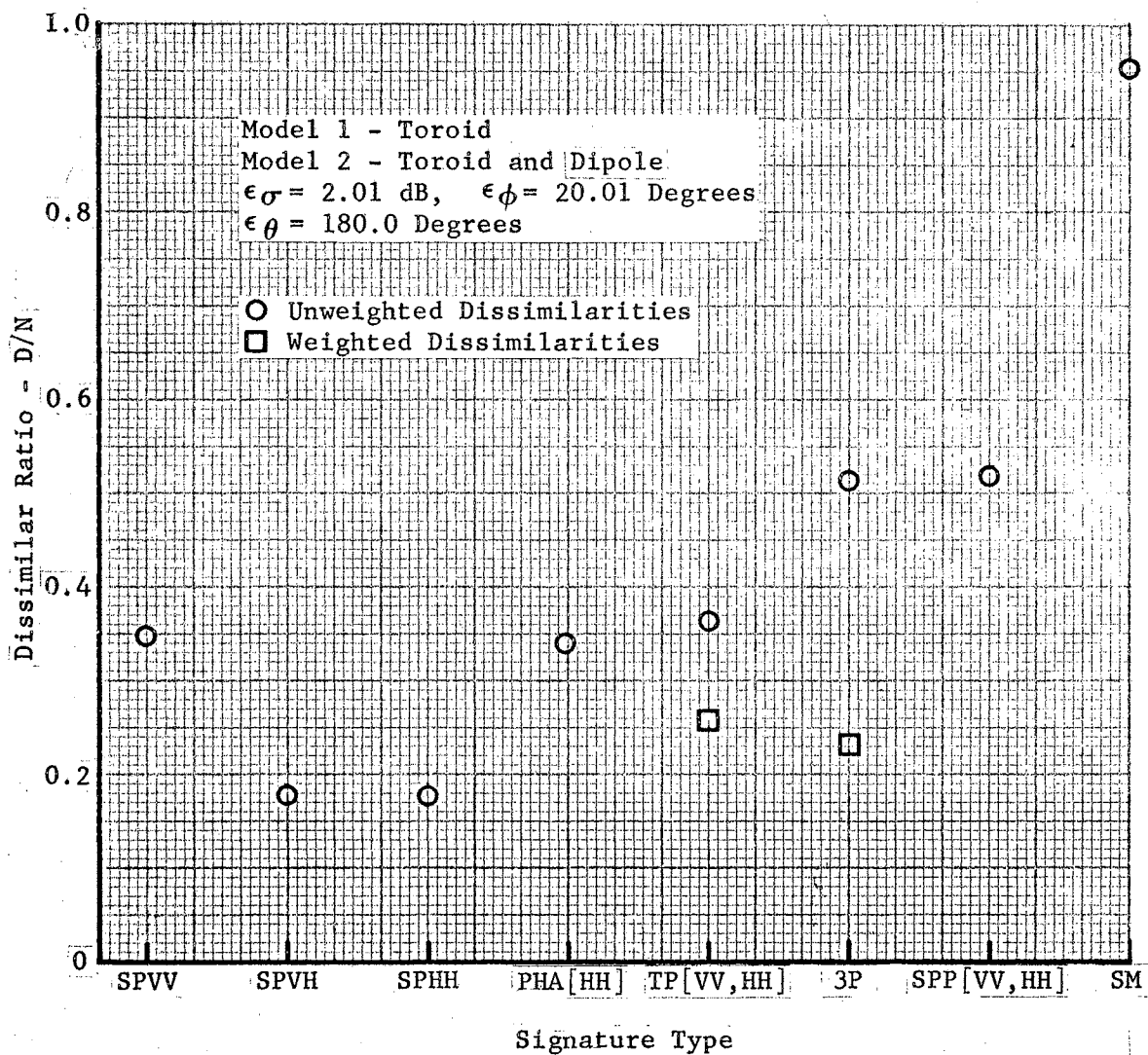


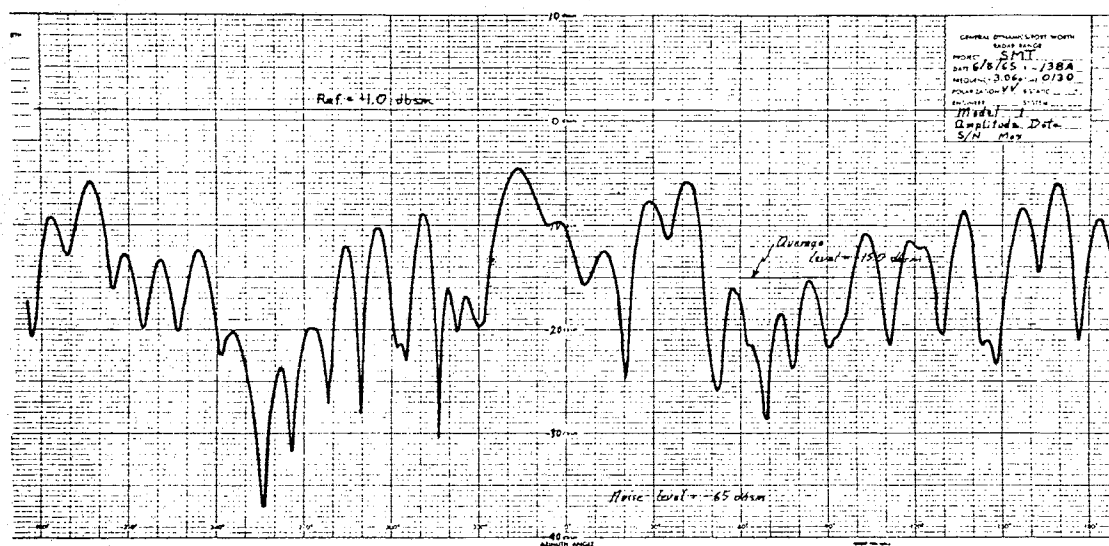
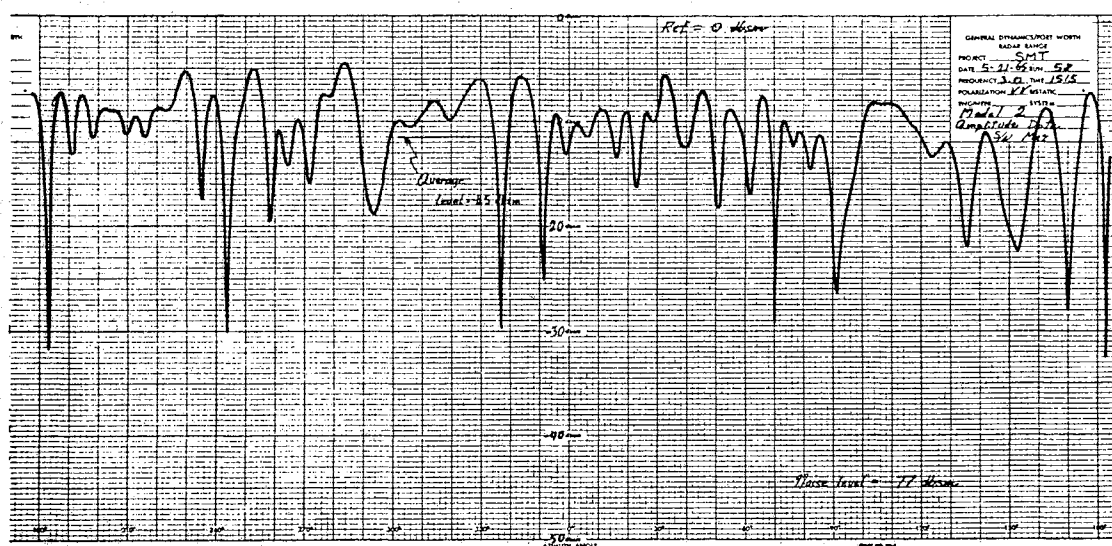
Figure 18. Dissimilar Ratio Comparison
 of Models 1 and 2

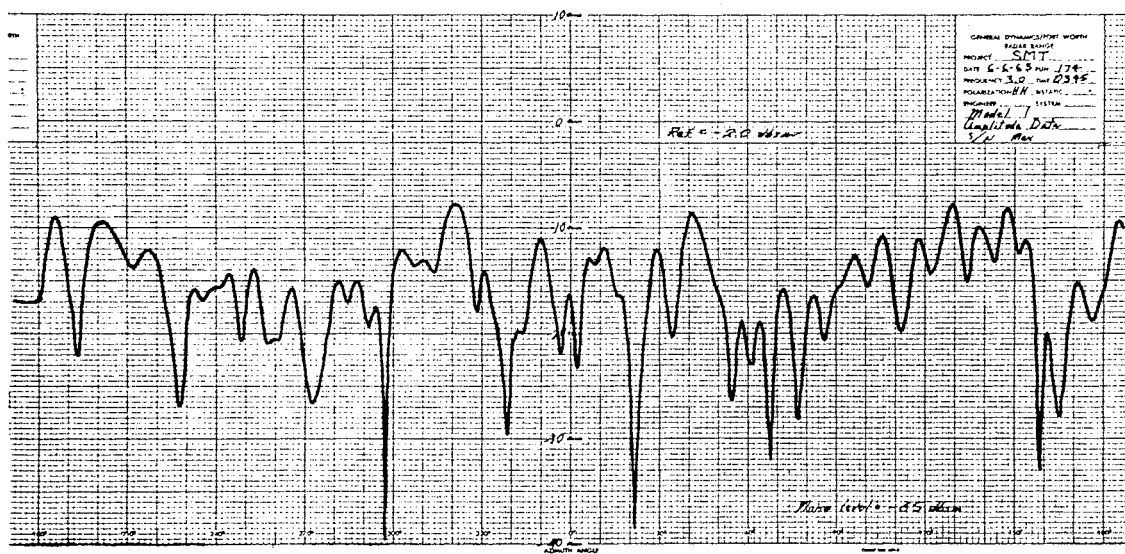
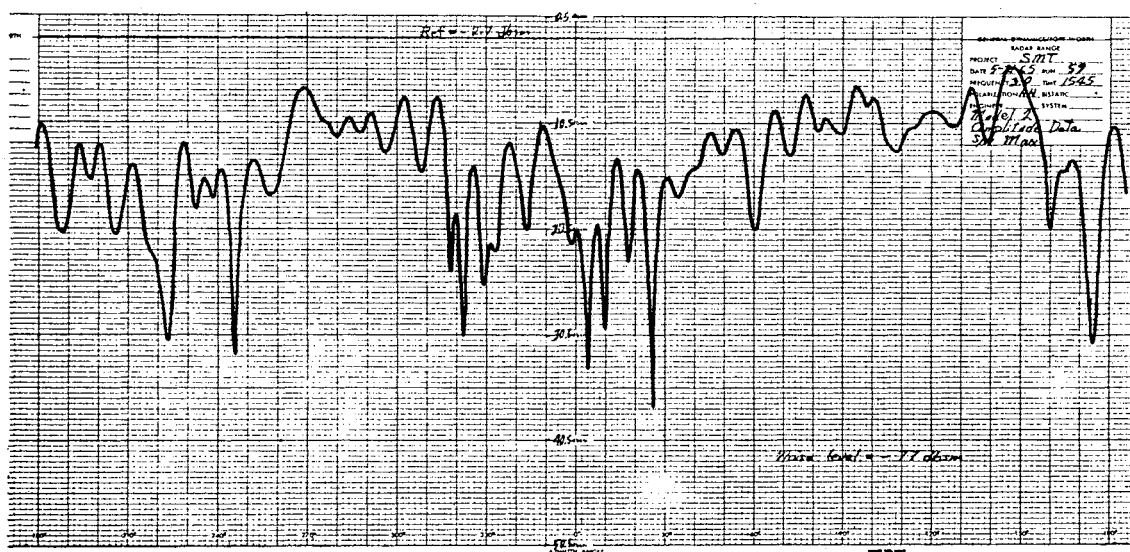
of the SM signatures are equivalent. This equivalence indicates that, at least at some aspects (possibly when the dipole is in the shadow region of the toroid), the two vehicles present similar signatures.

Figures 19 (a and b) and 20 (a and b) contain the measured cross section patterns of Models 1 and 2 obtained by use of the SPVV and SPHH signatures. The SPHH patterns are very similar (note the 60-degree aspect shift between these two patterns) while the SPVV patterns are quite different. One should also note that the dynamic range of the Model 1 SPVV data is considerably greater than that of the SPVV data related to Model 2.

The high value of D/N obtained by using the SM signature also reveals the unique nature of the SM. In fact, this result is particularly indicative of the unambiguous manner in which these two vehicles can be represented by the SM. However, it should be noted that this last statement can only be made with the a priori knowledge that the signature elements of Models 1 and 2 encompass the same basic dynamic ranges, a fact that is evident from the results obtained by using the lower dimensional subsets. It would be possible to obtain a value of D/N equal to unity if, for example, the dynamic ranges of two signature elements did not overlap. A technique for investigating this phenomenon was provided by incorporating the "Adjust Mean Value" option; however, the option was not used in this research as a result of the similarities in the values of k_a of the targets considered.

An interesting relationship (one which would be extremely difficult to analyze on a quantitative basis from observation of the pertinent cross section patterns) is quite easily detected from an examination of the data shown in Figure 18. This relationship indicates

Figure 19a. Model 1 Cross Section σ_{VV} Figure 19b. Model 2 Cross Section σ_{VV}

Figure 20a. Model 1 Cross Section σ_{HH} Figure 20b. Model 2 Cross Section σ_{HH}

that useful information may be contained in the sets of dissimilarities between the two vehicles in terms of different signature-types.

D4-2: $S_D(\text{Type})$ is defined as the set of dissimilar signatures obtained by using a particular signature type, pair of vehicles and set of error limits. Thus,

$$S_D(\text{Type}) = \left\{ A_i \mid \nexists B_k \ni B_k \approx A_i \right\}$$

where $A_i \in S^A$, $B_k \in S^B$ and $B_k \approx A_i$

$\Rightarrow a_{ij} - \epsilon_j \leq b_{kj} \leq a_{ij} + \epsilon_j \quad \forall j \in I_j$ and a given set of ϵ_j ; $j \in I_j$.

The set definition of dissimilarity (D4-1) and the subset definition (D4-3) may be used to establish the fact that, if a signature type X is a subset of signature type Y, then

$$S_D(Y) \supset S_D(X)$$

that is, all dissimilarities observed when X is used will also be observed when Y is used.

D4-3: Signature type X is a subset of signature type Y, denoted by $Y \supset X$, if every element of signature type X is also an element of signature type Y.

Theorem T4-1 provides proof of the fact that the relation

$$Y \supset X$$

implies that

$$S_D(Y) \supset S_D(X).$$

T4-1: Given: 1. Signature sets S^A and S^B and the set of dissimilarities $S_D(Y)$ and $S_D(X)$ for signature types

Y and X.

2. Assume $Y \supset X$

Then $S_D(Y) \supset S_D(X)$

Proof: 1. The bases signatures for S^A are identically the signature set

$$\{S_i \mid i = 1, 2, \dots, N_A\}$$

2. Let $A_m \in S_D(X)$ then

$$\forall B_k \in S^B \exists b_{kj_0} \rightarrow$$

$$b_{kj_0} \notin [a_{mj_0} - \epsilon_{j_0}, a_{mj_0} + \epsilon_{j_0}]$$

$$\forall k = 1, 2, \dots, N_B$$

where $j_0 \in I_{j_X}$

3. Assume $A_m \notin S_D(Y)$

Thus $\exists B_k \in S^B \rightarrow$

$$B_k \approx A_m$$

which contradicts (2) since $j_0 \in I_{j_Y}$

by definition.

$$\Rightarrow A_m \in S_D(Y)$$

4. Since this is true for every m,

$$S_D(Y) \supset S_D(X)$$

It is also necessary to define the difference between signature types (D4-4) in order to follow the ensuing argument.

D4-4: If $Y \supset X$, the signature type Y-X is defined as the signature

composed of elements which belong to Y but do not belong to X. Hence if $R = Y - X$, then

$$R_i = \left\{ r_{ij} \mid j \in I_{jy}, j \notin I_{jx} \right\}$$

If $Y \not\supset X$, $Y - X$ is undefined.

The set relationship established in T4-1 can be formulated into an equation for relating the sets of dissimilarities obtained by use of two signature types, one being a subset of the other. If $Y \supset X$, the difference between $S_D(Y)$ and $S_D(X)$ is given by

$$S_D(Y) - S_D(X) = S_D(Y-X) - S_D(X, Y-X) \quad (4-1)$$

This difference may be clarified by letting $Y = TP(VV, HH)$ and $X = SPVV$ so that $Y-X = TP-SPVV = SPHH$ and by obtaining

$$S_D(TP) - S_D(SPVV) = S_D(SPHH) - S_D(SPVV, SPHH) \quad (4-2)$$

where $S_D(SPVV, SPHH)$ is the set of signatures which are dissimilar in all elements of both signature types SPVV and SPHH. It should be noted that $S_D(TP)$, as used here, represents the set of signatures which have at least one dissimilar element in the TP signature.

Equation 4-2 is illustrated graphically in Figure 21. The sets of dissimilarities are shown as simply connected sets for illustration purposes; however, there is no such restriction in true signature space. All TP, SPVV, and SPHH signatures of a particular vehicle would belong to the signature space depicted in Figure 21. The set of signatures given by

$$S^A - S_D(TP) = \left\{ A_i \mid \exists B_k \ni B_k \approx A_i \quad \forall A_i \in S^A, B_k \in S^B \right\}$$

i.e., $S^A - S_D(TP)$ is the set of signatures belonging to S^A which are equivalent to at least one signature belonging to S^B .

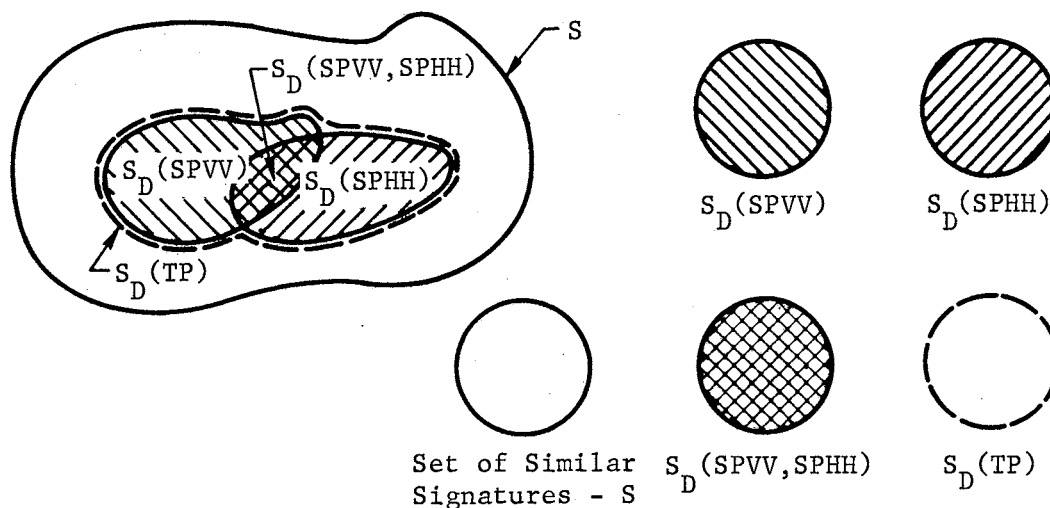


Figure 21. Relationship Between Sets of Dissimilar Signatures

As defined in D4-2, S_D represents a set of signatures. It is convenient to let N_D denote the number of signatures belonging to S_D . The data presented in Figure 18 can be used to compute the values of $N_D(TP)$, $N_D(SPVV)$, and $N_D(SPHH)$ directly from the values of D/N by N (888 in this case). Thus,

$$N_D(TP) = 323$$

$$N_D(SPVV) = 303$$

$$N_D(SPHH) = 156$$

Using Equation 4-2, with the values of N_D substituted for those of S_D , allows the number of signatures which are dissimilar in both σ_{VV} and

σ_{HH} to be computed as

$$\begin{aligned} N_D(\text{SPVV}, \text{SPHH}) &= N_D(\text{SPHH}) + N_D(\text{SPVV}) - N_D(\text{TP}) \\ &= 156 + 303 - 323 \\ &= 136 \end{aligned}$$

This relationship is illustrated in Figure 22.

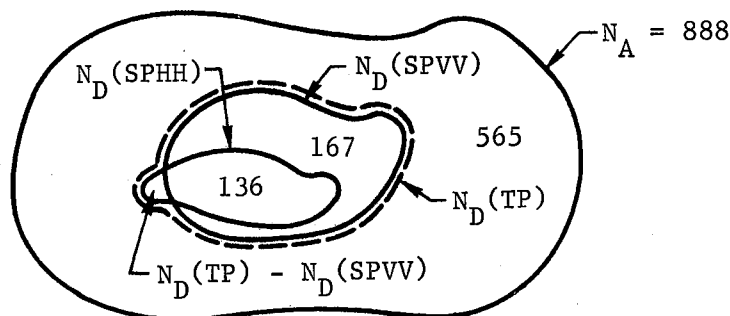


Figure 22. Relationship Between $N_D(\text{TP})$, $N_D(\text{SPVV})$, $N_D(\text{SPHH})$, and N_A of Models 1 and 2

In Figure 22, the numbers indicate the number of signatures in the signature set which are dissimilar in the elements comprising the designated signature type.

These results indicate that very few additional signature dissimilarities are obtained when TP signatures are used instead of SPVV signatures to compare Models 1 and 2. This lack of additional signature dissimilarities indicates the high degree of similarity between the two

vehicles when they are represented by SPHH signatures.

By use of a similar analysis, one can compute

$$N_D(3P) = N_D(TP) \cup N_D(SPVH) = N_D(TP) + N_D(SPVH) - N_D(TP, SPVH)$$

or

$$N_D(TP, SPVH) = N_D(TP) + N_D(SPVH) - N_D(3P)$$

where

$$S_D(Y) \cup S_D(Z) = \left\{ A \mid \nexists B_k \ni B_k \approx A \forall j \in I_{jY} \cup I_{jZ} \right\}$$

Thus $N_D(3P)$ can also be expressed as

$$\begin{aligned} N_D(3P) &= N_D(SPVV) \cup N_D(SPHH) \cup N_D(SPVH) \\ &= N_D(SPVV) + N_D(SPHH) + N_D(SPVH) - N_D(SPVV, SPHH) - \\ &\quad N_D(SPVV, SPVH) - N_D(SPVH, SPHH) + N_D(VV, HH, VH) \end{aligned} \quad (4-3)$$

as a result of the set definition of dissimilarity. The result expressed in Equation 4-3 can easily be established by reference to the relationship between the sets of dissimilarities of the SM and its subsets which is illustrated in Figure 23.

Using the relationships and results shown in Figure 18 allows the following data to be computed:

$$N_D(SPVV) = 303$$

$$N_D(SPVH) = 157$$

$$N_D(SPHH) = 156$$

$$N_D(SPVV, SPHH) = 136$$

$$N_D(SPVH, TP) = 26$$

The value of $N_D(SPVV, SPVH, SPHH)$ could also be computed if the signature types $TP(VV, VH)$ and $TP(VH, HH)$ had been utilized.

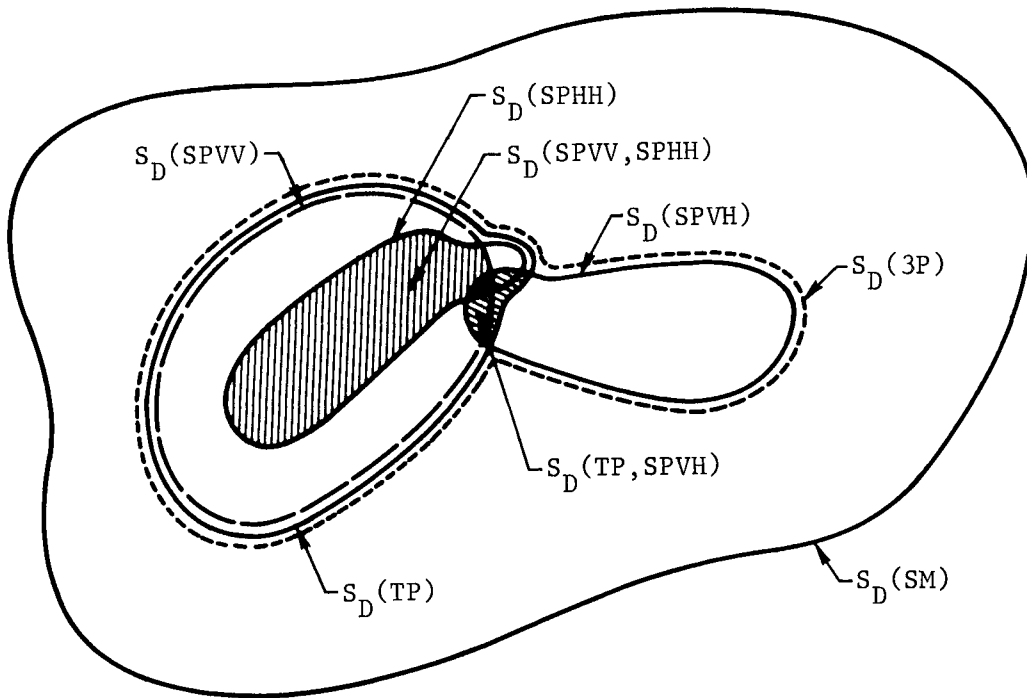


Figure 23. Sets of Dissimilarities Between Models 1 and 2

An upper bound on the value of $N_D(\text{SPVV}, \text{SPVH}, \text{SPHH})$ can be established by noting that

$$N_D(\text{SPVV}, \text{SPVH}, \text{SPHH}) \leq N_D(\text{SPVH}, \text{TP})$$

This result follows from the fact that

$$S_D(\text{SPVV}, \text{SPVH}, \text{SPHH}) \subset S_D(\text{SPVH}, \text{TP})$$

Thus

$$N_D(\text{SPVV}, \text{SPVH}, \text{SPHH}) \leq 26$$

The fact that $N_D(\text{SPVH}, \text{TP}) = 26$ also indicates that

$$N_D(\text{SPVH}, \text{SPVV}) \leq 26$$

and

$$N_D(\text{SPVH}, \text{SPHH}) \leq 26$$

which allows a lower bound to be determined by using the TP(VV, VH) signature. This lower bound is given by

$$\begin{aligned} N_D(\text{TP}(\text{VV}, \text{VH})) &= N_D(\text{SPVV}) + N_D(\text{SPVH}) - N_D(\text{SPVH}, \text{SPVV}) \\ &\geq 303 + 157 - 26 \end{aligned}$$

therefore,

$$N_D(\text{TP}(\text{VV}, \text{VH})) \geq 434$$

similarly,

$$N_D(\text{TP}(\text{HH}, \text{VH})) \geq 156 + 157 - 26 = 287$$

These results, based on the use of the cross section signatures discussed previously, lead to the following conclusions:

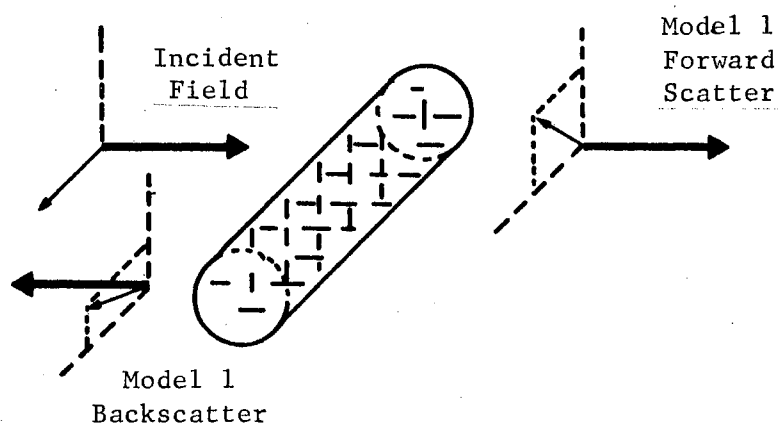
1. The relationship between $N_D(\text{SPVV})$, $N_D(\text{SPVH})$, and $N_D(\text{SPHH})$ indicates that the physical dissimilarities between Models 1 and 2 are primarily restricted to structure which preferentially scatters vertically polarized waves.
2. The fact that the intersection of $S_D(\text{SPVH})$ and $S_D(\text{SPVV})$ or $S_D(\text{SPHH})$ is very small indicates that one of the models produces considerably more depolarization of the incident wave than the other model.

The first of these conclusions is a logical result of the physical difference between Model 1 and Model 2. The addition of the vertical dipole to Model 1 to form Model 2 provides a structural difference which would indeed cause a change in the SPVV signature representations of the two models. Additionally, the fact that the dipole was designed

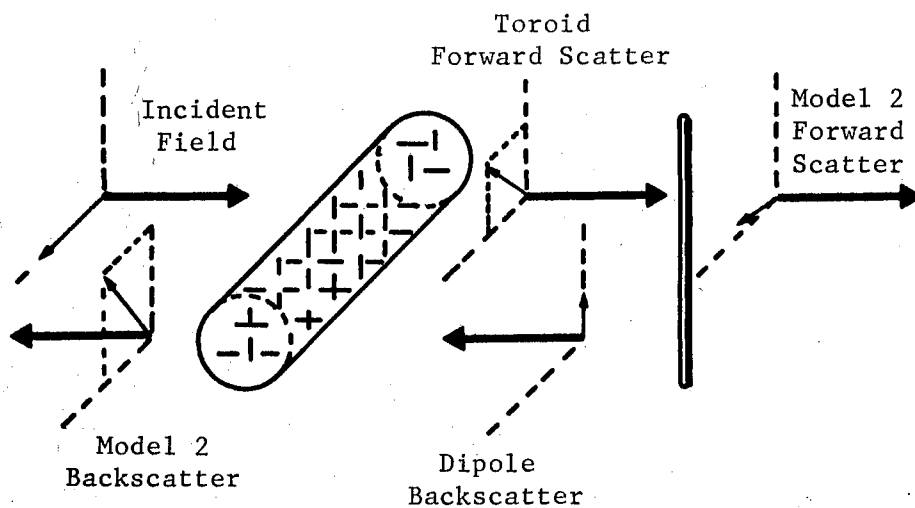
to present a significant value of cross section bears out the relative significance of the SPVV signature as a discriminant for comparing these two models.

The second conclusion is probably a result of the enhancement of depolarization caused by the dipole in the sense that energy which is depolarized by the toroid and normally scattered forward (away from the radar) could, with the addition of the dipole, now be scattered back toward the radar. Figure 24 is an illustration of the scattering phenomena exhibited by Model 1 and Model 2 (a horizontally polarized incident wave is assumed). The forward scattered wave is in general an elliptically polarized wave. In Figure 24, the dipole added to Model 1 to form Model 2 scatters some of the forward scattered energy (largely a vertically polarized component) back toward the transmitter.

A portion of this dipole scatter will be depolarized by the toroid, and some will be backscattered toward the dipole; however, some of this depolarized energy will be combined with the toroid backscatter to form a portion of the total backscattered wave intercepted by the radar receiving antenna. The example provided by this comparison of Models 1 and 2 is representative of the results to be expected when a comparison is made of two vehicles which are structurally quite different. In this instance, the structural differences are primarily sensitive to polarization as opposed to being, for example, sensitive to size. The computations of the sets of dissimilar signatures and the logical comparison of the results obtained for different signature types, including different values of ka , may well lead to the definition of an effective technique for determining the actual structural differences between vehicles.



Model 1 Backscatter



Model 2 Backscatter

Figure 24. Types of Backscatter Hypothesized for Models 1 and 2

The use of the set formation of dissimilar signatures leads to a simple means of computing the values of the unweighted dissimilar ratios. The weighted dissimilar ratio, W/N , is defined explicitly in D4-5.

D4-5: Given signature sets A and B of dimension n , let D_j be the number of signatures which exhibit exactly j dissimilar elements.

The weighted dissimilar number is then given by

$$W = \frac{1}{n} \sum_{j=0}^n jD_j \quad (4-4)$$

The weighted dissimilar ratio is the value of W/N_A .

For example, if $n = 3$

$$W = 1/3 \left(D_1 + 2D_2 + 3D_3 \right)$$

The values of the D_j 's may be determined directly from the unweighted dissimilar numbers if those values are available for all signatures of dimension j which are subsets of the signature type index set I_n . The number of subsets of dimension j which can be formed from a given n -dimensional signature is given by the binominal coefficient $\binom{n}{j} = \frac{n!}{j!(n-j)!}$, where $0 \leq j \leq n$. (23). The total number of signature types which can be formed from an n -dimensional signature is found by summing $\binom{n}{j}$ over all j from 1 to n (the zero-dimensional subset is meaningless in this case). Thus, one obtains

$$\sum_{j=1}^n \binom{n}{j} = 2^n - 1$$

a result which can be directly obtained by observing the form of Pascal's Triangle of the binomial coefficients. The comparison of SM signatures would then appear to involve the computation of $2^5 - 1 = 31$ separate values of D to provide data sufficient for calculating W ; consequently, this approach does not appear practical. However, the value of W in the case of a two-dimensional signature, such as the TP(VV,HH) type, is readily computed on the basis of the three values of N_D obtained for the SPVV, SPHH, and TP(VV,HH) signatures.

A simpler method of computing the weighted dissimilar ratio results from the fact that the value of the summation $\sum_{j=1}^n jD_j$ is identically equal to the sum of the number of dissimilarities obtained by using the n possible one-dimensional signatures belonging to the pertinent signature-type index set, I_n . Let k represent the k^{th} signature element. Then

$$\sum_{j=1}^n jD_j = \sum_{k=1}^n N_D(k) \quad (4-6)$$

Equation 4-6 can be established in the following manner: For the case of $n = 1$, the value of D_1 represents the number of signatures which are dissimilar in exactly 1 element. It follows that

$$D_1 = N_D(1)$$

For the case of $n = 2$, the value of D_2 represents the number of signatures which are dissimilar in exactly 2 elements; therefore,

$$D_1 + 2D_2 = N_D(1) + N_D(2) \quad (4-7)$$

since $N_D(1) + N_D(2)$ equals the sum of the signatures which are dissimilar in either element 1 or element 2. Thus those signatures which are dissimilar in both elements will be counted twice, and this value will be exactly accounted for by the value of $2D_2$.

Similarly, for the case of $n = 3$, the addition of $N_D(3)$ to the right-hand side of Equation 4-7 adds a number of single third-element dissimilarities to D_1 , twice the number of 2-element dissimilarities to D_2 , and three times the number of 3-element dissimilarities to D_3 . Thus,

$$D_1 + 2D_2 + 3D_3 = N_D(1) + N_D(2) + N_D(3)$$

If the case

$$\sum_{j=1}^{n-1} jD_j = \sum_{k=1}^{n-1} N_D(k)$$

is assumed for $n - 1$, then Equation 4-6 is established by induction. Equation 4-6 was used to compute the data presented in Table VII in the form of a comparison of the unweighted and weighted dissimilar numbers. The corresponding dissimilar ratios are plotted in Figure 18 for comparison.

TABLE VII
COMPARISON OF D/N AND W/N

Signature Type	D	W	D/N	W/N
SPVV	303	303	.341	.341
SPVH	157	157	.177	.177
SPHH	156	156	.176	.176
PHA(HH)	303	303	.341	.341
TP(VV,HH)	323	229	.353	.258
3P	454	205	.512	.231
SPP(VV,HH)	462	303	.341	.341
SM ²	848	244	.955	.275

A comparison of the weighted and unweighted dissimilar ratios computed for Models 1 and 2 clearly demonstrates the degree of bias toward dissimilarity that is exhibited in the unweighted case. However, this bias is not necessarily unrealistic because the use of measurement error limits of 2 dB on cross section and 20 degrees on phase tends to weight the measure toward similarity. Also, the inherent uniqueness of the SM signature tends to result in a large value of dissimilarity between these two vehicles because of the large differences between the σ_{VV} and σ_{VH} signatures of the two vehicles.

4.3.2 Generic Vehicles. Figure 25 contains data obtained by using

²By assuming that the value of D/N of the PHA(VH) signature is 0.341 (the same as that determined for the PHA(HH) signature), the value of W/N(SM) can be computed.

the SSDP to compute a measure of the similitude between Model C1 and Models C2, CY5, and F5. Error limits of 3 dB on cross section and 20 degrees on phase were utilized. Additionally, in order to investigate the effects of signature order, a value of D/N was computed for the case in which no aspect angle correlation was used ($\epsilon_\theta = 180$ degrees) and for the case where the signature sets were correlated to within ± 10 degrees ($\epsilon_\theta = 10$ degrees). The signature sets in each case consisted of alternate signatures over the theta (θ) interval from 0 (nose-on) to 180 (tail-on) degrees. In each case, the signature sets of each of the two models used in the comparison covered identical intervals in theta.

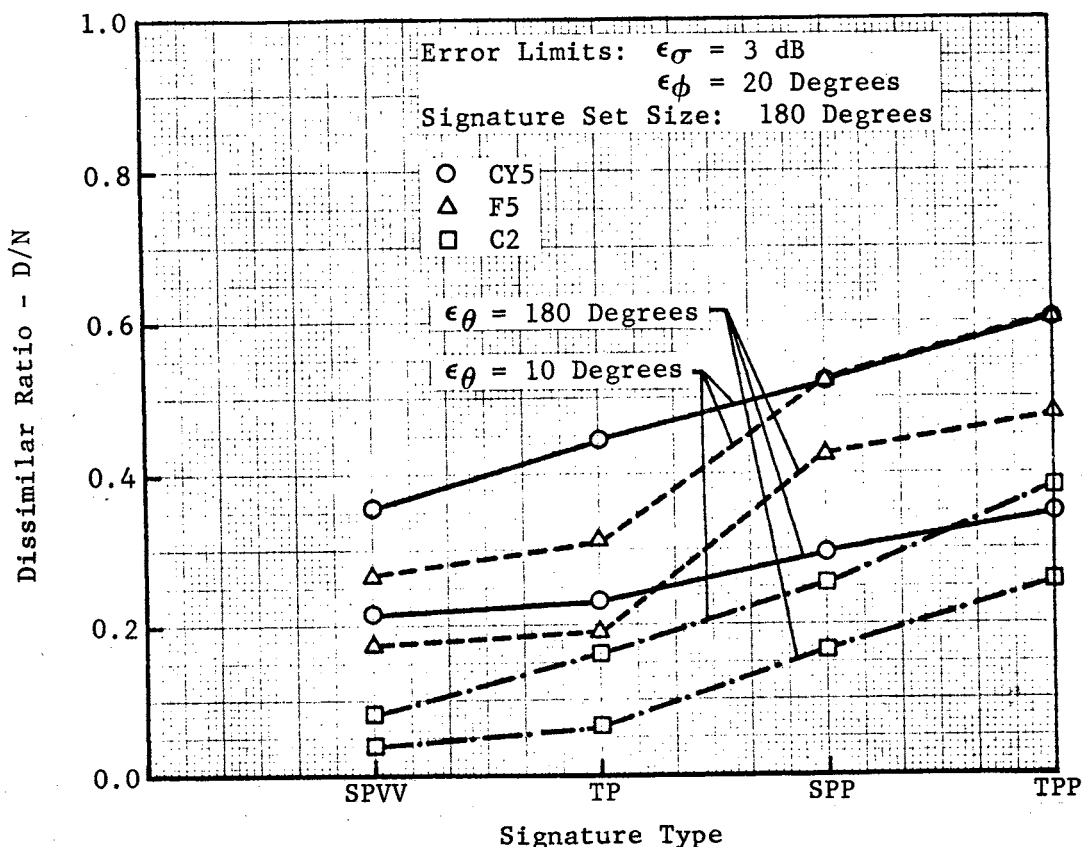


Figure 25. Vehicle Similitude to Model C1 Established by Use of the Dissimilar Ratio

An examination of the data shown in Figure 25 results in the following conclusions with regard to the generic shapes:

1. The two cones C1 and C2 are more similar to each other than to the frustrum or the cylinder.
2. The cone is more similar to the frustrum than to the cylinder when cross section signatures are used; however, the opposite is true when phase is utilized.
3. In general, the use of azimuth correlation in computing D/N results in an increase in the value of D/N.
4. In the case of these vehicles, the rate of change of D/N obtained with a change in signature type is relatively independent of the type of models which are being compared.
5. By comparing these results to those in Section 3.4 it is apparent that two vehicles may exhibit similar values of ambiguity and still exhibit signature dissimilarities on which to base a measure of their similitude.

Although the data shown in Figure 25 illustrates the relative similitude between Model C1 and the other models; the difference between these comparisons of the different models might not appear as great as might be desired. On the contrary, this data indicates that Cone C1 is approximately five times as similar to Cone C2 as to Cylinder CY5 when the SPVV signature is utilized with and without aspect angle correlation. This difference becomes smaller as additional signature elements are utilized; however, this result is to be expected because of the correlation between signature elements of the generic vehicles. This correlation is further indicated in terms of the ambiguity data contained in Figure 13.

It should be pointed out that the fact that identical values of D/N are obtained when a vehicle is compared to two different vehicles does not indicate that the two vehicles are identical. For example, the comparison of a cylinder to a much smaller cylinder and to a much larger cylinder could conceivably result in identical values of D/N even though the small and the large cylinder are quite different. This case occurred in comparisons between Models C1 and F5 and Models C1 and CY5 when SPP and TPP signatures were used. However, a comparison of Models CY5 and F5, based on the use of the SPVV and SPP signatures, resulted in values of D/N of .1260 and .3562, respectively.

Figure 26 contains an illustration of the relationship between the values of D/N of Models C1, F5, and CY5. The length of the sides of the triangles shown in this figure are scaled in terms of the computed values of D/N. The triangle formed by using the SPP signatures indicates that Models F5 and CY5 are nearly as different as the Model pairs C1-F5 and C1-CY5. The results obtained by using SPVV signatures are also shown.

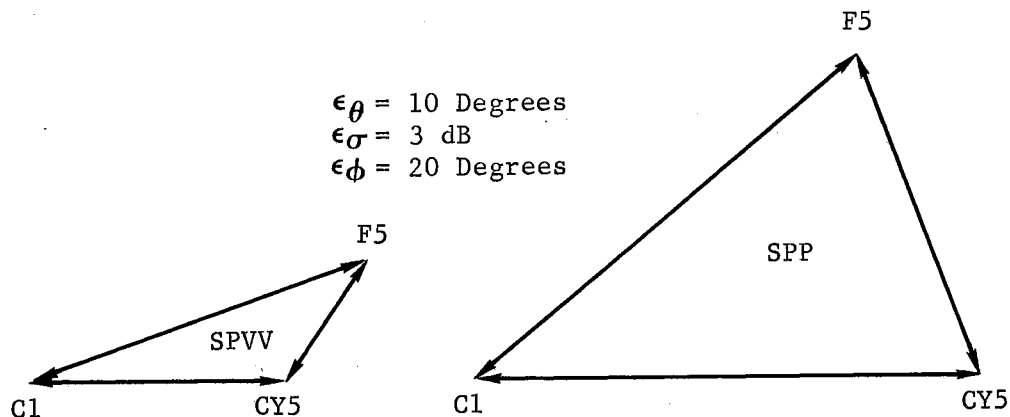


Figure 26. Dissimilar Ratio Relationship Between Models C1, F5, and CY5

Conclusions 1 and 2 can be compared quite well to similar conclusions which might be drawn on the basis of the physical dissimilarities between these vehicles. A visual comparison of these vehicles is sufficient to establish an order of their physical dissimilarities; however, these dissimilarities can be placed on a quantitative basis in the following manner.

In the case of these smooth, symmetrical, generic shapes, a set of four physical discriminants may be defined for each vehicle:

1. S is the number of surfaces producing significant specular reflections in the theta interval which comprises a signature set.
2. P is the number of pairs of surfaces producing identical specular reflections in a signature set.
3. L is the largest characteristic length of the vehicle.
4. R is the largest characteristic radius of the vehicle.

A cone, for example, would exhibit $S = 0$ and $P = 0$ in a 180-degree rotation from 0 to 180 degrees, but it would exhibit $S = 3$ and $P = 2$ if 360 degrees of rotation were allowed. A cylinder would exhibit $S = 3$ and $P = 1$ for 180 degrees, but it would exhibit $S = 4$ and $P = 2$ for 360 degrees of rotation.

A quantitative measure of the physical similitude between vehicles A and B can then be formed as

$$P(A,B) = \frac{1}{4} \left(\frac{S_A}{S_B} + \frac{P_A}{P_B} + \frac{L_A}{L_B} + \frac{R_A}{R_B} \right)$$

where, for example, each ratio is formed as the smaller of

$$\frac{P_A}{P_B} \text{ or } \frac{P_B}{P_A}$$

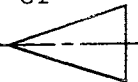


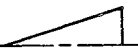
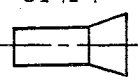
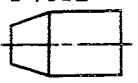
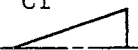
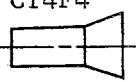
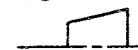

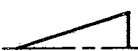

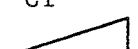
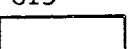
The physical dissimilar ratio, D_p , can then be computed as $D_p = 1 - P(A,B)$. Note that, since the value of $P(A,B)$ is restricted to the range between 0 and unity, the value of D_p will also lie between 0 and 1. Table VIII contains the results of computing D_p for the comparison of C1-C2, C1-CY5, C1-F5, C1-CY4F4, and CY4F4-F4CY2 by using SPVV and other signatures. The shape of the vehicle indicates whether 180 or 360 degrees of rotation were utilized to form the signature set.

This particular technique for defining physical similitude is in no sense optimum; in fact, a great deal of intuition is necessary, for example, in determining what constitutes a "significant" specular reflection. As used here, "significant" is referenced to characteristics significant in terms of wavelength, i.e., the regions which are large enough in wavelength to produce true specular reflection. As simple as the technique is, the computed values of D_p show a remarkable degree of correlation with the computed values of D/N , as indicated in Table VIII. Most of these data were computed without aspect angle correlation; hence, such vehicles as CY4F4 and F4CY2 should indeed be quite similar. The use of aspect angle correlation and SPVV signatures provides an even better correlation between D_p and D/N for the comparisons in which order was used.

4.3.3 Composite Generic Vehicles. The data contained in Figure 27 are the results of comparing vehicle Model A1 with Models A2 and A3. Models A2 and A3 were constructed to represent various degrees of

Table VIII

Comparison of Physical and Statistical Dissimilar Ratios

Vehicle A	Vehicle B	ϵ_{σ} dB	S_A/S_B	P_A/P_B	L_A/L_B	R_A/R_B	$W(A,B)$	D_P	D/N SPVV $\epsilon_{\theta}=10$	D/N SPVV $\epsilon_{\theta}=180$	D/N TP $\epsilon_{\theta}=180$	D/N SPP $\epsilon_{\theta}=180$	D/N TPP $\epsilon_{\theta}=180$
C1 	C2 	2.	1.	1.	.75	1.	.940	.060	--	.0517	--	--	--
C1 	C2 	3.	1.	1.	.75	1.	.940	.060	.0781	.0359	.0607	.1648	.2515
CY4F4 	F4CY2 	2.	1.	1.	.975	1.	.990	.010	--	.0380	--	--	--
C1 	CY4F4 	2.	.5	.5	.985	1.	.746	.254	--	.1410	.2002	--	--
F5 	CY5 	3.	1.	0.	.430	1.	.607	.393	.1260	--	--	--	--
C1 	F5 	3.	.67	0.	.630	1.	.574	.426	.2659	.1807	.1832	.4237	--
C1 	CY5 	3.	.67	0.	.688	.842	.544	.456	.3572	.2107	.2268	.2912	.3475

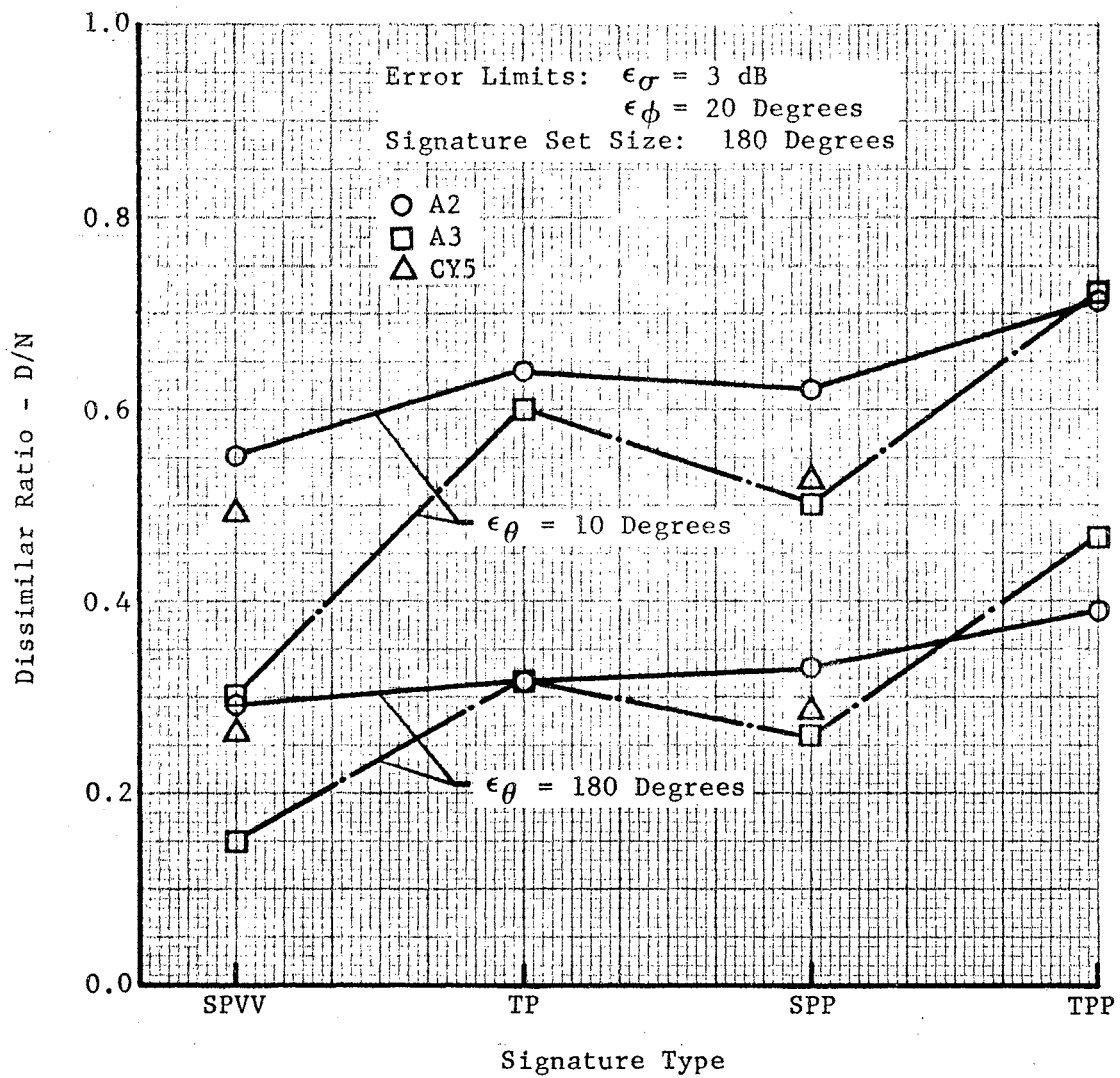


Figure 27. Vehicle Similitude To Model A1 Established By Use of the Dissimilar Ratio

physical synthesis of Model A1 which was itself a smooth model composed of generic surfaces and was designed to provide a close approximation of a typical aerospace vehicle. The measured amplitude plots of these three vehicles are shown in Appendix C.

The results of these comparisons indicate that the similitude between Models A1 and A2 is approximately the same as that between A1 and A3 except in the case of SPVV signatures. In this case, the difference between Models A1 and A2 appears to be about twice that between A1 and A3. An examination of the pertinent cross section patterns reveals the following:

1. On the basis of their SPVV and SPHH signatures, Models A1 and A2 are fairly similar in the regions of (0, 50) degrees and (80, 100) degrees, but they are quite different elsewhere. In other words, they appear to be similar at nose-on and at broadside.
2. When SPVV signatures are used, Models A1 and A3 appear to be fairly similar over a broad region centered at 90 degrees; however, they are very different in the regions near 0 and 180 degrees.
3. When SPHH signatures are used, the differences between Models A1 and A3 are much greater, a fact that can be very well correlated with the large increase in D/N observed when the TP signature is used.

Also plotted in Figure 27 are the results of comparing Models A1 and CY5 by using SPP and SPVV signatures with and without aspect angle correlation. These results indicate that these two vehicles, which are radically different in length, still exhibit approximately the same

value of similitude as, for example, Models A1 and A2. The fact that Model A1 is a composite model in which Model CY5 is used in its construction and the fact that their cross section patterns in the theta region near 180 degrees are very similar (within 3 dB) indicate that the above result is plausible.

An examination of the dissimilar ratio data contained in Figures 25 and 27 reveals the fact that the use of phase in general does not provide the discrimination which might be expected from an examination of the measured phase patterns. The exception occurs when Models C1 and F5 are compared. It should be noted, however, that differential phase is being used as a discriminant and that, while measured (TV, RV) and (TH, RH) phase may contain many cycles, the difference between these values may be relatively constant. In fact, if the phase center of the scatterer is spatially located at the same point in the radar line of sight for both (TV, RV) and (TH, RH) polarization conditions, the resulting relative phase will be constant (zero). When phase error limits of ± 20 degrees are used, it is expected that there may be regions of aspect angles in which the use of phase as a discriminant will result in few additional dissimilarities. All of the vehicles shown in Figures 25 and 27 are composed of smooth, highly conductive surfaces as opposed to the wire toroid used to construct Models 1 and 2. Figures 28 and 29 contain plots of differential phase of some of the generic and composite vehicles considered above. Note that in these plots relative phase may vary between ± 360 degrees; however, the absolute values of phase were used in computing D/N. Reflection of the curves for $-\emptyset$ about the line $\emptyset = 0$ corresponds to taking the absolute value of \emptyset . These plots were made by using a Stromberg-Carlson SC4020

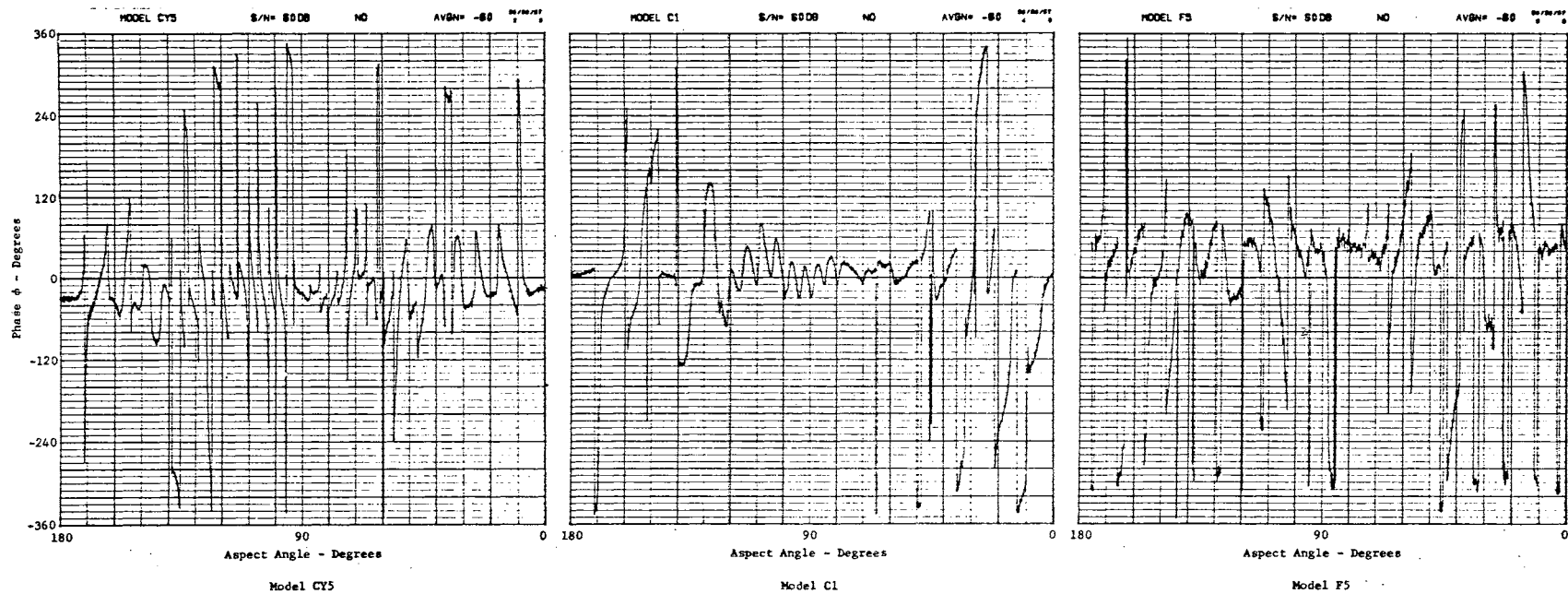


Figure 28. Differential Phase Exhibited by Models CY5, C1, and F5

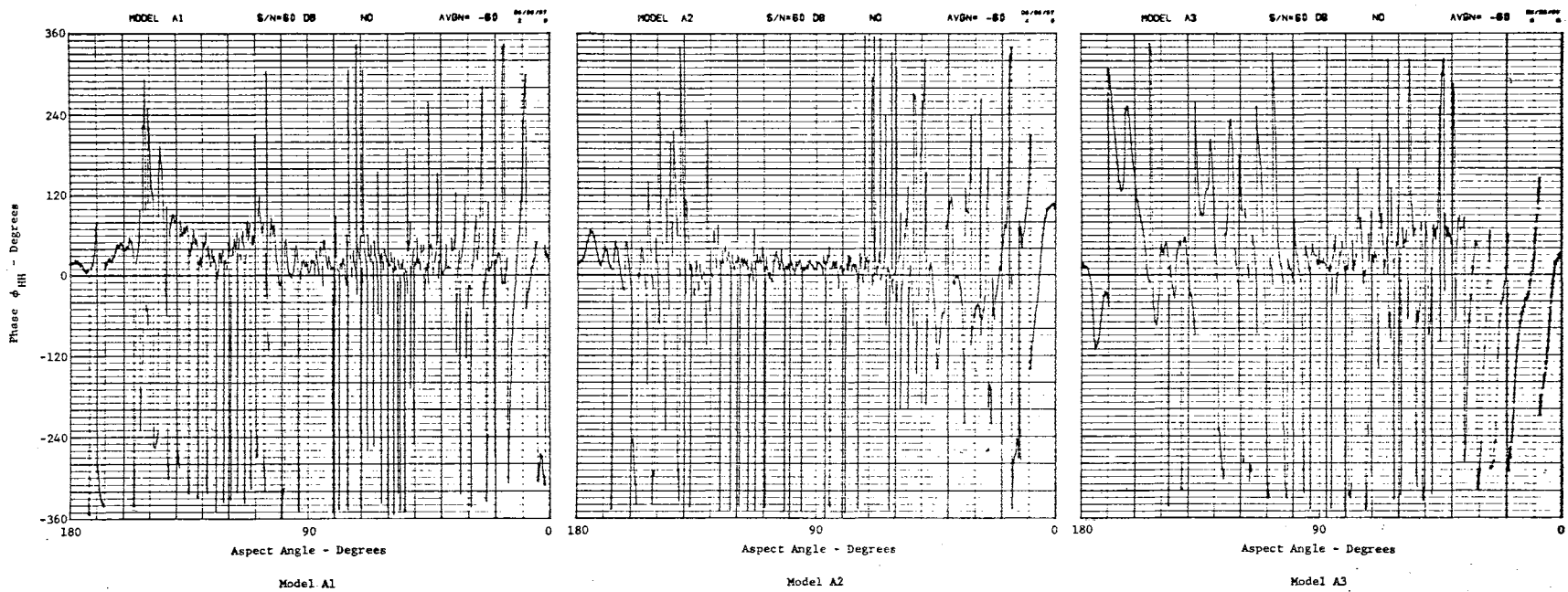


Figure 29. Differential Phase Exhibited by Models A1, A2, and A3

Automatic plotter in conjunction with the IBM 7040/7090 system.

An examination of the phase records in Figure 28 indicates that, although the differential phase of Model C1 is approximately zero over a broad region centered at 80 degrees (the specular point of the cone), the differential phase of Model F5 is approximately 40 degrees over the same angular region. An average difference in the phase signatures of about 40 degrees is also evident in the regions near the end-on aspects of these two targets. In contrast to Models C1 and F5, a comparison of the phase signatures of Models C1 and CY5 indicates a much smaller number of dissimilarities would exist. Note that the difference between the phase signatures of Models C1 and F5 would be approximately the same when the absolute value of \emptyset is used, but the phase signatures of Model C1 and CY5 would become much more similar.

The differential phase data presented in Figure 29 shows a much higher degree of similarity between the phase signatures of Models A1 and A2 than those of Models A1 and A3. This fact is also evident from the small change in the values of D/N obtained when phase signature elements are used, as indicated in Figure 27.

4.4 Conclusions. The analysis of this measure of vehicle similitude on the basis of radar signature dissimilarities has resulted in the formulation of a set of primary conclusions, as follows:

1. A useful degree of correlation does exist between the dissimilar ratio and the physical dissimilarities between vehicles.
2. The use of complex signatures, such as those which might be obtained by using a coherent radar or a scattering matrix radar, provides a better measure of vehicle similitude than

that obtained by using a conventional radar (single polarization-amplitude only).

3. The availability of order information, i.e., the ability to determine the orientation of two vehicles relative to each other provides a significant increase in the degree of confidence one would have in making a decision as to the similitude between two scattering vehicles.

The relationship which was obtained between the computed values of the dissimilar ratio and the structural differences between Models 1 and 2 provides a clear indication of the feasibility of employing the dissimilar ratio as a measure of vehicle similitude. The data obtained by using C-band measurements of a set of generic vehicles also shows the usefulness of the dissimilar ratio.

The results analyzed in this chapter were computed on the basis of radar signatures of target models which were constrained to rotate in a horizontal plane containing the radar line of sight. In addition, a high signal-to-noise level was maintained in the measurement system at all times. Consequently, care must be observed in attempting to extrapolate these results in an effort to solve identification and discrimination problems on the basis of signatures obtained in an operational radar environment.

The feasibility of utilizing the equivalence class concept in an operational radar environment is certainly of interest to a large number of investigators. Therefore, the differences between static and dynamic signature measurements need to be discussed in terms of the manner in which these differences might limit the application of the concept to practical problems of interest. Some of the pertinent

aspects of dynamic signature measurements are discussed in Chapter V.

CHAPTER V

SUMMARY AND RECOMMENDATIONS

5.1 Summary. The research investigation considered herein has been primarily directed toward an examination of the feasibility of utilizing equivalence class techniques to enhance the application of automatic decision making processes to radar signature analysis. This research was precipitated by difficulties which have been attendant on efforts to utilize multidimensional radar signatures in conventional decision making processes, notably, those involving human analysts. The approach taken herein has been that of developing an Equivalence Class Technique (ECT) that can be used to construct a contraction mapping of a multidimensional signature set into a set of parameters to which decision rules may be applied. Two specific applications of such a mapping to problems of concern to the radar signature analyst have been discussed in detail in order to establish a quantitative measure of the utility of the ECT.

The basis for the ECT is the fact that signatures which exhibit a set of common properties may be logically called equivalent relative to these properties. The nature of the properties selected to form a basis for this equivalence determines to a great extent the significance of the mapping and, ultimately, the confidence level that can be attached to any resulting decision. The properties used in this research were selected in an effort (1) to emphasize the physical significance of

errors in signature measurements, (2) to achieve a significant reduction in computer storage requirements, and (3) to retain only that information necessary for making meaningful decisions.

The extraction of meaningful discriminants from the equivalence class mapping of a signature set was the subject of the investigation of signature-type ambiguity. A relationship between the number, size, and diameter of the equivalence classes was investigated and used to form a measure of how uniquely a vehicle can be represented by different types of signatures obtained under various degrees of measurement accuracy. The results of this research provided a great deal of information concerning the interdependence of the elements of the target scattering matrix of a number of vehicle types. The radar designer will also be interested in the comparative effects on the ambiguity of system measurement resolution and signature dimension which were revealed in the ambiguity investigation.

An application of the ECT in forming a measure of the similitude between two vehicles on the basis of their signature representations was discussed in Chapter IV. In this research, a dissimilar ratio was formed as a measure of the differences between the equivalence class mappings of two vehicles. The relationship between this measure and parameters, including signature-type, signature set size, and vehicle symmetry, was examined for a number of different vehicles. This investigation also revealed a potentially useful identification aid in the relationship between sets of dissimilar signatures of different signature-types. This phenomena was not extensively investigated because of a lack of suitable vehicle measurements; however, data on a particular pair of vehicles provided information sufficient to warrant

further interest.

In order to establish a meaningful basis for evaluating the dissimilar ratio, a physical dissimilar ratio was defined in terms of certain distinguishing features of typical bodies of revolution. This measure of physical dissimilarity incorporated dimensional properties and properties of symmetry of the vehicles being compared, and it appeared to represent a useful measure of similitude. The dissimilar ratio computed on the basis of the radar signature representations of the vehicles compared quite favorably with the physical dissimilar ratio.

The signature sets used in this research were composed of subsets of the measured scattering matrices of vehicle models. These measurements were obtained by using a ground plane radar range under conditions which represented a precise synthesis of a free-space environment. The vehicle models represented a broad spectrum of physical complexity and an order of magnitude range in ka . Details of the measurement technique, the measurement system, and the model specifications have been documented in the appendices.

5.2 Recommendations for Further Research. In this research, primary emphasis has been placed on defining the amount of information contained in certain multidimensional radar signatures and defining an efficient technique for extracting and automatically processing only that information which can be used in making particular decisions in radar signature analysis. The results presented were computed on the basis of the radar signatures of targets that were constrained to rotate in a plane passing through the radar line of sight. In addition, the orientation of the vehicle was known exactly during each signature

measurement. Also, a high signal-to-noise ratio was maintained at all times. Consequently, the extrapolation of these results to identification and discrimination problems on the basis of signatures obtained in an operational radar environment would involve the investigation of a number of phenomena. The relationship between the dynamic signatures of a vehicle and that obtained under static (radar range) conditions may be classified into three categories:

1. Environmental
2. Calibration
3. Vehicle Motion and Orientation.

Environmental considerations would include ionospheric propagation phenomena, such as Faraday rotation and birefringence. These non-reciprocal and anisotropic effects may produce a linear rotation of the propagating wave and/or a differential phase shift between orthogonal linear polarizations. A brief analysis of these effects on scattering matrix measurements is given by Beckel and Bates (24). They also indicate the target conditions under which these effects can be calibrated out of SM measurements; however, they note that a cooperative target is generally required to achieve this calibration. Other techniques, such as the use of multiple frequency signatures, may facilitate the removal of these effects, and they should be investigated.

The calibration of an operational radar to provide accurate cross section and phase measurements is a second consideration. Calibration on a radar range is fairly simple, but calibration in the operational case may involve the use of known satellites, precision spheres carried aloft by weather balloons, or possibly some ground-based technique of calibration via the side lobes of the radar antenna. The use of

signatures formed as the ratios of cross section at different polarizations and the use of directly measured differential phase elements bears investigation on the basis of the attendant reduction in calibration requirements.

The problems which are connected with the motion of a space object appear to place the severest restrictions on the application of automated techniques of radar signature analysis. In the first place, signatures measured directly by use of an operational radar must be based or indexed in terms of time rather than orientation angle. In order to utilize signatures of this type, conventional practices involve the determining of the transformation between the index of the signatures and the vehicle orientation angle. If the target geometry is known, this problem may be simple; however, in general, a satellite may be tumbling, spinning, or precessing through space, and its relative motion with respect to the radar may be quite complicated. Nevertheless, under some conditions, equivalence class mappings made on the basis of a time index may be useful. The use of highly unique signature representations may, for example, reduce the necessity of determining the parameters of body motion. It must also be pointed out that a certain amount of identification information is available in the form of the motion exhibited by a space vehicle. For example, the fact that a vehicle is inertially stable, earth stable, radar stable, or tumbling may be significant to the identification of the vehicles.

A major problem in obtaining dynamic signature measurements is that which results from the component of vehicle velocity along the radar line. The high velocity of a satellite causes the satellite's range to change quite rapidly; consequently, there is a resultant rapid

change in the measured phase terms. If the time interval between measurements of phase elements of the scattering matrix is large, the resulting measurement of differential phase may be considerably in error. Techniques for removing this range rate term include that of measuring all elements of a SM during a very short time interval by simultaneously measuring this term on the basis of multiple polarizations, or by removing the range rate term by using either differential range data, doppler frequency techniques, or multiple frequencies.

An investigation of the relative usefulness of other multidimensional signatures based on different frequencies and/or bistatic angles could proceed along the same lines of this research. The usefulness of multiple frequencies in obtaining information on body motion, Faraday rotation, and range rate constitutes an additional motivation for an investigation of this type.

The formulation of equivalence classes based on signature properties other than those considered herein should result in additional information regarding the feasibility of using ECT's as a basis for radar signature analysis. The ambiguity measure would, for example, be a reasonable criterion for examining the utility of signatures in which cross section ratios were used as elements, and this measure would be directly applicable to the evaluation of multiple frequency signatures.

BIBLIOGRAPHY

1. Skolnik, M. I. Introduction to Radar Systems, McGraw-Hill, New York, N. Y. (1962).
2. "Special Issue on Radar Reflectivity." Proceedings of the IEEE, Vol. 53, No. 8. (1965).
3. Kennaugh, E. Polarization Properties of Radar Reflections, Antenna Lab., The Ohio State University Research Foundation, Columbus, Ohio. RADC Contract AF28(099)-90, Project Report 389-12(AD2494), March 1, 1952.
4. Copeland, J. R. "Radar Target Classification by Polarization Properties." Proceedings of the IEEE, Vol. 48. (1960) 1290-1296.
5. Bojarski, N. N. Signal Processing Studies and Analysis, Technical Report No. RADC-TR-66-830, Rome Air Development Center, Rome, N. Y. (April, 1967).
6. Heasley, C. C. Jr. "Some Communication Aspects of Character-Sensing Systems." Proceedings of the Western Joint Computer Conference, (1959) 176-180.
7. Kamentsky, L. A. "The Simulation of Three Machines Which Read Rows of Handwritten Arabic Numbers." IRE Transactions on Electronic Computers, Vol. EC-10. (1961) 489-502.
8. Kerr, D. E. ed. Propagation of Short Radio Waves, Massachusetts Institute of Technology Radiation Series. McGraw-Hill, New York, N. Y. (1951).
9. Huynen, J. R. "Measurement of the Target Scattering Matrix." Proceedings of the IEEE, Vol. 53, No. 8. (1965) 936-946.
10. Martinson, L. W., Perry, R. P., and Howard, T. B. Wide Band Baseline Radar Study, Technical Report No. RADC-TR-67-72, Rome Air Development Center, Rome, N. Y. (1967).
11. Kuhl, F. and Covelli, R. "Object Identification by Multiple Observations of the Target Scattering Matrix." Proceedings of the IEEE, Vol. 53, No. 8. (1965) 1110-1115.
12. Radar Reflectivity Measurements Symposium, Technical Report RADC-TDR-64-25, Vol. 1. (April, 1964).

13. Blacksmith, P. Jr., Hiatt, R. E., and Mack, R. B. "Introduction to Radar Cross-Section Measurements." Proceedings of the IEEE, Vol. 53, No. 8. (1965) 901-920.
14. Kennaugh, E. M. and Moffatt, D. L. "Transient and Impulse Response Approximations." Ibid. 893-901.
15. Rheinstein, J. "Scattering of Short Pulses of Electromagnetic Waves." Ibid. 1069-1070.
16. Kouyoumjian, R. G. and Peters, L. Jr. "Range Requirements in Radar Cross-Section Measurements." Ibid. 920-928.
17. Sebestyen, G. S. "Recognition of Membership in Classes." IRE Transactions on Information Theory, Vol. IT-7 (1961) 44-50.
18. Sinclair, G. Modification of the Radar Range Equation for Arbitrary Targets and Arbitrary Polarization, Report 302-19, Antenna Laboratory, The Ohio State University Research Foundation, Columbus, Ohio. (September, 1948).
19. Ridenour, L. N. Radar System Engineering, Radiation Laboratory Series, Vol. 1. McGraw-Hill, New York, N. Y. (1947).
20. Graves, C. D. "Radar Polarization Power Scattering Matrix." Proceedings of the IRE, Vol. , No. . (1956) 248-252.
21. Gruver, G. W. Scattering Matrix Utilization Study, Technical Report No. RADC-TR-67-392, Rome Air Development Center, Rome, N. Y. (August, 1967).
22. Experimental and Analytical Investigation of Target Scattering Matrices, Technical Report No. RADC-TR-65-298, Rome Air Development Center, Rome, N. Y. (December, 1965).
23. Parzen, E. Modern Probability Theory and Its Applications, John Wiley and Sons, Inc., New York, N. Y. (1960) Chapter V.
24. Bickel, S. H. and Bates, R. T. H. "Effects of Magnetic-Ionic Propagation on the Polarization Scattering Matrix." Proceedings of the IEEE, Vol. 53, No. 8. (1965) 1089-1091.
25. An Analysis of the Scattering Matrix Measurements Capabilities of a Ground Plane Radar Cross-Section Range, Technical Documentary Report No. RADC-TDR- 64-317, Rome Air Development Center, Rome, N. Y. (June, 1964).
26. RAT SCAT Phase Measurement System, Report No. FZE-344, General Dynamics, Fort Worth, Texas.
27. Freeny, C. C. "Target Support Parameters Associated with Radar Reflectivity Measurements." Proceedings of the IEEE, Vol. 53, No. 8. (1965) 929-936.

28. Heart, E. E. and Fritsch, P. C. "A Method of Measuring Small Radar Cross Sections by Digital Vector-Field Subtraction." Radar Reflectivity Measurements Symposium, Technical Documentary Report No. RADC-TDR-64-25, Rome Aire Development Center, Rome, N. Y. (April, 1964).

APPENDIX A

SCATTERING MATRIX MEASUREMENTS

A.1 The Scattering Matrix. The monostatic Scattering Matrix (SM) of an object at a single frequency and a fixed orientation with respect to the RLOS completely represents the polarization characteristics of the object in terms of that frequency, orientation, and transmitter-receiver geometry. (3). This fact, that the radar cross section of an object at any polarization conditions of the radar can be computed on the basis of the SM, has stimulated a great deal of interest in SM measurements. This appendix contains a brief discussion of the formulation of the target SM and a description of the conditions under which the SM of an object can be measured by use of a ground plane radar range. The primary source of the material presented in this appendix is Reference 25, and the reader is referred to that document for more detailed information. This reference also contains an interesting discussion of the effects of errors in the measurement of the elements of the SM and the manner in which these errors propagate through computations of cross section at other polarizations.

A general electromagnetic plane wave propagating in the +z direction of a right-hand cartesian coordinate system, such as that shown in Figure 30, can be described by the orthogonal pair of vectors E_x and E_y where

$$E_x = \mathcal{E} \sin \gamma e^{i(\omega t - kz)} \quad (\text{A-1a})$$

$$E_y = \mathcal{E} \cos \gamma e^{i(\omega t - kz - \delta)} \quad (\text{A-1b})$$

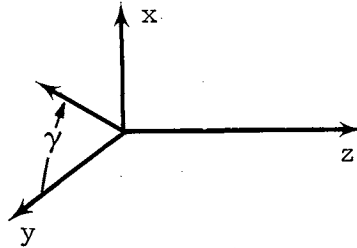


Figure 30. Coordinate System

Here, \mathcal{E} is an amplitude term, γ is an angle, $0 \leq \gamma \leq 90$ degrees, which represents the orientation of the linear polarization that would result if δ were zero, and δ is the phase angle between the E_x and E_y components of the wave. ω and k represent angular frequency and wave number, respectively. The sign of δ determines the sense (direction of rotation) of the wave relative to the direction of propagation. If δ is positive, the wave described in Equations A-1 would be assigned a left-hand sense. If $\delta \leq 0$, a right-hand sense would be assigned.¹ The wave represented by Equations A-1 is, in general, an elliptically polarized wave, i.e., the tip of the polarization vector would, in general, be traced out in the form of an ellipse in the x-y plane.

In matrix notation, a transmitted wave can be described as

¹This definition is in accordance with the IRE Standards on Radio Propagation.

$$\mathbf{E}_T = \begin{bmatrix} E_{TX} \\ E_{TY} \end{bmatrix} = \xi \begin{bmatrix} \sin \gamma_t \\ \cos \gamma_t e^{j\delta_t} \end{bmatrix} = \xi \hat{q} \quad (\text{A-2})$$

where the $e^{j(\omega t - kz)}$ term has been suppressed and \hat{q} is a unit column matrix used to define the polarization of the transmitted wave or the polarization of the transmitting antenna.

The polarization of a receiving antenna will be defined by \hat{p} where

$$\hat{p} = \begin{bmatrix} \sin \gamma_r \\ \cos \gamma_r e^{j\delta_r} \end{bmatrix} \quad (\text{A-3})$$

The coupling between two antennas is given by the voltage generated in the receiving antenna terminals by a received wave; the coupling can be expressed by

$$v = \hat{p}^{*t} \hat{q} \quad (\text{A-4})$$

where the asterisk denotes the complex conjugate and the lower case t denotes the transpose matrix. Equation A-4 may be written as

$$v = \begin{bmatrix} \sin \gamma_r, \cos \gamma_r e^{-j\delta_r} \end{bmatrix} \begin{bmatrix} \sin \gamma_t \\ \cos \gamma_t e^{j\delta_t} \end{bmatrix}$$

which can be further expanded to give

$$v = \sin \gamma_r \sin \gamma_t + \cos \gamma_r \cos \gamma_t e^{j(\delta_t - \delta_r)} \quad (\text{A-5})$$

The complex conjugate is necessary in order that the two antennas be described in terms of the same coordinate system relative to the direction of propagation. If the two antennas are identically polarized, ($\gamma_r = \gamma_t$ and $\delta_r = \delta_t$) the resulting voltage is unity. On

the contrary, if the two antennas are orthogonally polarized ($\gamma_r = \pi/2 - \gamma_t$ and $\delta_r = \pi + \delta_t$) the resulting voltage is zero.

Under the assumption that the intervening medium along the propagation path between two antennas is both homogeneous and isotropic, the matrix notation

$$\begin{bmatrix} E_1^s \\ E_2^s \end{bmatrix} = [S] \begin{bmatrix} E_1^i \\ E_2^i \end{bmatrix} \quad (A-6)$$

can be used to express the field strength of a scattered wave (denoted by superscript s) relative to that of an incident wave (denoted by superscript i). The subscripts 1 and 2 may denote any system of bases vectors which span the two-dimensional complex space of a plane wave. Examples of such bases vectors include vertical and horizontal polarizations and right circular and left circular polarizations. The matrix $[S]$ is called the scattering matrix.

The definition of radar cross section allows one to deduce that the magnitude of the elements of $[S]$ must be identically equal to the square root of the radar cross section of the object relative to the pertinent polarization conditions. Thus,

$$[S] = \begin{bmatrix} a_{11}e^{j\psi_{11}} & a_{12}e^{j\psi_{12}} \\ a_{21}e^{j\psi_{21}} & a_{22}e^{j\psi_{22}} \end{bmatrix} = \begin{bmatrix} \sqrt{\sigma_{11}} e^{j\psi_{11}} & \sqrt{\sigma_{12}} e^{j\psi_{12}} \\ \sqrt{\sigma_{21}} e^{j\psi_{21}} & \sqrt{\sigma_{22}} e^{j\psi_{22}} \end{bmatrix} \quad (A-7)$$

where the first subscript refers to the polarization of the incident wave and the second to that of the scattered wave.

On the basis of the reciprocity theorem, if the transmitting and

receiving antenna are at the same point, the off-diagonal terms of the scattering matrix must be equal in the case of a linear scatterer. A linear scatter is defined as one in which the principle of superposition holds.

The measurement of the cross section terms of the SM in a free space environment would involve only a measurement of the coupling between the radar transmitter and receiver under the three polarization conditions described by the subscripts 11, 12, and 22. A phase reference for the phase terms of S can be established by factoring out the $e^{j\psi_{11}}$ term from each element to obtain

$$[S] = e^{j\psi_{11}} \begin{bmatrix} a_{11} & a_{12}e^{j\phi_{12}} \\ a_{12}e^{j\phi_{12}} & a_{22}e^{j\phi_{22}} \end{bmatrix}$$

where $\phi_{12} = \psi_{12} - \psi_{11}$ and $\phi_{22} = \psi_{22} - \psi_{11}$. The factor $e^{j\psi_{11}}$ can be ignored since it is a function of the radar range.

A.2 Calibration. In order to measure the true value of radar cross section, an absolute measure of the coupling between the radar transmitter and receiver must be available. However, since the radar cross section of an object is generally desired relative to a square meter, calibration can be most easily obtained by comparing the coupling obtained via the target to the coupling obtained via an object of known cross section. A precision sphere is commonly used as a primary calibration standard since its cross section is insensitive to the orientation of the sphere and is readily available as a function of ka . (8).

In order to obtain accurate comparative measurements of this type,

a number of conditions must be satisfied. The frequency stability and the power level stability of the radar must be such that negligible drift is exhibited during the period between calibration and measurement. Additionally, the target and the calibration object must occupy essentially the same volume in space to assure identical illumination in terms of the radar coverage diagram. A technique whereby the specification of frequency and power drift can be considerably relaxed is discussed in Section A.3 along with a method whereby a fixed-position secondary standard is used to eliminate the necessity of measuring the primary standard prior to each target measurement.

Phase measurements relative to a range term may be obtained by comparing the phase of the target signal with that of a reference signal and a coherent oscillator. The difference between the target phase and the reference phase is converted to a voltage and is used to servo a calibrated phase shifter to minimize this voltage. The resulting change in the calibrated phase shifter represents the measured phase, modulo 2π . Reference 26 contains a detailed discussion of the amplitude and phase measurement systems utilized to obtain the signatures used in this research. Appendix B contains a brief description of that system.

A.3 The Ground Plane Radar Range. The discussions in Sections A.1 and A.2 apply when the energy transfer between the radar and the target is effected by means of the direct path along the RLOS only. In the case where the target is also illuminated by a wave that is reflected from a flat ground plane, additional considerations are necessary.

A primary problem associated with obtaining accurate measurements of the scattering characteristics of an object is that of maintaining

the target-environment relationship which would exist in an operational case. For example, the radar cross section of a satellite in its free space environment may be quite different from that measured under laboratory conditions where external structural support must be provided for the target and where other structures, such as the earth itself, tend to influence the scattered return.

The target support problem can generally be handled by applying various techniques to reduce the radar cross section of the support to a value considerably less than that of the target. (27). If such a value cannot be achieved because of the required support size, vector subtraction techniques may be utilized to subtract the background contribution from that of the target. (28).

The effects of the proximity of the earth to both the target and the radar antennas has until recently posed a more serious problem. Ground effects have been eliminated to some extent by aiming the antennas upward at a suspended target, but the attendant target support problems have been such that this solution is not generally feasible.

In most recently implemented radar scattering facilities, the ground plane effect has been used rather than eliminated. (25). This approach has been made possible as a result of the development of techniques whereby the ground plane effects can be quite effectively defined by use of a calibrated target. However, the application of these calibration techniques for the purpose of obtaining accurate cross section and phase measurements is dependent on meeting a number of conditions. These conditions are discussed in the following paragraphs with reference to the nomenclature of Figure 30. A complete discussion of the ground plane range is contained in Reference 24 which

has been used as the source of much of the following discussion. The ground plane shown in Figure 31 is assumed to be flat and smooth relative to λ .

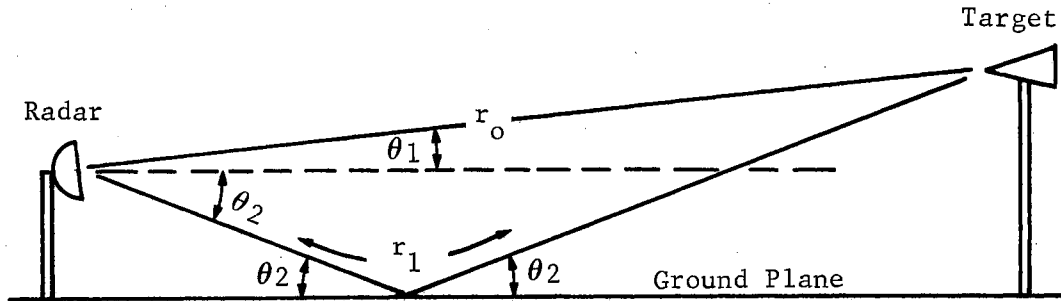


Figure 31. The Ground Plane Radar

The field which illuminates the target shown in Figure 31 is a result of the vector addition of the direct wave (path along r_0) and the reflected wave (path along r_1). The field at the target may be generally described as

$$\bar{E} = \bar{E}_{r_0} + \bar{E}_{r_1} = E_0 \left(f(\theta_1) + \rho f(\theta_2) e^{j(\xi + \Delta)} \right) \quad (\text{A-8})$$

where $f(\theta)$ is the antenna pattern factor referenced to the antenna boresite, $\rho e^{j\xi}$ is the complex coefficient of reflection of the earth at point P, and $\Delta = k(r_1 - r_0)$. If the antenna patterns are sufficiently broad, or if θ_1 and θ_2 are very small, the approximation $f(\theta) \cong 1$ allows \bar{E} to be written

$$\bar{E} = E_0 (1 + \rho e^{j(\xi + \Delta)}) \quad (\text{A-9})$$

It is assumed that the fields at the target decay as $1/r_0$, in other words, the target is in the far field of the radar antennas. This dependence on $1/r_0$ has been suppressed since $r_0 \cong r_1$ in terms of amplitude.

The complex coefficient of reflection is a function of the polarization of the incident fields at the point of reflection as well as such ground constants as the conductivity and the dielectric constant. The properties of the soil will be assumed to be constant during a measurement sequence to the extent that they will be ignored in terms of the explicit manner in which they enter into the following discussion. In the case of horizontal polarization of the incident wave,

$$\rho_h e^{j\xi_h} = \frac{\sin\theta_2 - \sqrt{(k_1/k_o)^2 - \cos^2\theta_2}}{\sin\theta_2 + \sqrt{(k_1/k_o)^2 - \cos^2\theta_2}} \quad (A-10)$$

Similarly, in the case of vertical polarization

$$\rho_v e^{j\xi_v} = \frac{(k_1/k_o)^2 \sin\theta_2 - \sqrt{(k_1/k_o)^2 - \cos^2\theta_2}}{(k_1/k_o)^2 \sin\theta_2 + \sqrt{(k_1/k_o)^2 - \cos^2\theta_2}} \quad (A-11)$$

where θ_2 is the grazing angle shown in Figure 31 and (k_1/k_o) is the complex dielectric constant of the ground.

Substitution of the relations in Equations A-12a and b may be made in Equation A-9;

$$\Gamma_h e^{j\mu_h} = 1 + \rho_h e^{j(\xi_h + \Delta)} \quad (A-12a)$$

and

$$\Gamma_v e^{j\mu_v} = 1 + \rho_v e^{j(\xi_v + \Delta)} \quad (A-12b)$$

in order to describe the field at the target as follows:

$$\bar{E}_\alpha = E_o \Gamma_\mu e^{j\mu} \quad (A-13)$$

where the subscript α indicates the polarization of the incident wave.

In general, the complex reflection coefficient of the ground is

sensitive to polarization, the result being that the vertical coverage patterns at the target may be different in the case of horizontal and vertical polarizations.

The transformation which results when a wave is reflected by a smooth flat earth can also be cast in a matrix notation similar to that given in Equation A-6 for the SM. Again, if the $1/r$ dependence of the fields is ignored, the scattered field at the surface of the earth can be expressed as

$$\begin{bmatrix} E_v^s \\ E_h^s \end{bmatrix} = [T] \begin{bmatrix} E_v^i \\ E_h^i \end{bmatrix} \quad (A-14)$$

where the matrix $[T]$ represents the ground plane polarization dependence and is given by

$$[T] = \begin{bmatrix} \Gamma_v e^{j\mu_v} & 0 \\ 0 & \Gamma_h e^{j\mu_h} \end{bmatrix}$$

$[T]$ is actually the bistatic SM of the ground plane at grazing incidence. No cross polarization terms will be evident if the ground is sufficiently homogeneous and smooth.

It is assumed that the x axis of the coordinate system shown in Figure A-1 is perpendicular to the ground plane shown in Figure A-2. Thus, when $\gamma = 0$ the polarization is horizontal.

The polarization of the wave at the radar receiver can now be expressed in terms of the transmitter polarization, the ground plane matrix, and the SM of the target as follows:

$$\begin{bmatrix} E_{Rv} \\ E_{Rh} \end{bmatrix} = [T_R] [S] [T_T] \begin{bmatrix} E_{Tv} \\ E_{Th} \end{bmatrix} \quad (A-15)$$

where $E_{Tv} = \sin \alpha_t$ and $E_{Th} = \cos \alpha_t$ as a result of the specification of linear polarization. The subscripts T and R on the $[T]$ matrices allow the effects of the ground plane transformation along the two-way path to be explicitly revealed. The voltage at the terminals of the radar receiver can now be expressed as

$$E^R = E_A^T e^{j\phi_R} e^{j\phi_T} \begin{bmatrix} \beta_{Rv} \sin \alpha_r & \beta_{Rh} \cos \alpha_r \end{bmatrix} \begin{bmatrix} \Gamma_{Rv} e^{j\mu_v} & 0 \\ 0 & \Gamma_{Rh} e^{j\mu_h} \end{bmatrix} \begin{bmatrix} \sqrt{\sigma_{vv}} e^{j\psi_{vv}} & \sqrt{\sigma_{vh}} e^{j\psi_{vh}} \\ \sqrt{\sigma_{vh}} e^{j\psi_{vh}} & \sqrt{\sigma_{hh}} e^{j\psi_{hh}} \end{bmatrix} \begin{bmatrix} \Gamma_{Tv} e^{j\mu_v} & 0 \\ 0 & \Gamma_{Th} e^{j\mu_h} \end{bmatrix} \begin{bmatrix} \beta_{Tv} \sin \alpha_t \\ \beta_{Th} \cos \alpha_t \end{bmatrix} \quad (A-16)$$

A^R and A^T represent receiver and transmitter amplitude controls, and similar phase controls are represented by $e^{j\phi_R}$ and $e^{j\phi_T}$. The β 's in the polarization matrices represent gains of the various field components under the assumption that the vertical and horizontal channels can be completely isolated. The constant terms of Equation A-16 can be combined to give

$$E^R = E^{T'} \begin{bmatrix} \rho_{Rv} \sin \alpha_r & \rho_{Rh} \cos \alpha_r \end{bmatrix} [S] \begin{bmatrix} \rho_{Tv} \sin \alpha_t \\ \rho_{Th} \cos \alpha_t \end{bmatrix} \quad (A-17)$$

where $E^{T'} = E_A^T e^{j\phi_R} e^{j\phi_T}$ and $\rho_{ij} = \beta_{ij} \Gamma_{ij}$. Under the assumption that $\alpha_r = \alpha_t = 0$ (to enable the use of horizontally polarized transmitter and receiving antennas), Equation A-17 can be reduced to

$$E_{hh}^R = E^{T'} \rho_{Rh} \rho_{Th} \sqrt{\sigma_{hh}} e^{j\psi_{hh}} \quad (A-18)$$

If the target were replaced with a sphere, Equation A-18 would give

$$E_{hh}^{Rs} = E^{T'} \rho_{Rh} \rho_{Th} \sigma_{hh}^s e^{j\psi_{hh}^s} \quad (A-19)$$

where the superscript s signifies that the target is a sphere.

Elimination of the common terms between Equations A-18 and A-19 allows the relationship between the target cross section and that of the sphere to be expressed.

$$\sigma_{hh} = \sigma_{hh}^s \left| \frac{E_{hh}^R}{E_{hh}^{Rs}} \right|^2 \quad (A-20)$$

In a similar manner, the value of σ_{vv} of the target can be determined in terms of σ_{vv}^s for a sphere on the basis of

$$\sigma_{vv} = \sigma_{vv}^s \left| \frac{E_{vv}^R}{E_{vv}^{Rs}} \right|^2 \quad (A-21)$$

Inspection of Equations A-20 and A-21 will reveal that the amplitude effects of the ground plane can be completely compensated for during the calibration process, provided that identical propagation paths are used in measuring the target and the sphere.

Compensation for the phase components of the ground plane transformation can be accomplished in a similar manner by considering the phase component of the received signal in Equation A-16.

In order to calibrate the cross polarized cross section terms, it is necessary to consider the product of the magnitude of E_{vh}^R and E_{hv}^R . This product is given by

$$\left| E_{vh}^R \right| \left| E_{hv}^R \right| = \left| E^{T'} \right|^2 \left| \rho_{Rv} \rho_{Th} \right| \left| \rho_{Rh} \rho_{Tv} \right| \sigma_{vh} \quad (A-22)$$

Similarly, the product $\left| E_{vv}^{Rs} \right| \left| E_{hh}^{Rs} \right|$ is given by

$$\left| E_{vv}^{Rs} \right| \left| E_{hh}^{Rs} \right| = \left| E^{T'} \right|^2 \left| \rho_{Rv} \rho_{Tv} \rho_{Rh} \rho_{Th} \right| \sigma^s \quad (A-23)$$

where the symmetry of the sphere is used to establish the relationship $\sigma_{vv}^s = \sigma_{hh}^s = \sigma^s$. Equations A-22 and A-23 can now be combined to give

$$\sigma_{vh} = \sigma^s \frac{\left| E_{vh}^R \right| \left| E_{hv}^R \right|}{\left| E_{vv}^{Rs} \right| \left| E_{hh}^{Rs} \right|}$$

The cross polarized term can also be calibrated by using a 45-degree dipole as a calibration target.

In general, scattering matrix measurements made on a ground plane radar range are obtained by using a sphere at the target area as a primary standard and a secondary standard, such as a corner reflector, located outside of the target area. The sequence of measurements set forth in Table IX is generally followed. It is assumed that the radar consists of a coherent, pulsed, range-gated radar similar to that subsequently described in Appendix B.

The use of a secondary standard is facilitated by the use of a range-gated radar system. By gating the receiver on only during the period of time when the radar returns are received from the target, scattering contributions from the corner reflector and other background-contributing scatterers can be reduced. Similarly, by moving the range gate to the range of the corner reflector, a fixed reference can be established without the necessity of replacing the target with the primary standard. The geometry of a typical ground plane radar range

is subsequently shown in Appendix B in terms of the relative position of the radar, the secondary standard, and the target or primary standard.

TABLE IX
SCATTERING MATRIX MEASUREMENT PROCEDURE

I. Precalibration

- a. Place the sphere in the position normally occupied by the target.
- b. Place the range gate over the sphere.
- c. Adjust the system amplitude control to obtain the computed value of σ^S .
- d. Adjust the system phase control to give zero.
- e. Place the range gate over the corner reflector.
- f. Record the measured cross section and the phase of the corner reflector.
- g. Repeat Steps I.a through I.f at all polarizations of interest.

II. Target Measurement

- a. Place the range gate over the corner reflector.
- b. Adjust the system to obtain the cross section and phase recorded in I.f.
- c. Replace the sphere with the target.
- d. Place the range gate over the target.
- e. Record the cross section and the phase of the target.
- f. Repeat Steps II.a through II.e at all polarizations of interest.

TABLE IX (Continued)

III. Post-Calibration

- a. Repeat Part II with the sphere used as the target.
- b. Results obtained from II.e should agree with those obtained from I.c and I.d.

A.4 Scattering Matrix Computations. The form of the scattering matrix is determined as a function of the bases vectors used to describe the incident and scattered polarizations. If, for example, bases vectors representing left and right circular polarizations are used, the scattering matrix could take the form

$$\begin{bmatrix} S_c \end{bmatrix} = \begin{bmatrix} \sqrt{\sigma_{RR}} e^{j\psi_{RR}} & \sqrt{\sigma_{LR}} e^{j\psi_{LR}} \\ \sqrt{\sigma_{RL}} e^{j\psi_{RL}} & \sqrt{\sigma_{LL}} e^{j\psi_{LL}} \end{bmatrix} \quad (A-24)$$

However, the elements of the matrix in Equation A-24 can also be computed directly from the elements of the SM in Equation A-16 by noting the result of a change of bases vectors. Prior to a discussion of a change in bases, the radar cross section of a target will be explicitly defined as

$$\sigma = vv^* = |v|^2 = \left| \hat{p}^t \begin{bmatrix} S \end{bmatrix} \hat{q} \right|^2 \quad (A-25)$$

where \hat{p}^t is used rather than \hat{p}^{*t} , as a result of the change in direction inherent to the backscatter process. Thus, the complex radar cross section obtained from use of transmitter polarization t and receiver polarization r becomes

$$\sqrt{\sigma_{tr}} e^{j\psi_{tr}} = \hat{p}^t [S] \hat{q} \quad (A-26)$$

or

$$\sqrt{\sigma_{tr}} e^{j\psi_{tr}} = \begin{bmatrix} \sin\gamma_r & \cos\gamma_r e^{j\delta_r} \end{bmatrix} \begin{bmatrix} \sqrt{\sigma_{vv}} e^{j\psi_{vv}} & \sqrt{\sigma_{vh}} e^{j\psi_{vh}} \\ \sqrt{\sigma_{hv}} e^{j\psi_{hv}} & \sqrt{\sigma_{hh}} e^{j\psi_{hh}} \end{bmatrix} \begin{bmatrix} \sin\gamma_t \\ \cos\gamma_t e^{j\delta_t} \end{bmatrix} \quad (A-27)$$

Equation A-27 can be used to compute the elements of the circular polarized scattering matrix $[S_c]$ by substituting the correct values for γ_r , δ_r , γ_t , and δ_t into the polarization vectors. For example, the transmit-left-circular, receive-right-circular values would be given by

$$\sqrt{\sigma_{LR}} e^{j\psi_{LR}} = \frac{1}{2} \begin{bmatrix} 1 & -j \end{bmatrix} [S] \begin{bmatrix} 1 \\ j \end{bmatrix} \quad (A-28)$$

since $\gamma_r = \pi/4$, $\delta_r = -\pi/2$, $\gamma_t = \pi/4$, and $\delta_t = \pi/2$ are the values which represent this polarization condition.

The component vectors of \hat{q} span the space of plane waves to which this research is limited. An arbitrary plane wave is represented in terms of these components by the parameters γ_t and δ_t . The particular polarization condition \hat{q} can be represented in terms of any other pair of bases vectors by premultiplying q by a suitable transformation matrix $[A]$ which relates the components of the original set of bases vectors to the second set. If \hat{p}_1 represents the polarization in terms of the bases denoted by the subscript 1, then

$$\hat{p}_2 = [A] \hat{p}_1 \quad (A-29)$$

would represent the polarization in terms of the bases denoted by the

subscript 2. The transformation matrix, $[A]$, must be a unitary matrix i.e., the condition

$$[A]^t^* [A] = [I] \quad (A-30)$$

must be satisfied where $[I]$ is the identity matrix. It can easily be shown that, if $[A]$ is unitary, then $[A]$ has an inverse $[A]^{-1}$ defined by

$$[A]^{-1}[A] = [A][A]^{-1} = [I]$$

where $[I]$ is the identity matrix. Therefore, the relations

$$\hat{p}^t = \hat{p}^t [A][A]^{-1}$$

and

$$\hat{q} = [A]^{-1} [A] \hat{q}$$

can be inserted in Equation A-26 to give

$$\sqrt{\sigma_{tr}} e^{j\psi_{tr}} = \hat{p}^t [A^t] [A^t]^{-1} [S] [A]^{-1} [A] \hat{q} \quad (A-31)$$

Regrouping the terms of Equation A-31 allows this relation to be expressed as

$$\sqrt{\sigma_{tr}} e^{j\psi_{tr}} = \left[[A] \hat{p} \right]^t \left[[A^t]^{-1} [S] [A]^{-1} \right] \left[[A] \hat{q} \right] \quad (A-32)$$

where the relationship $\left[[B] [C] \right]^t = [C]^t [B]^t$ has been incorporated. The term $[A] \hat{q}$ is identically equal to the transmitter polarization representation in terms of the new bases. Similarly, the matrix $\left[[A] \hat{p} \right]^t$ is simply the transpose of the \hat{p}_2 matrix of Equation A-29. Thus, the matrix

$$[S'] = [A^t]^{-1} [S] [A]^{-1} = \left[[A]^{-1} \right]^t [S] [A]^{-1}$$

must be the scattering matrix representation of the target in terms of the new bases. The unitary matrix

$$[A] = \frac{1}{2} \begin{bmatrix} 1 & -j \\ 1 & j \end{bmatrix}$$

is the transformation matrix which is used to transform the polarization bases from linear ($\gamma = 0$ and $\gamma = \pi/2$) to a circular bases. For example, if $\gamma = \pi/4$ and $\delta = \pi/2$, the transformation gives

$$[A] \begin{bmatrix} \sin \pi/4 \\ \cos \pi/4 e^{j\pi/2} \end{bmatrix} = \frac{1}{2} \begin{bmatrix} 2 \\ 0 \end{bmatrix} = \begin{bmatrix} 1 \\ 0 \end{bmatrix}$$

which denotes the left- circular polarization basis vector. Similarly, the vector $\begin{bmatrix} 0 \\ 1 \end{bmatrix}$ denotes the right-circular polarization basis vector.

The circularly polarized scattering matrix

$$[S_c] = \begin{bmatrix} \sqrt{\sigma_{LL}} e^{j\psi_{LL}} & \sqrt{\sigma_{RL}} e^{j\psi_{RL}} \\ \sqrt{\sigma_{LR}} e^{j\psi_{LR}} & \sqrt{\sigma_{RR}} e^{j\psi_{RR}} \end{bmatrix}$$

can be computed in terms of the elements of the linear scattering matrix $[S]$ by use of the transformation

$$[S_c] = -\frac{1}{2} \begin{bmatrix} j & -1 \\ j & 1 \end{bmatrix} \begin{bmatrix} \sqrt{\sigma_{vv}} e^{j\psi_{vv}} & \sqrt{\sigma_{hv}} e^{j\psi_{hv}} \\ \sqrt{\sigma_{vh}} e^{j\psi_{vh}} & \sqrt{\sigma_{hh}} e^{j\psi_{hh}} \end{bmatrix} \begin{bmatrix} j & j \\ -1 & -1 \end{bmatrix}$$

(A-33)

Expanding Equation A-33 gives the desired results.

$$\sqrt{\sigma_{LL}} e^{j\psi_{LL}} = \sqrt{\sigma_{VV}} e^{j\psi_{VV}} - \sqrt{\sigma_{hh}} e^{j\psi_{hh}} + j(\sqrt{\sigma_{hv}} e^{j\psi_{hv}} + \sqrt{\sigma_{vh}} e^{j\psi_{vh}})$$

$$\sqrt{\sigma_{RL}} e^{j\psi_{RL}} = \sqrt{\sigma_{VV}} e^{j\psi_{VV}} + \sqrt{\sigma_{hh}} e^{j\psi_{hh}} - j(\sqrt{\sigma_{hv}} e^{j\psi_{hv}} - \sqrt{\sigma_{vh}} e^{j\psi_{vh}})$$

$$\sqrt{\sigma_{LR}} e^{j\psi_{LR}} = \sqrt{\sigma_{VV}} e^{j\psi_{VV}} + \sqrt{\sigma_{hh}} e^{j\psi_{hh}} + j(\sqrt{\sigma_{hv}} e^{j\psi_{hv}} - \sqrt{\sigma_{vh}} e^{j\psi_{vh}})$$

$$\sqrt{\sigma_{RR}} e^{j\psi_{RR}} = \sqrt{\sigma_{VV}} e^{j\psi_{VV}} - \sqrt{\sigma_{hh}} e^{j\psi_{hh}} - j(\sqrt{\sigma_{hv}} e^{j\psi_{hv}} + \sqrt{\sigma_{vh}} e^{j\psi_{vh}})$$

On the basis of reciprocity, which can be used to establish the fact that $\sqrt{\sigma_{vh}} e^{j\psi_{vh}} = \sqrt{\sigma_{hv}} e^{j\psi_{hv}}$, these results can be simplified to yield

$$\sqrt{\sigma_{LL}} e^{j\psi_{LL}} = \sqrt{\sigma_{VV}} e^{j\psi_{VV}} - \sqrt{\sigma_{hh}} e^{j\psi_{hh}} + 2j \sqrt{\sigma_{vh}} e^{j\psi_{vh}}$$

$$\sqrt{\sigma_{RR}} e^{j\psi_{RR}} = \sqrt{\sigma_{VV}} e^{j\psi_{VV}} - \sqrt{\sigma_{hh}} e^{j\psi_{hh}} - 2j \sqrt{\sigma_{vh}} e^{j\psi_{vh}}$$

$$\sqrt{\sigma_{RL}} e^{j\psi_{RL}} = \sqrt{\sigma_{RL}} e^{j\psi_{RL}} = \sqrt{\sigma_{hh}} e^{j\psi_{hh}} + \sqrt{\sigma_{VV}} e^{j\psi_{VV}}$$

As an additional example, the matrix

$$\begin{bmatrix} B \end{bmatrix} = \frac{1}{2} \begin{bmatrix} 1 & 1 \\ -1 & 1 \end{bmatrix}$$

can be used to effect a transformation from the linear bases ($\gamma = 0$) and ($\gamma = \pi/2$) to the linear bases ($\gamma = \pi/4$) and ($\gamma = -\pi/4$).

The computation procedure described in the preceding paragraphs was used by Freeny (22) to demonstrate the accuracy of the measurement system subsequently described in Appendix B. This accuracy was demonstrated by comparing computed and measured results obtained by use of 45-degree linear polarizations.

APPENDIX B

GENERAL DYNAMICS SIGNATURE MEASUREMENT SYSTEM

B.1 Radar Range Description. The radar signature measurements used in this research were obtained by the author through use of the radar range at the Fort Worth facilities of General Dynamics. This range consists of approximately 70 acres of flat land which is suitable for the implementation of a ground plane radar range such as that described in Appendix A. In order to achieve the greatest possible flexibility, all of the radar equipment used on this range has been made mobile with the exception of three permanent target rotator pits which enable the simultaneous operation of three separate radar measurement systems.

The ground plane radar used to obtain the measurements analyzed in this research consists of a mobile van containing the radar electronic equipment, a pair of mobile antennas, and the target rotator and associated calibration equipment. Figure 32 is a photograph of the radar range showing the equipment van, antennas, and a target supported over the target rotator by a tripod of styrofoam columns.

The equipment used for recording measured signature data consists of both analog and digital recording units which are contained in the van and are synchronized with the target rotator through a servo system.

B.2 Electronics System. The radar used for these measurements consists of a coherent pulsed radar which incorporates a range-gated



Figure 32. Radar Range at the Fort Worth Division of General Dynamics

system to provide target-environment isolation. A dual antenna system is used in order to allow bistatic operation, although the data obtained for this research was obtained by using a bistatic angle of approximately zero. Both amplitude and absolute phase measurements are obtained with this system. Figure 33 is an interior view of the equipment van showing the components of the radar transmitter and receiver.

The transmitter consists of a coherent oscillator which drives a pair of travelling wave tubes in series to provide approximately one kilowatt of output power.

The receiving system is a unique system designed and built at the Fort Worth Division. Basically, the system is a typical superheterodyne receiver which incorporates a variable range gate that is manually controlled to gate a 60-megahertz IF amplifier on during the time interval of the range gate. This variable range gate is controlled by the operator so that the source of the target signal can be varied between the target rotator and the secondary standard to calibrate the system. Within the system, a fixed range gate is utilized to turn on the receiver at a range at which no target is present in order to inject a reference signal. This reference signal is a 60-megahertz pulse which is injected from a pulsed coherent oscillator through a linear attenuator and a variable phase shifter. The remainder of the receiver circuitry is used to compare the amplitude and phase of the target signal with that of the reference signal. The difference between the target and reference signals is applied to an amplitude servo and a phase servo which, if differences exist, are used to drive the calibrated attenuator and the variable phase shifter to force the two signals to correspond in amplitude and phase. The resulting changes in the

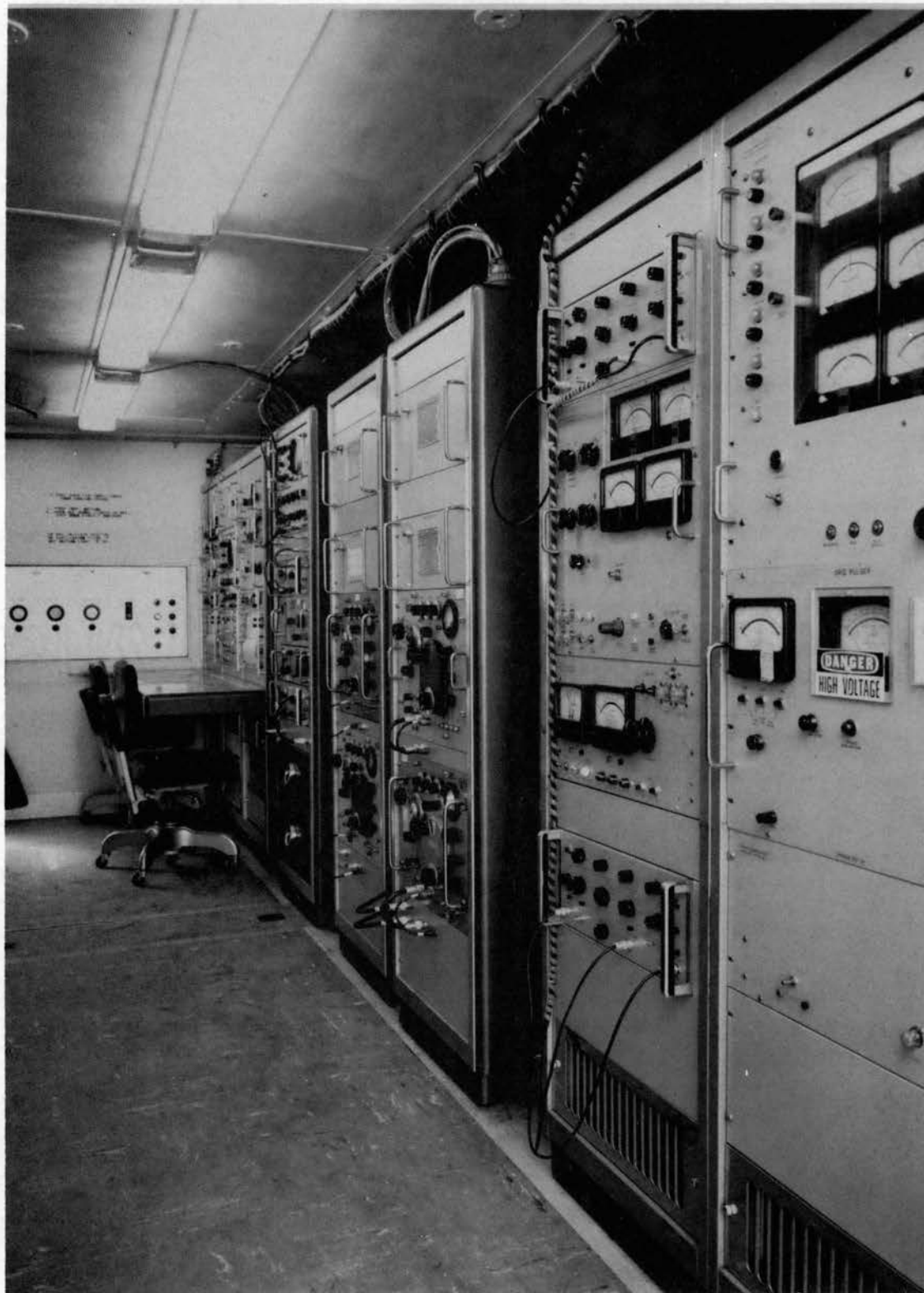


Figure 33. Interior of Electronic Equipment Van

attenuator and the phase shifter are used to drive a pair of analog recorders and are also encoded to provide a digital output which is recorded on punch paper tape. During the calibration process, the outputs of the attenuator and the phase shifter are calibrated to provide radar cross section and absolute phase.

Figure 34 is a block diagram of the radar receiver and its associated amplitude and phase circuitry. The amplitude linearity of the system is 0.5 dB and its phase linearity is 2.0 degrees.

The frequency of the radar system is controlled by locking the master and local oscillators to a Mansons Laboratory Synthesizer which provides a short-term frequency stability of one part in 10^9 . A permanent monitoring device is used to assure that the difference between the frequency of the master oscillator and that of the local oscillator is maintained at exactly 60 megahertz. The transmitter pulse shape is also permanently displayed during all measurements.

The recording system records cross section to the nearest 0.1 dB, phase to the nearest degree (modulo 360 degrees), and aspect angle to the nearest 0.1 degree. The dynamic range of the cross section measurement system is 50 dB.

B.3 Range Setup Procedure. In order to achieve accurate signature measurements, a number of detailed setup procedures are necessary. These include

1. Adjustment of the antenna heights and pointing direction to obtain maximum sensitivity and a uniform field and phase across the volume to be occupied by the target
2. Adjustment of the target rotator so that the target actually rotates in the plane of the radar beam

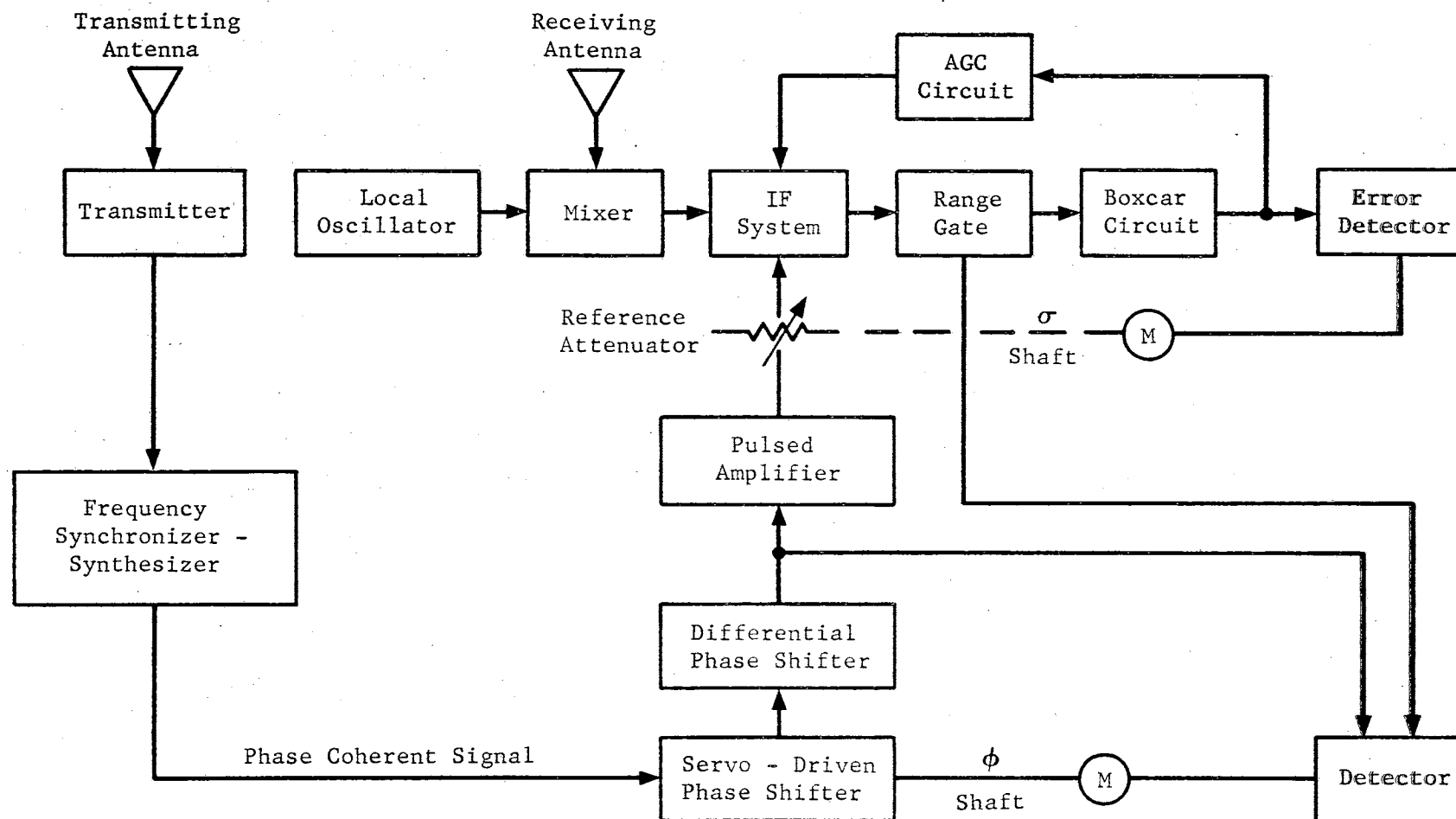


Figure 34. Block Diagram of Electronic Measurement System

3. Use of all possible means to reduce the cross section of the target support, the target rotator, and the other back-scattering mechanisms which might be located in the target range gate
4. Calibration of the radar via a primary standard and calibration of a secondary standard.

The antenna heights are adjusted so that the target is located in the first lobe of the radar interference pattern. The relationship

$$H_A = \frac{r\lambda}{4H_T}$$

is used to provide an initial height, where

H_A = antenna height

H_T = target height

λ = wavelength.

Final adjustment is achieved by maximizing the return from a calibration target.

The uniformity of the field in the target area is determined by raising a calibration probe (usually a sphere or corner reflector) through the region where the target will be located and recording the signal return as a function of the height of the probe. If a large amplitude gradient exists across the target volume, the radar range must be increased.

The tilt angle of the rotator is adjusted so that the radar cross section of both sides of a flat plate are identical. Use of this action assures that the target will rotate in the plane of the radar beam, which generally is not parallel to the ground.

The background cross section may be reduced (1) by tuning the

support column by means of small changes in frequency so that the reflections from the front and the back of the column cancel (if this technique is acceptable) or (2) by physically changing the column size. The column may also be tilted to obtain a very low background over most aspect angles. Use of this tilting process essentially positions the column so that the radar sees a null in the column's backscatter pattern; however, this result cannot be obtained through the entire rotation of the target from 0 to 360 degrees in aspect. Additional reduction may be achieved by using Radar Absorbing Material (RAM) to reduce the backscatter from the edge of the rotator pit and by assuring that the surrounding area is clear of backscattering sources. The backgrounds achieved during the measurements used in this research averaged less than -40 dBsm, well below the value of a typical target which exhibited specular cross sections greater than zero dBsm.

Calibration was achieved by using a precision sphere for a primary standard and a corner reflector for a secondary standard. The secondary standard was measured before and after each measurement run so that system changes could be detected and corrected before the target was removed from the rotator.

B.4 Signature Measurement Procedures. During each measurement sequence, the following items were continuously monitored to assure the accuracy of all measurements:

1. Repeatability of all measurements were assured by rotating and recording all signatures over at least 380 degrees.
2. Phase closure within ± 8 degrees was achieved during all measurements.
3. The position of the phase center of both the ψ_{vv} and ψ_{hh}

terms was checked at a specular point on each target to insure accurate phase calibration. $\psi_{vv} = \psi_{hh} \pm 8$ degrees was necessary for acceptance.

4. The accuracies of the digital encoders were checked before and after each measurement by noting the limiting values on the digital display.
5. The absolute accuracy of cross section measurements was checked against computed values of the cross section of the generic shapes on the basis of the physical optics approximation. These values checked within ± 1 dB.

The accuracy of this system has been demonstrated countless times, and this facility is without doubt one of the most versatile and accurate static radar scattering ranges in the world.

APPENDIX C

VEHICLE MODEL DATA

In Table X, the values of k_a (electrical diameter) and k_l (electrical length) are specified for each of the vehicle models used in this research. The method of constructing the generic shapes and the composite models formed from these shapes is indicated in Figure 35 for the case of a cone-cylinder. The tolerance on the model dimensions was 0.002 inch, which corresponds to less than one electrical degree in terms of a two-way path. This is a significantly greater constraint than that placed on the measurement accuracy of the phase measurement system. Figure 36 is a photograph of the generic shapes from which most of the models used in this research were constructed. The data in the photograph in Figure 37 provide an indication of how typical vehicle models were constructed by use of the generic models. All of these models were fabricated from solid aluminum.

The data in Table XI illustrate the manner in which the generic vehicles were utilized to construct Models A1, A2, and A3. The order of construction from left to right corresponds to the ordering from nose-on (zero degree) to tail-on (180 degrees).

Figures 38 through 47 contain measured cross section plots of v_v as a function of aspect angle for Models C1, F5, CY5, C1CY1F3, A1, A2, and A3.

TABLE X
DESCRIPTION OF MODELS

Model Designation	Model Type	ka	kl
1	Toroid	31.0	31.0
2	Toroid and Dipole	31.0	31.0
3	Typical Aerospace Vehicle	69.0	12.0
C1	Cone	20.0	24.0
C2	Cone	20.0	50.4
CY5	Cylinder	23.6	55.0
F3	Frustrum	23.6	10.7
F5	Frustrum	23.6	23.2
C1F2CY5	Cone-Frustrum-Cylinder	23.6	86.0
C1CY3	Cone-Cylinder	20.0	47.6
C1CY1F3	Cone-Cylinder-Frustrum	23.6	68.3
CY3	Cylinder	20.0	33.6
CY4F4	Cylinder-Flare	20.0	37.9
F4CY2	Frustrum-Cylinder	20.0	38.0
A1	Typical Aerospace Vehicle Model	23.6	167.5
A2	First Order Synthesis of Model A1	23.6	160.0
A3	Second Order Synthesis of Model A1	23.6	174.5

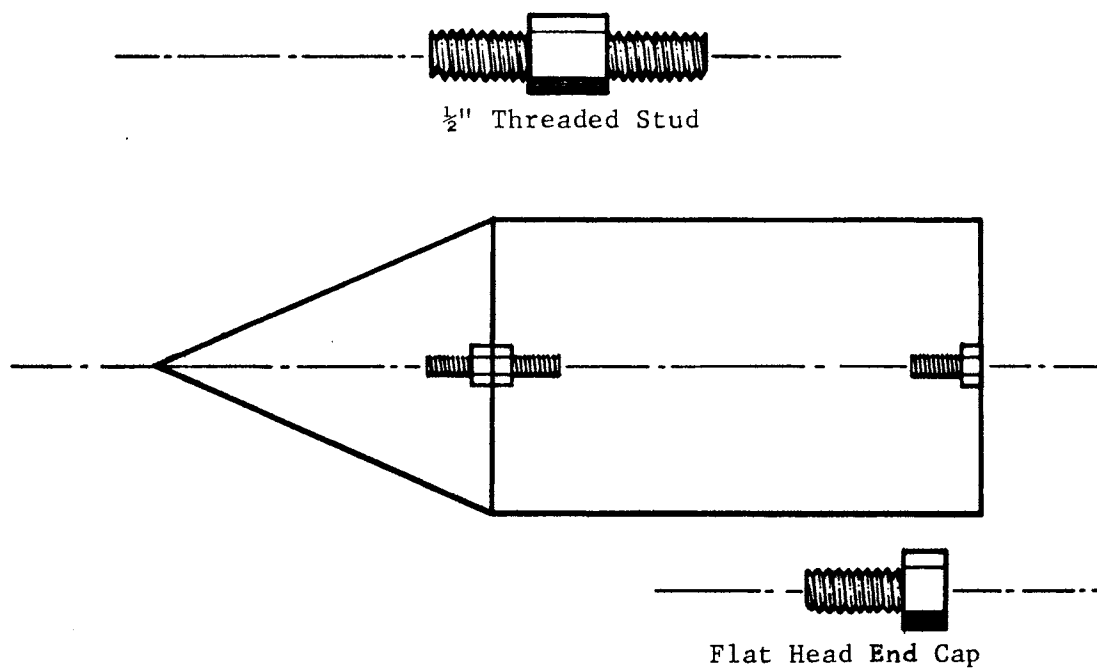


Figure 35. Construction of Composite Vehicles

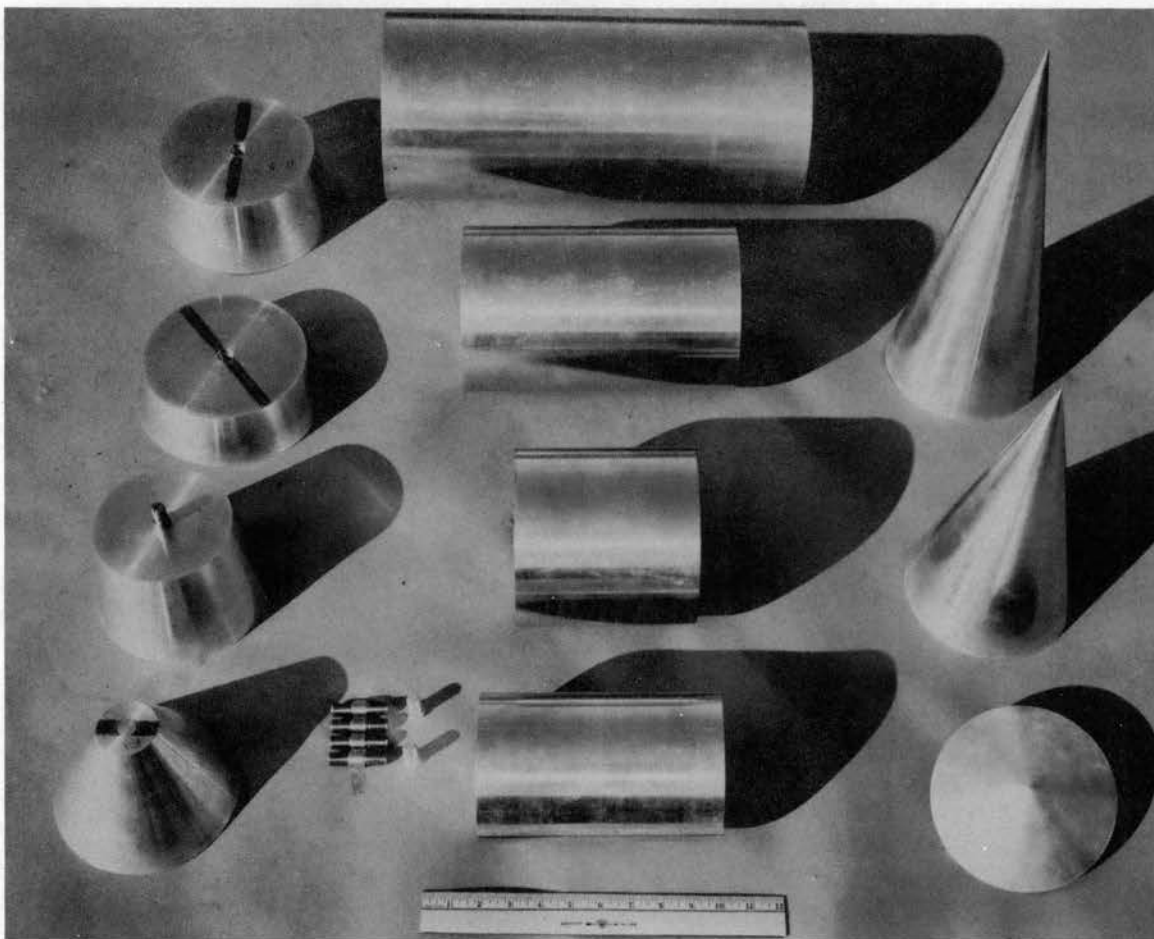


Figure 36. Typical Generic Vehicles

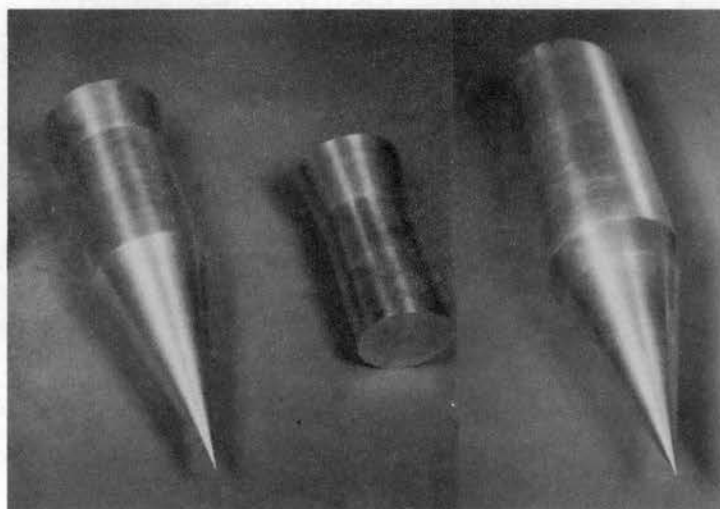


Figure 37. Typical Composite Generic Vehicles

TABLE XI
CONSTRUCTION OF MODELS A1, A2, and A3

Model	Generic Shapes Utilized							
A1	P1	F4	CY2	F2	CY5	F3	CY3	F1
A2		C1	CY3	F3	CY5	F2	CY1	F1
A3		H1	CY1	CY2	CY5	CY3	C3	

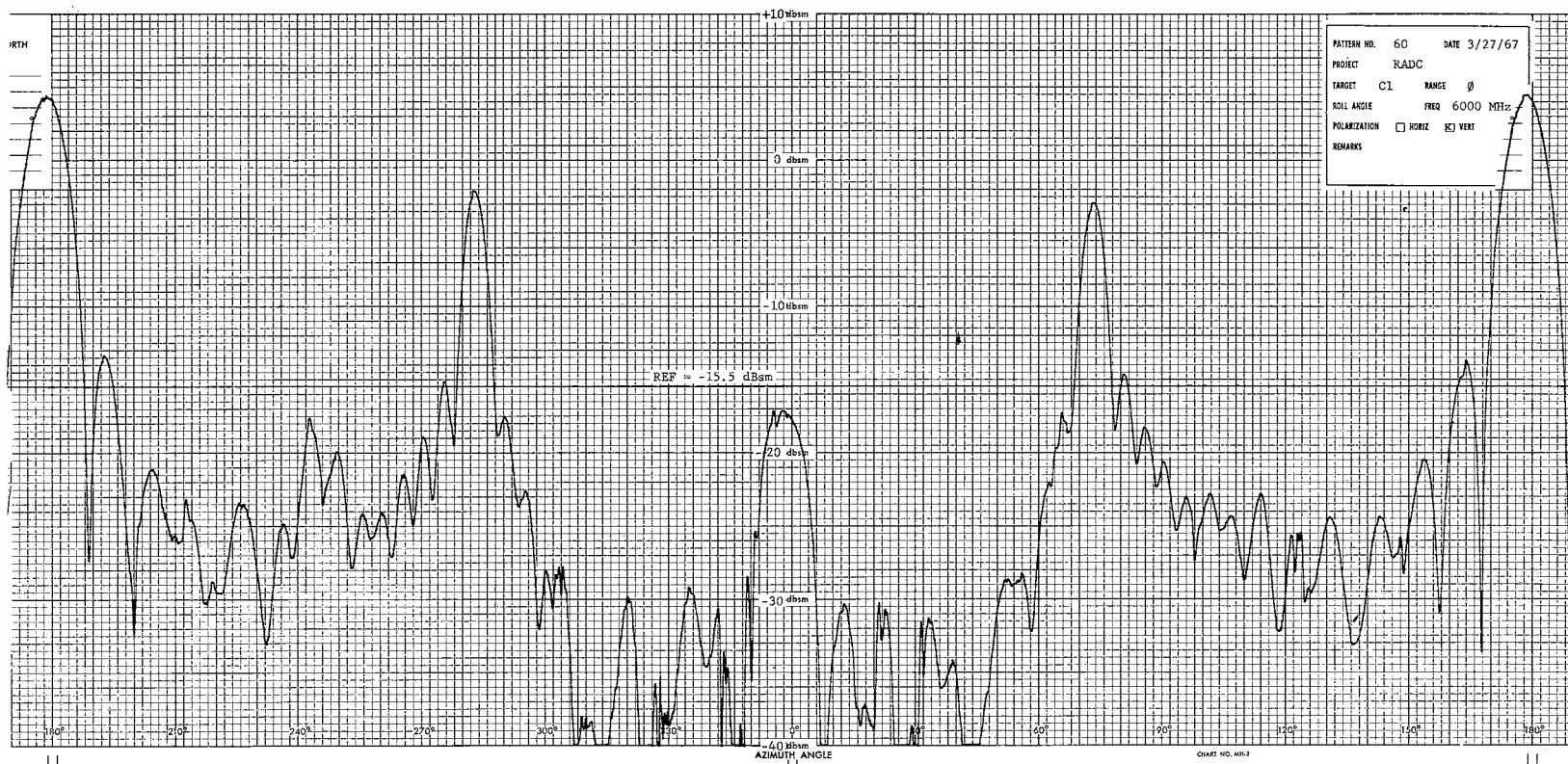


Figure 38. Model C1 Cross Section σ_{vv}

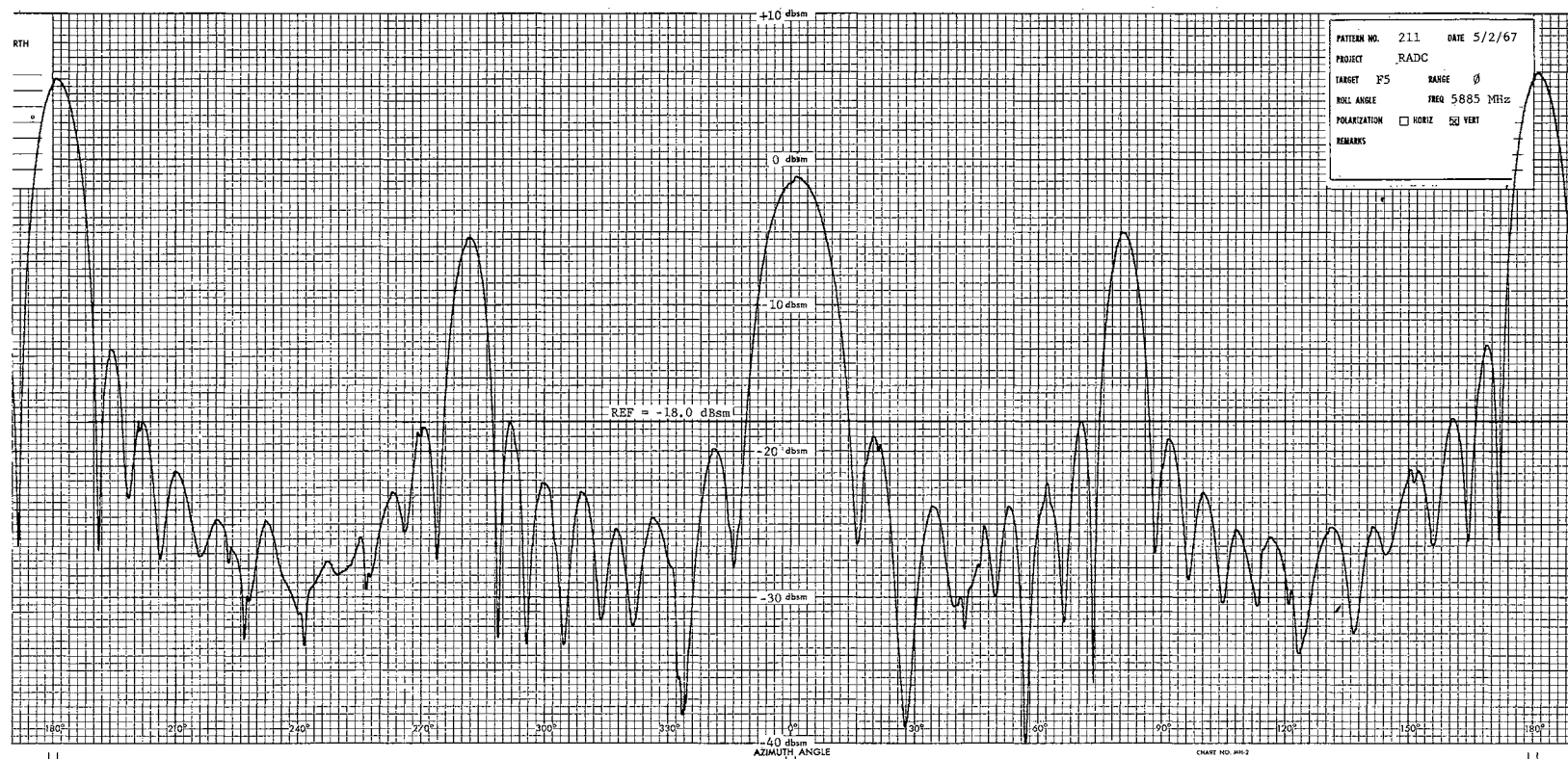


Figure 39. Model F5 Cross Section σ_{VV}

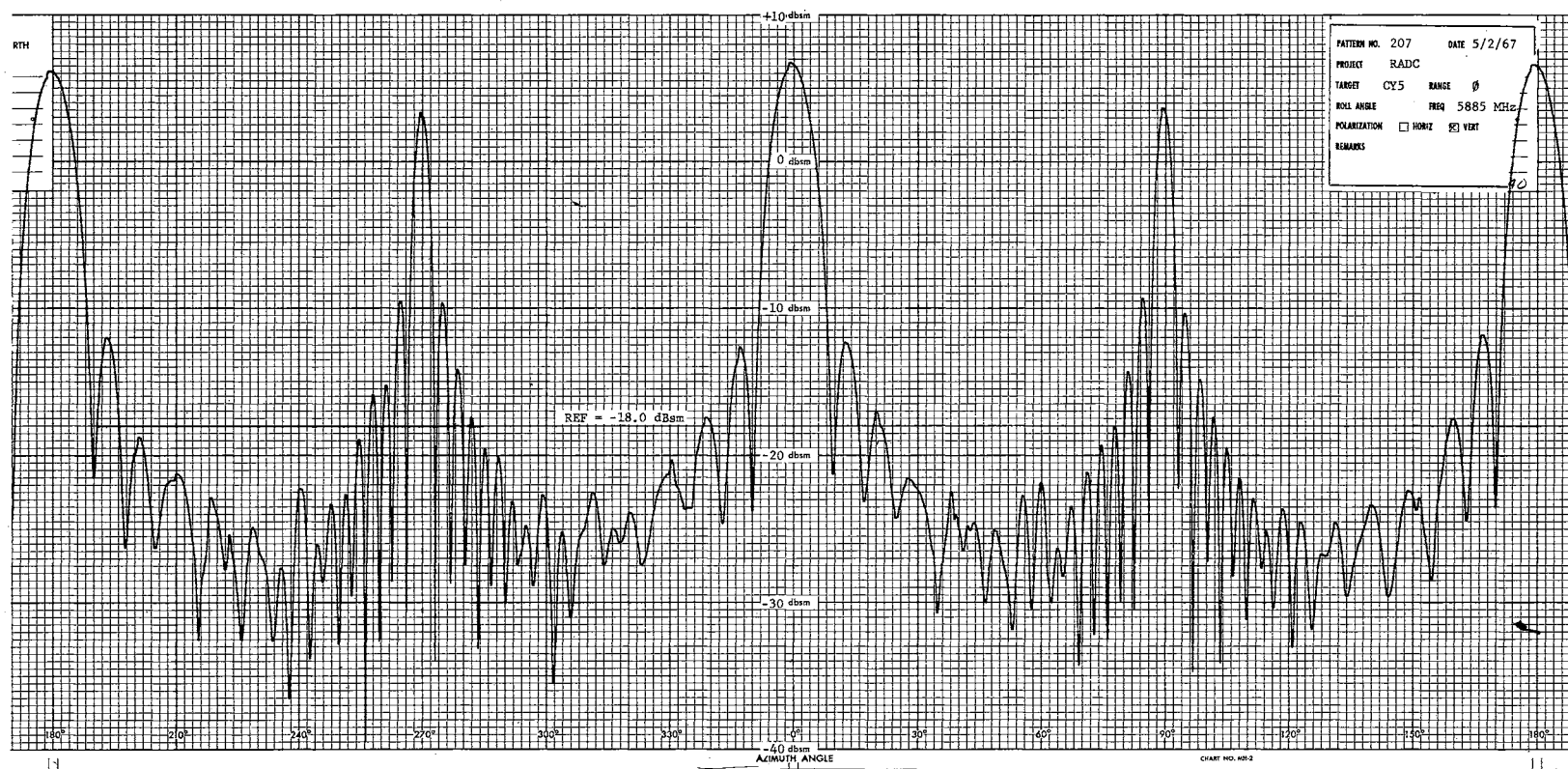


Figure 40. Model CY5 Cross Section σ_{VV}

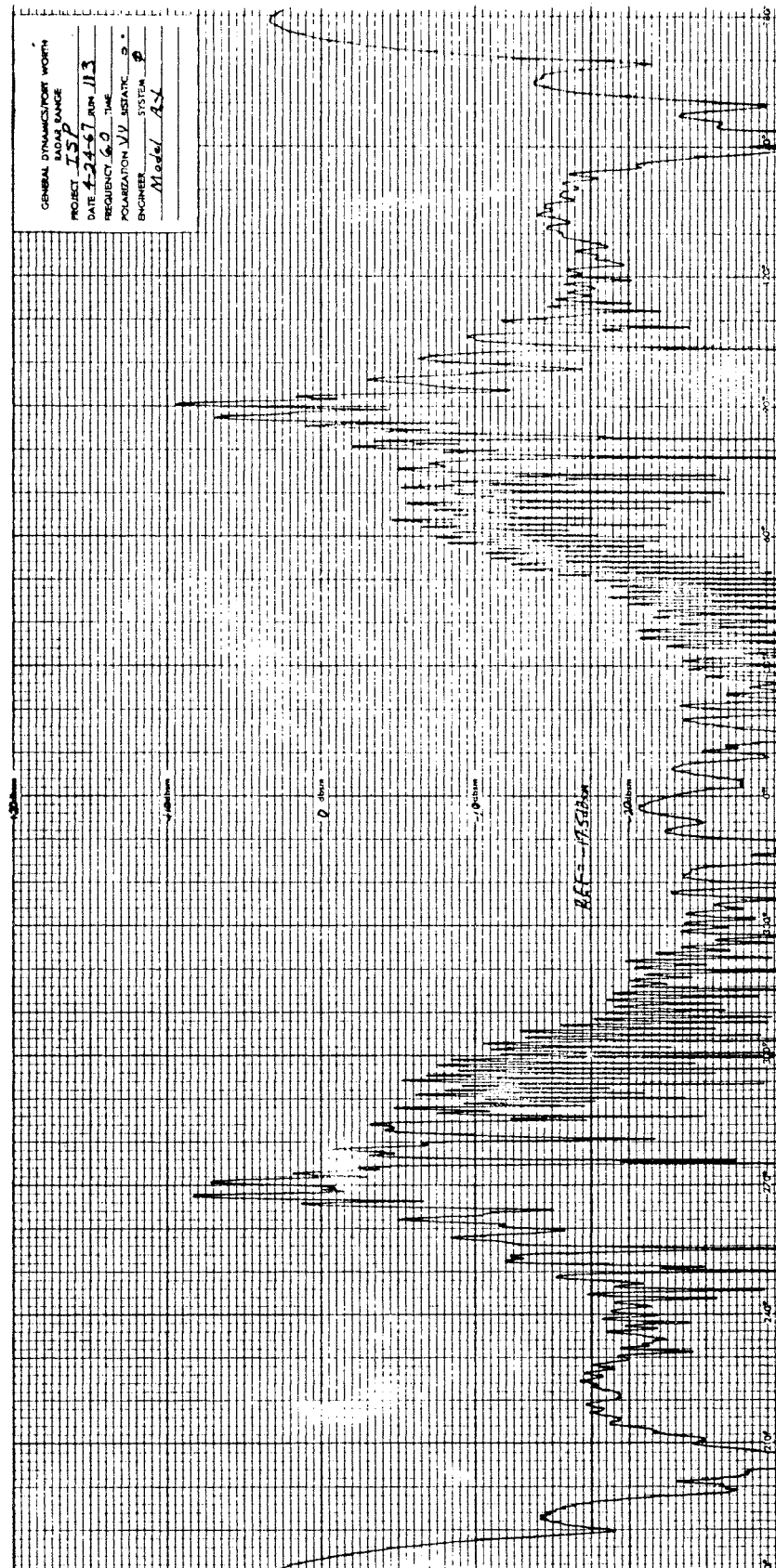


Figure 42. Model Al Cross Section σ_{vV}

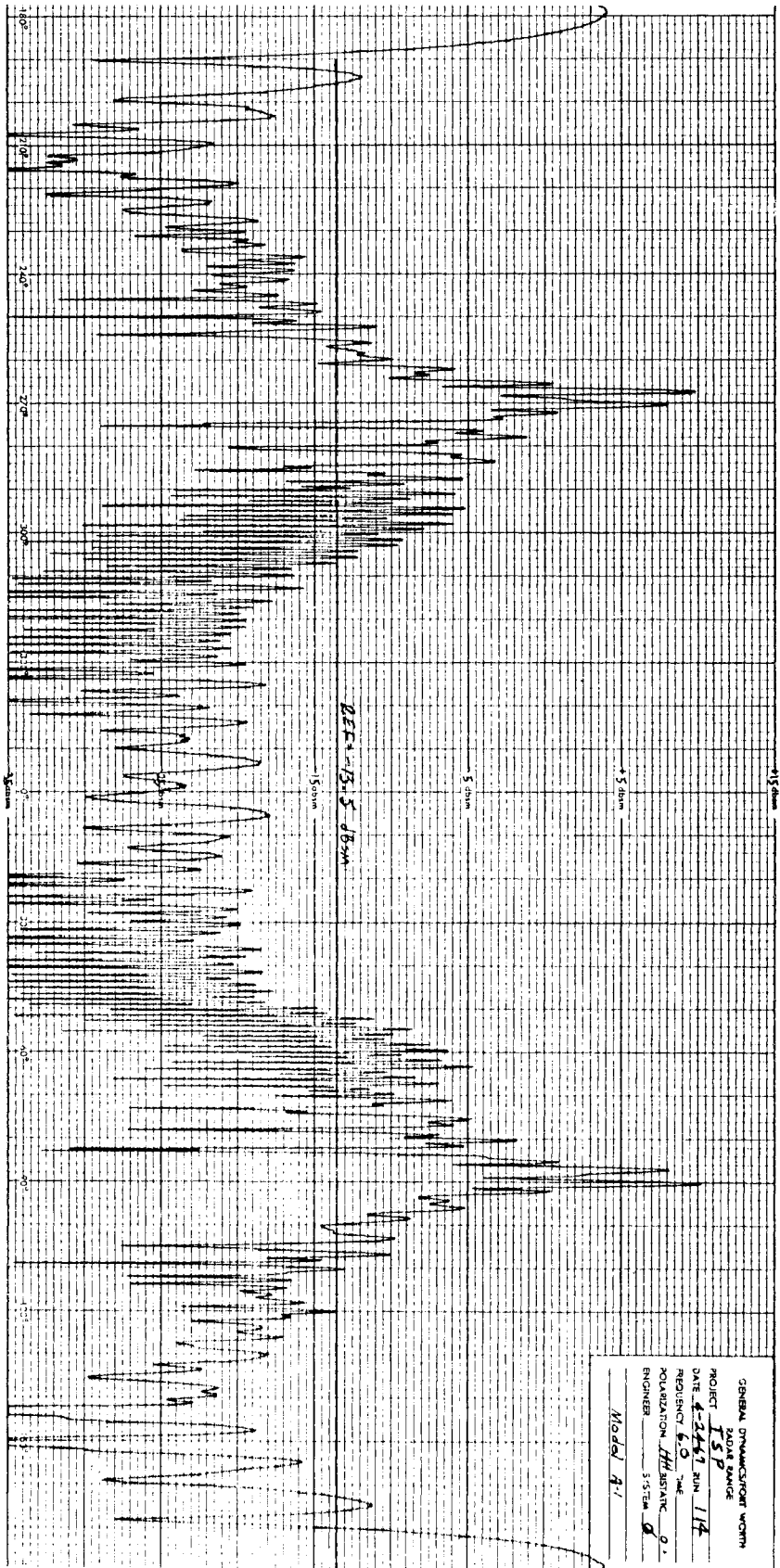
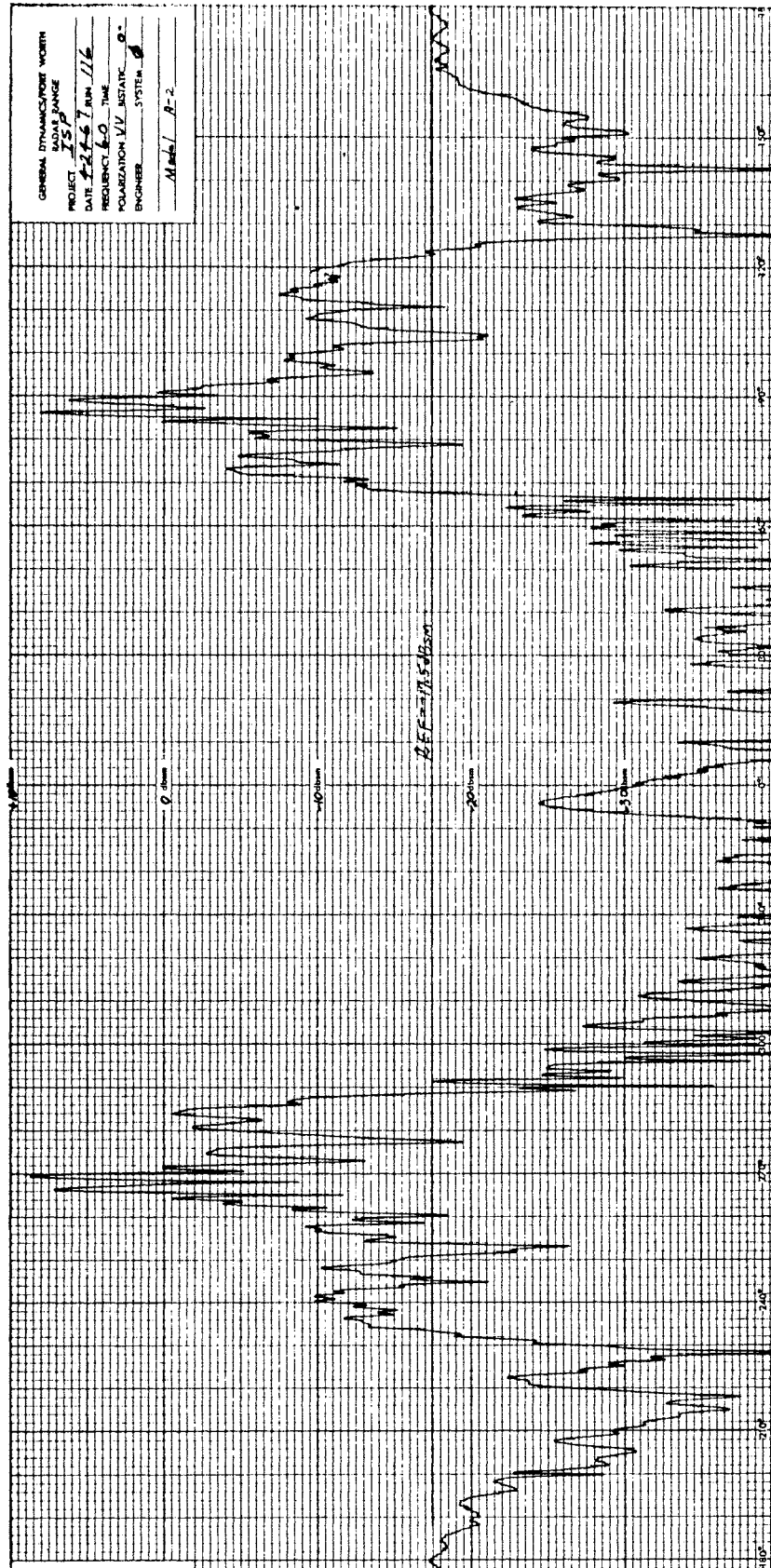
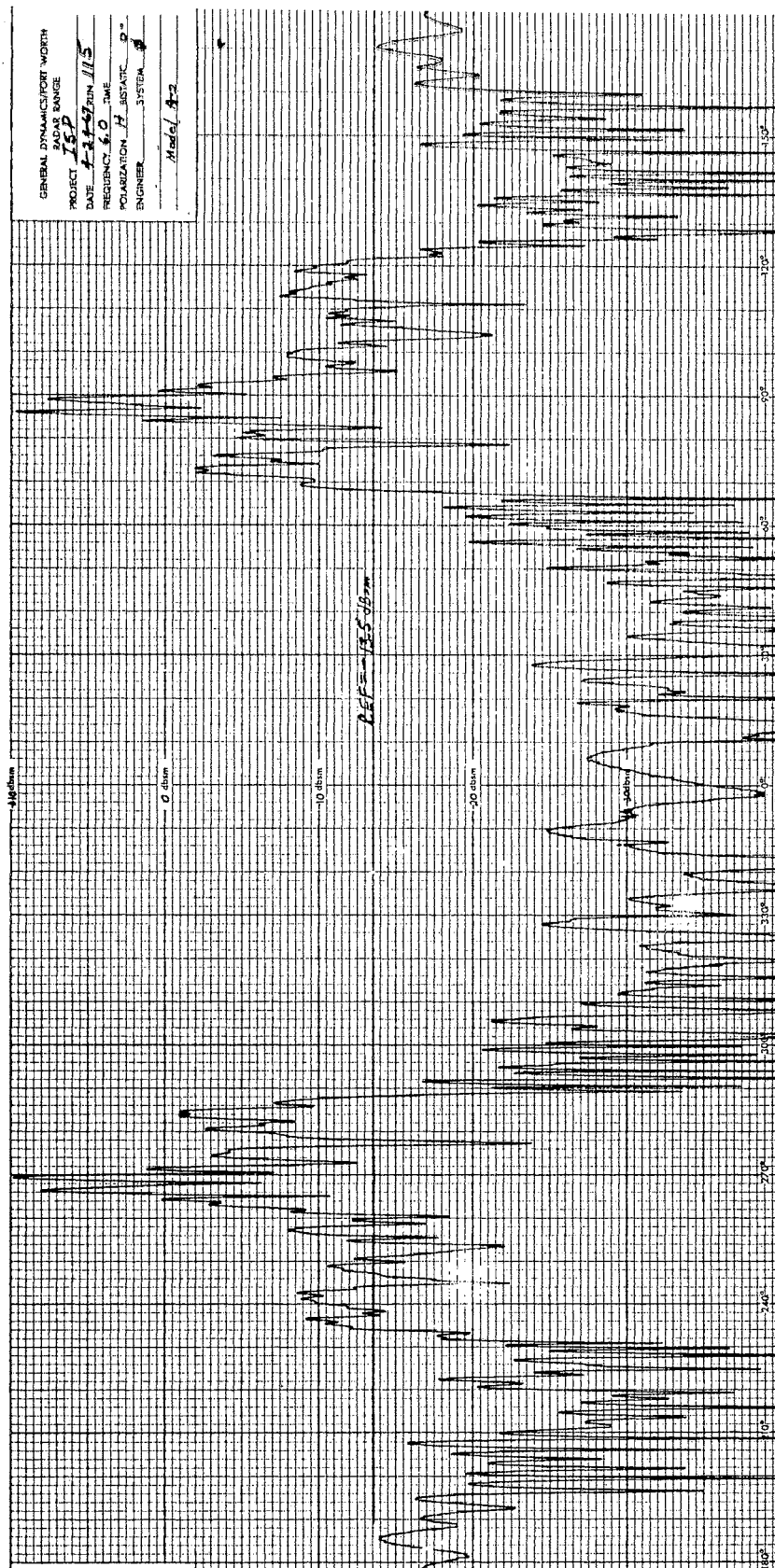
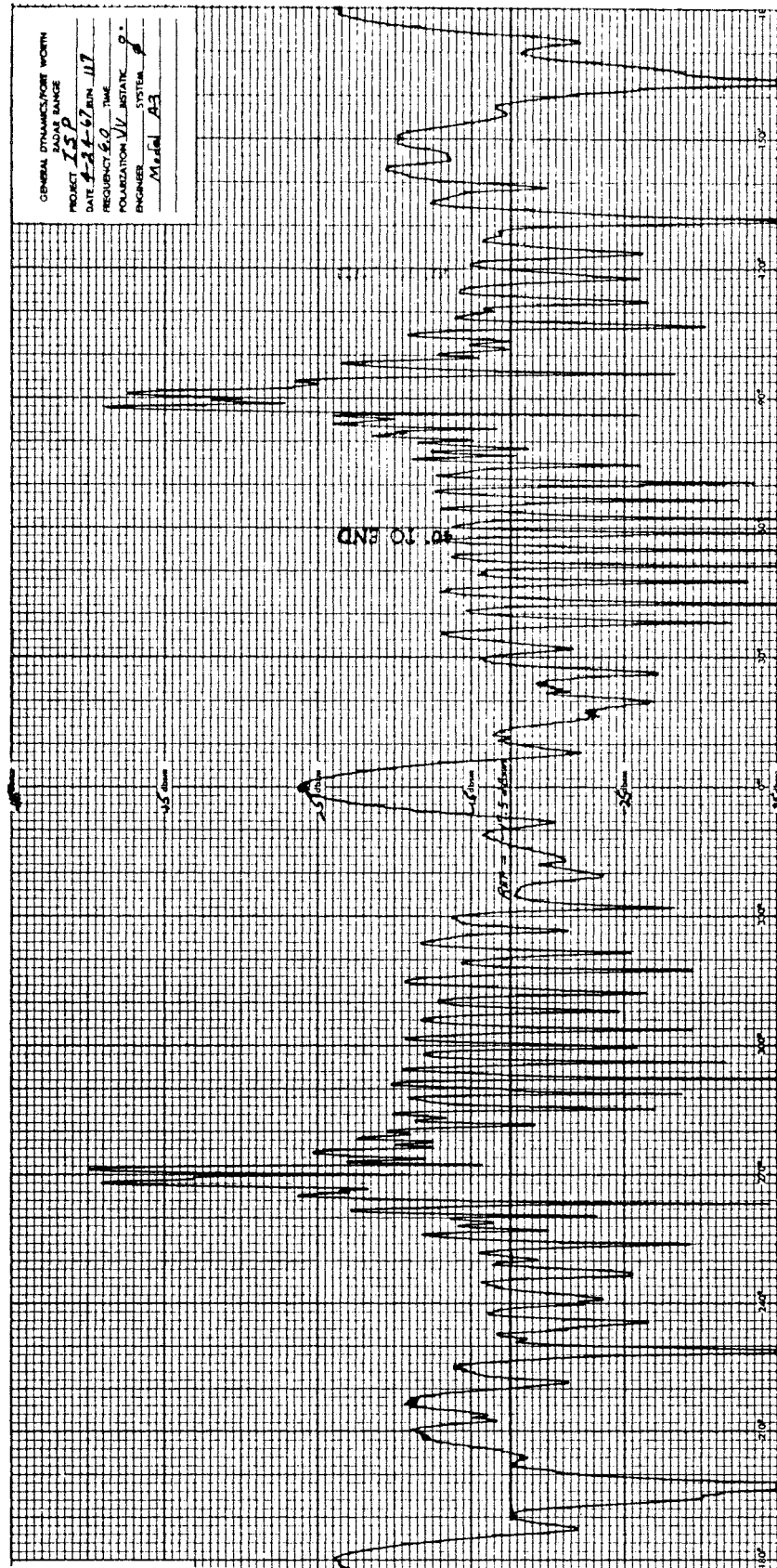
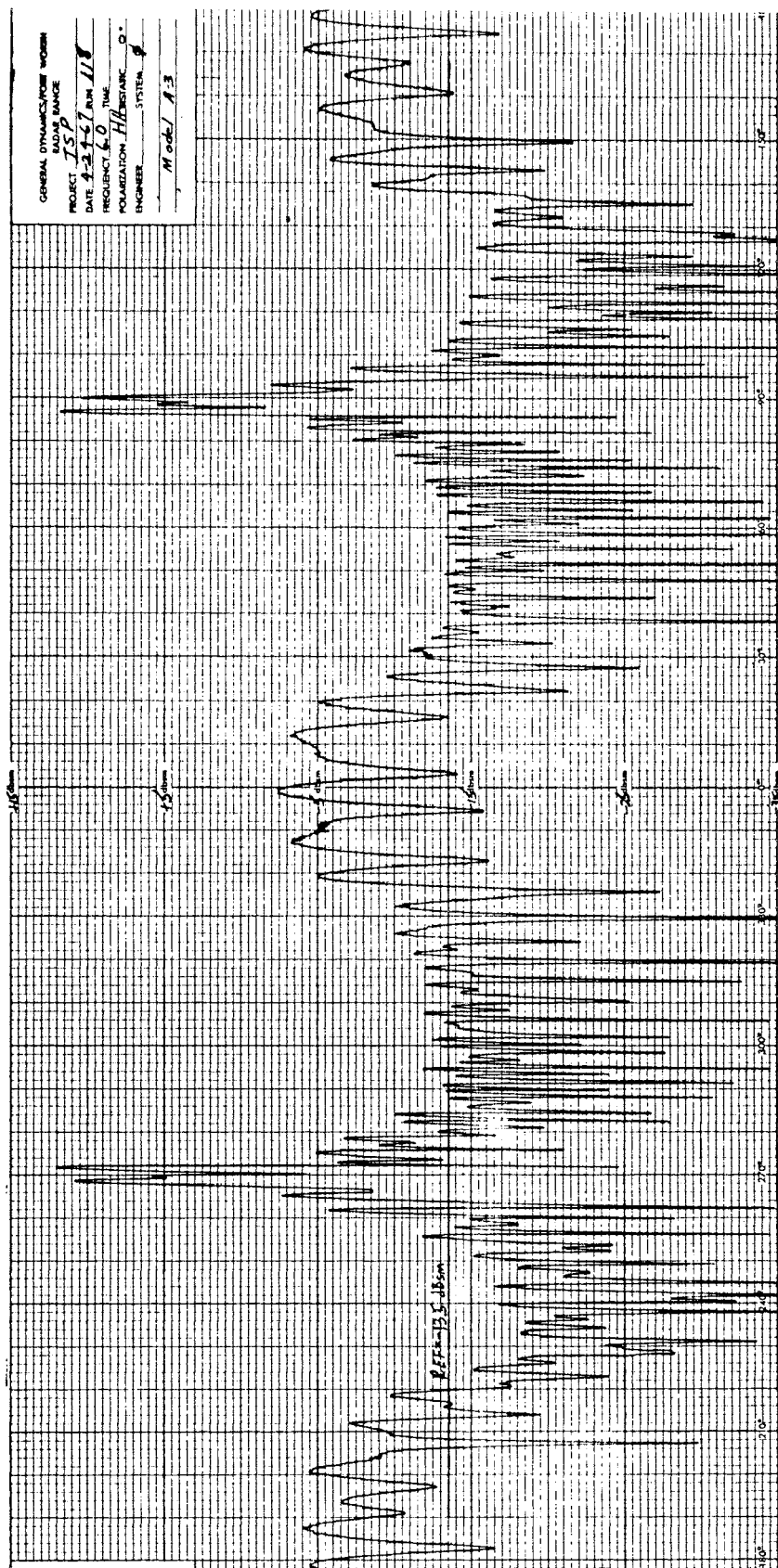


Figure 43. Model A2 Cross Section σ_{vv}

Figure 44. Model A3 Cross Section σ_{vv}

Figure 45. Model A1 Cross Section σ_{hh}



Figure 47. Model A3 Cross Section σ_{hh}

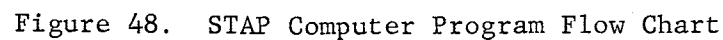
APPENDIX D

COMPUTER PROGRAMS STAP AND SSDP

D.1 General. This appendix contains documentation pertaining to the Signature Type Ambiguity Program (STAP) and the Statistical Signature Dissimilarity Program (SSDP). Section D.2 contains a listing of the STAP program in Fortran IV language, a flow chart, and a sample problem output. Section D.3 contains similar documentation on the SSDP program. Both of these programs were written for use with an IBM 7040/7090 direct-coupled computer system.

D.2 STAP Computer Program. Figure 48 is a flow chart of the STAP program. Following Figure 48 is a complete Fortran IV language listing of the STAP program. Figure 49 is a sample problem output listing and also contains the pertinent input data.

D.3 SSDP Computer Program. Figure 50 is a flow chart of the SSDP program. The Fortran IV listing of the program follows Figure 50. A sample problem output listing is shown in Figure 51.



STAP SOURCE STATEMENT

```

C   SIGNATURE TYPE AMBIGUITY
C
COMMON /AA1/SMAT(2250,6),IS(7), M1(6), ACUT1, ACUT2, ACUT3,
1  ACUT4
DIMENSION AP(3700), E(3700),EE1(6), EE2(6),E1(6)
CALL GSTART(3HH65,M)
REWIND 9
NO11=-1
ACUT1=180.
ACUT2=0.
ACUT3=360.
ACUT4=181.
20 CALL PROB
READ(5,1005) NNN,TN,MN,SN,SAN,NS ,AVGNA
21 READ(5,1000) K,A1,A2,A3,A4,A5,J
GO TO (30,40,50,60,70,80,90,100) ,K
30 NO=J
GO TO 21
40 ISAN=J
AVGN=A2
NSS=J
GO TO 21
50 M1(2)=A1+.1
M1(3)=A2+.1
M1(4)=A3+.1
M1(5)=A4+.1
M1(6)=A5+.1
GO TO 21
60 E1(2)=A1
E1(3)=A2
E1(4)=A3
E1(5)=A4
E1(6)=A5
GO TO 21
70 ACUT1=A1
ACUT2=A2
ACUT3=A3
ACUT4=A4
ISMVAR=A5+.1
GO TO 21
80 IOPT=A1+.1
GO TO 21
90 DNORMA = A1
GO TO 21
100 WRITE(6,1006) NNN,TN,MN,WN,SAN,AVGNA,NS,
1 E1(2),E1(3),E1(4),E1(5),E1(6),
2ACUT1, ACUT2, ACUT3, ACUT4, ISMVAR
C
C   FIND CORRECT SCATTERING MATRIX DATA ON TAPE
C

```



```

      CALL STATUS(IS)
      CALL EOFPRO
      IF (NO .NE. NO11) GO TO 101
      DO 105 I = 1, NUM
105  SMAT(I,1) = ABS(SMAT(I,1))
      GO TO 180
101  IF (NO11 .EQ. -1) GO TO 103
102  READ (9)
      IF ( IEOF(9) ) 102,102,103
103  READ (9)
      LOC=103
      IF (IEOF(9)) 104,104,550
104  READ (9) NO1
      LOC=104
      IF (IEOF(9)) 106,106,550
106  IF (NO .EQ. NO1) GO TO 140
110  READ (9)
      IF (IEOF(9)) 110,110,103
C    READ IN SCATTERING MATRIX
140  I=1
      NUM=0
141  READ (9) (SMAT(I,J),J=1,6)
      SMAT(I,5) = ABS(SMAT(I,5))
      SMAT(I,6) = ABS(SMAT(I,6))
      LOC=141
      IF (IEOF(9)) 143,143,179
143  IF ( SMAT(I,1) .LE. ACUT1 .AND. SMAT(I,1) .GE. ACUT2 .OR.
1    SMAT(I,1) .LE. ACUT3 .AND. SMAT(I,1) .GE. ACUT4 ) GO TO 142
      GO TO 180
142  IF (ISMVAR .LT. 1 ) GO TO 147
      DO 145 IJ=1, ISMVAR
144  READ(9)
      LOC=144
      IF (IEOF(9)) 145,145,179
145  CONTINUE
147  NUM=NUM + 1
      I=I+1
      GO TO 141
179  BACKSPACE 9
C
C    CHECK FOR SYNTHESIZING ADDITIVE NOISE SUBROUTINE
180  IF(ISAN .EQ. 1 ) CALL SANSUB( NUM, AVGN, $190)
C
C    CHECK FOR NOISE SUBTRACTION SUBROUTINE
      IF(NSS .EQ. 2 ) CALL NSSSUB ( NUM, AVGN, $190)
190  I1=1
      CALL EOFMON
      K=1
      AVGSIZ=0.
      AVGDIA=0.
      ICONT=0.
      II=1

```



```

200 IF(SMAT(I1,1) .GE. 0.0 ) GO TO 205
    I1=I1+1
    K=I1
    IF (K .GT. NUM) GO TO 290
    GO TO 200
205 IND = 0
    DO 210 IJ=2,6
        IF (M1(IJ) .EQ. 0) GO TO 210
        EE1(IJ) = SMAT(K,IJ) - E1(IJ)
        EE2(IJ) = SMAT(K,IJ) + E1(IJ)
210 CONTINUE
220 ICONT = ICONT + 1
    E( ICONT ) = SMAT(K,1)
    SMAT(K,1) = -SMAT(K,1)
    K = K + 1
    IF ( K .GT. NUM ) GO TO 245
    KLIM = 2
227 DO 230 IJ = KLIM,6
    IF(M1(IJ) .EQ. 0 ) GO TO 230
    IF( IJ .GE. 5) GO TO 2228
228 IF(SMAT(K,1) .LT. 0.0 .OR. (SMAT(K,IJ) .LT. EE1(IJ)
1 .OR. SMAT(K,IJ) .GT. EE2(IJ))) GO TO 232
230 CONTINUE
    GO TO 220
2228 IF( IND .NE. 0) GO TO 2232
    IF(EE1(IJ) .LT. 0.) GO TO 2229
    IF(EE2(IJ) .GT. 360.) GO TO 2230
    IF(SMAT(K,1) .LT. 0.0 .OR. (SMAT(K,IJ) .LT. EE1(IJ) .OR.
1SMAT(K,IJ) .GT. EE2(IJ))) GO TO 232
    GO TO 2234
2229 EE1(IJ) = EE1(IJ) + 360.
    IND = 1
    GO TO 2232
2230 EE2(IJ) = EE2(IJ) - 360.
    IND = 1
2232 IF(SMAT(K,1) .LT. 0.0 .OR. (SMAT(K,IJ) .GT. EE2(IJ) .AND.
1SMAT(K,IJ) .LT. EE1(IJ))) GO TO 232
2234 IF(IJ .EQ. 6) GO TO 220
    KLIM = 6
    GO TO 227
232 K = K + 1
    IF ( K .LE. NUM ) GO TO 227
245 IF (ICONT .EQ. 0) GO TO 290
250 DICONT = ICONT
    DNUM = NUM
    CCS = DICONT/DNUM
    AVGSIZ = CCS + AVGSIZ
    DAXM = 0.
    DO 260 I = 1, ICONT
    DO 260 IJ = I, ICONT
        IF ( DAXM .LT. AMOD(ABS(E(I) - E(IJ)),180.)) DAXM = AMOD(ABS(E(I)
1 E(IJ)),180.)
260 CONTINUE

```



```

      DK = DAXM/DNORMA
      AVGDIA = DK + AVGDIA
      AP(II) = 1./ 3.0 *(CCS**2 + DK**2 )
      WRITE(6,1001) II,CCS,II,DK
      IF (IOPT .NE. 1) GO TO 270
      WRITE(6,1003) (E(IJ),IJ =1,ICON)
270  II = II + 1
      II = II + 1
      ICON = 0
      K = II
      IF (II .LE. NUM ) GO TO 200
290  AA = 0.
      ICN = II - 1
      DCN = ICN
      ENNOEC = 1. - DCN/FLOAT(NUM)
      DO 300 IJ = 1, ICN
      AP(IJ) = SQRT(1./3. *(ENNOEC**2) AP(IJ))
300  AA = 1./ (DCN )*AP(IJ) + AA
      AVGSIZ = AVGSIZ /DCN
      AVGDIA = AVGDIA /DCN
      DA = 0.
      DO 310 IJ = 1, ICN
310  DA = (1./DCN*(AP(IJ) -AA)**2) + DA
      DA = SQRT(DA)
      WRITE(6,1011) (AP(I),I =1,ICN)
      WRITE(6,1004) AA,DA,ENNOEC
      WRITE(6,1013) AVGSIZ, AVGDIZ, NUM
      NO11 = NO
1000 FORMAT(I2,2X5E10.4,3XI4)
1001 FORMAT(1X4H C(S I4,2H)= F10.4,5X4H D(S I4,2H)= F10.4 )
1002 FORMAT(31H SCATTERING MATRIX DATA NUMBER I4,23H DOESN'T EXIST ON
      ITAPE )
1003 FORMAT(47H AZIMUTH VALUES IN THIS EQUIVALENCE CLASS ARE /(5F6.1))
1004 FORMAT(1X5HAVGA-F9.4,5HVARA- F10.4,8H 1-K/N= F8.4)
1005 FORMAT(8A5)
1006 FORMAT( 1X 40H SMUS - STATISTICAL SIGNATURE AMBIGUITY /
      1 1X 16H SIGNATURE TYPE A5 /
      2 1X 16H SM TAPE NUMBER A5, 14H MODEL NUMBER A5 /
      3 1X 6H S/N= A5 ,3H DB /
      4 1X 5H SAN = A5 , 5X6H AVGN = A5 /
      5 1X 20H NOISE SUBTRACTION = A5 /
      6 1X 18H ERROR LIMITS ARE /
      71X6H E(1)=F6.3,6H E(2)=F6.3,6H E(3)=F6.3,6H E(4)=F6.1,6H E(5)=F6.1
      8/ 1X7H ACUT1=F6.1,7H ACUT2= F6.1,7H ACUT3= F6.1,7H ACUT4= F6.1 /
      91X 8H ISMVAR = I2 )
1008 FORMAT(I3)
1009 FORMAT(1XI4)
1010 FORMAT(6F10.3)
1011 FORMAT( 28H NORMALIZED AMBIGUITY VECTOR / (5F10.4))
      GO TO 20
      550 WRITE(6,1012) LOC
1012 FORMAT( 32H END OF FILE ERROR AT STATEMENT I4 )

```



```

1013 FORMAT (1X, 8HAVGSIZ =,F6.4,10H  AVGDIA =,F6.4, 7H  NUM =,I4)
      GO TO 20
      END

```

```

      SUBROUTINE SANSUB(NUM,AVGN ,*)
C
C      SUBROUTINE FOR SYNTHESIZING ADDITIVE NOISE
C
      COMMON /AA1/SMAT(2250,6),IS(7), M1(6), ACUT1,  ACUT2,  ACUT3,
1 ACUT4
      DO 50 I=1,NUM
      DO 50 J=2,4
      IF(M1(J) .EQ. 0 ) GO TO 50
      EIJ - 10.*ALOG10(1. + 10.**((AVGN -SMAT(I,J))/10. ) )
      SMAT(I,J) = SMAT(I,J) + EIJ
50 CONTINUE
      RETURN 1
      END

```

```

      SUBROUTINE NSSSUB(NUM,  AVGN,*)
C
C      NOISE SUBTRACTION SUBROUTINE
C
      COMMON /AA1/SMAT(2250,6),IS(7), M1(6), ACUT1,  ACUT2,  ACUT3,
1 ACUT4
      DO 50 I=1, NUM
      DO 50 J=2,4
      IF(M1(J) .EQ. 0) GO TO 50
      IF ( SMAT(I,J) - AVGN .GT. 0.0433 ) GO TO 40
      SMAT(I,J) = AVGN - 20.0
      GO TO 50
40 SMAT(I,J) = AVGN + 10.*ALOG10( 10. **((SMAT(I,J) -AVGN)*.1) -1. )
50 CONTINUE
      RETURN 1
      END

```


GENERAL DYNAMICS
FORT WORTH DIVISION

7090 PROCEDURE H65
PROBLEM 064371-012

SMUS - STATISTICAL SIGNATURE AMBIGUITY

SIGNATURE TYPE SPVV

SM TAPE NUMBER 62368 MODEL NUMBER F5

S/N = NO AVGN = -60 DB

SAN = NO NOISE SUBTRACTION = NO

ERROR LIMITS ARE

E(1)= 3.010 E(2)= 0. E(3)= 0. E(4)= 0. E(5)= 0.

ACUT1= 175.8 ACUT2= 0. ACUT3= 360.0 ACUT4= 355.8

ISMVAR = 0

C(S 1)=	0.0055	D(S 1)=	0.0050
C(S 2)=	0.0036	D(S 2)=	0.5672
C(S 3)=	0.0255	D(S 3)=	0.9989
C(S 4)=	0.0734	D(S 4)=	0.9783
C(S 5)=	0.0322	D(S 5)=	0.9244
C(S 6)=	0.0370	D(S 6)=	0.9094
C(S 7)=	0.0607	D(S 7)=	0.8983
C(S 8)=	0.0977	D(S 8)=	0.8889
C(S 9)=	0.2864	D(S 9)=	0.8822
C(S 10)=	0.2676	D(S 10)=	0.7900
C(S 11)=	0.0801	D(S 11)=	0.7828
C(S 12)=	0.0303	D(S 12)=	0.4511

NORMALIZED AMBIGUITY VECTOR

0.5732	0.6601	0.8132	0.8058	0.7834
0.7776	0.7738	0.7714	0.7848	0.7486
0.7314	0.6298			

AVGA = 0.7377 VARA = 0.0728 1-K/N = 0.9927

AVGSIZ = 0.0833 AVGDIA = 0.7564 NUM = 1648

INPUT DATA

SPVV 62368 F5 60 NO NO -60

1						3
2		-60.				0
3	1.	0.	0.	0.	0.	
4	3.01	0.	0.	0.	0.	
5	175.8	0.	360.	355.8	0.	
6	0.					
7	180.					

Figure 49. STAP Sample Problem Output Listing

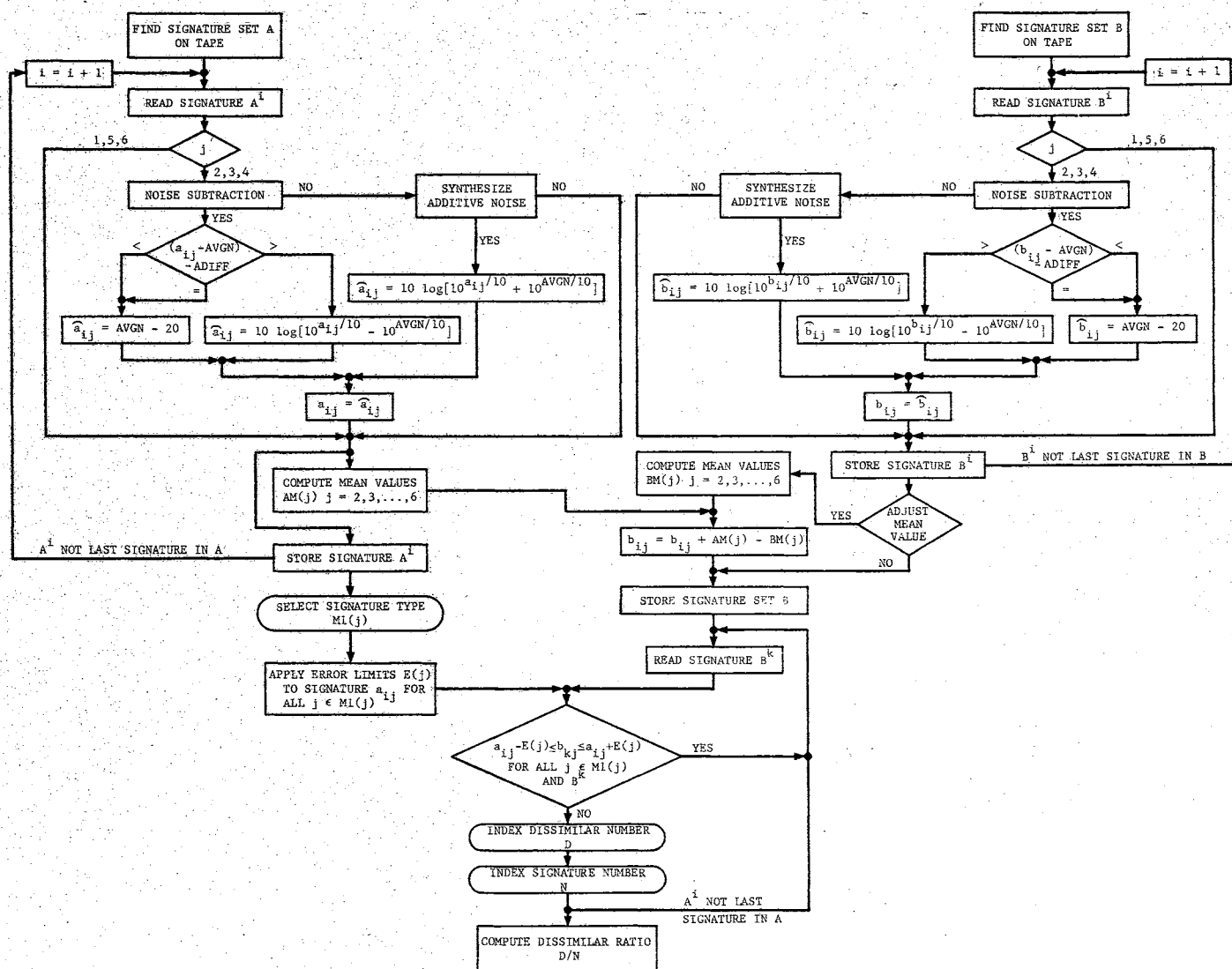


Figure 50. SSDP Computer Program Flow Chart

SSDP SOURCE STATEMENT

C
C
C
C
C

STATISTICAL DISSIMILAR RATIO COMPUTATION

```

COMMON /AA1/SMAT(1125,6),IS(7), M1(6), ACUT1, ACUT2, ACUT3, ACUT4
DIMENSION EE1(6), EE2(6), E1(6), AM(6), BM(6),SMATA(1125,6)
CALL GSTART(3HH64,M)
NTAL =-1
NTBL =-1
ACUT1=180.
ACUT2=0.
ACUT3=360.
ACUT4=180.
NAL =-1
NBL =-1
20 CALL PROB
IREWA=1
IREWB=1
READ(5,1002) NN1,NTA1 , MN1,SN1,SAN1, NS1, AAGN1, CCNS1,
1          NTB1 , MN2,SN2,SAN2, NS2, AAGN2, CCNS2, ADJMV1
21 READ(5,1003) K,A1,A2,A3, A4, A5, A6,J
GO TO (30,40,50,60,70,80,90,100),K
30 NA = A1 +.1
NTA = A2 + .1
NB = A3 +.1
NTB = A4 +.1
IF(NTA .EQ. 1) NTA = 9
IF(NTA .NE. 9) NTA = 10
IF(NTB .EQ. 1) NTB = 9
IF(NTB .NE. 9) NTB = 10
GO TO 21
40 ISANA = J
CRSMNA = A1
NSSA = J
AVGNA = A1
ICCNSA = A2 + .1
GO TO 21
50 M1(1)= A1 + .1
M1(2)= A2+ .1
M1(3)= A3+ .1
M1(4)= A4+ .1
M1(5)= A5+ .1
M1(6)= A6+ .1
GO TO 21
60 E1(1)=A1
E1(2)=A2
E1(3)=A3
E1(4)=A4
E1(5)=A5

```



```

      E1(6)=A6
      GO TO 21
70 ACUT1=A1
      ACUT2=A2
      ACUT3=A3
      ACUT4=A4
      ISMVAR=A5 + .1
      GO TO 21
80 ISANB=J
      CRSMNB=A1
      AVGNB=A1
      ICCNSB=A2 + .1
      GO TO 21
90 IADJMV = A1 + .1
      ISKIPA = 0
      ISKIPB = 0
      IF(A2 .GT. 0.0) ISKIPA = A2 + 0.1
      IF(A2 .LT. 0.0) ISKIPB = ABS(A2) + 0.1
      GO TO 21
100 WRITE(6,1000) NNN1,NTA1, MN1, SN1, SAN1, AAGN1, NS1, CCNS1,
1      NTB1, MN2, SN2, SAN2, AAGN2, NS2, CCNS2,
2 E1(2), E1(3),E1(4), E1(5), E1(6),E1(1),
3 ACUT1,ACUT2,ACUT3,ACUT4, ISMVAR,ADJMV1
      CALL EOFPRO
C
C      FIND CORRECT SCATTERING MATRIX A ON TAPE UNIT NTA
C
      IF(NTA .EQ. NTAL .AND. NA .EQ. NAL) GO TO 230
      IF((NTA .EQ. NTAL .AND. NA .GE. NAL ) .OR. (NTA .EQ. NTBL
1.AND. NA .GE. NBL )) IREWA=0
      IF((NTB .EQ. NTBL.AND. NB .GE. NBL ) .OR. (NTB .EQ. NTAL
1.AND. NB .GE. NAL )) IREWB=0
      BACKSPACE NTA
      BACKSPACE NTB
      IF(IREWA .EQ. 1) REWIND NTA
      IF(IREWB .EQ. 1) REWIND NTB
      IF(IREWA .EQ. 1 .or. NTA .EQ. NTB) GO TO 111
110 READ (NTA)
      IF(IEOR(NTA)) 110,110,111
111 IF(IREWB .EQ. 1 .OR. (IREWA .EQ. 1 .AND. NTA .EQ. NTB))GO TO 120
      IF(NTA .EQ. NTB) GO TO 120
112 READ (NTB)
      IF(IEOF(NTB)) 112,112,120
120 IF(NAL .EQ. NA .AND. NTAL .EQ. NTA) GO TO 230
130 READ (NTA)
      LOC = 130
      IF ( IEOF(NTA)) 131,131,550
131 READ(NTA) NOA
      LOC=131
      IF(IEOF(NTA)) 132,132,550
132 IF(NA .EQ. NOA ) GO TO 180
140 READ (NTA)

```



```

      LOC=140
      IF(IEOF(9)) 140,140,130
C
C      READ IN SCATTERING MATRIX A
C
180 IF (ISKIPA .EQ. 0) GO TO 181
      DO 179 I=1,ISKIPA
179 READ (NTA)
181 I=1
      NUMA=0
190 READ (NTA) (SMAT(I,J),J=1,6
      SMAT(I,5) = ABS(SMAT(K,5))
      SMAT(I,6) = ABS(SMAT(I,6))
      LOC=190
      IF (IEOF(NTA)) 195,195,550
195 IF ( SMAT(I,1) .LE. ACUT1 .AND. SMAT(I,1) .GE. ACUT2 .OR.
      1 SMAT(I,1) .LE. ACUT3 .AND. SMAT(I,1) .GE. ACUT4 ) GO TO 205
      GO TO 230
205 IF (ISMVAR .LT. 1 ) GO TO 220
      DO 210 IJ=1,ISMVAR
209 READ (NTA)
      LOC=209
      IF(IEOF(NTA)) 210,210,550
210 CONTINUE
220 NUMA = NUMA + 1
      I = I + 1
      GO TO 190
C
C      CHECK SMA FOR SYNTHESIZING ADDITIVE NOISE
C
230 IF ( ISANA .EQ. 1 ) CALL SANSUB(NUMA,CRSMNA,$250)
C
C      CHECK SMA FOR NOISE SUBTRACTION SUBROUTINE
C
      IF (NSSA .EQ. 2 ) CALL NSSSUB(NUMA,ICCNSA,AVGNA,$250)
250 DO 255 J=2,6
255 AM(J)=0.
      DNUMA= NUMA
      DO 270 J=2,6
      DO 260 I=1,NUMA
260 AM(J)= SMAT(I,J) + AM(J)
270 AM(J)= AM(J)/DNUMA
      DO 280 I=1,NUMA
      DO 280 J=1,6
280 SMATA(I,J) = SMAT(I,J)
      NUMB=NUMA
      IF(NAL .EQ. NA .AND. NTAL .EQ. NTA) GO TO 310
290 IF (NTB .NE. NTA ) GO TO 300
295 READ (NTB)
      IF(IEOF(NTB)) 295,295,300
300 IF((NA .EQ. NB .AND. NTA .EQ. NTB) .AND. (NTAL .NE. NTA .OR.
      INA .NE. NAL )) GO TO 410
310 IF(NTB .NE. NTBL .OR. NB .NE. NBL ) GO TO 312

```



```

      DO 311 I = 1, NUMB
311  SMAT(I,1)=ABS(SMAT(I,1))
      GO TO 410
312  READ(NTB)
      LOC=310
      IF (IEOF(NTB)) 315,315,550
315  READ(NTB) NOB
      LOC=315
      IF(IEOF(NTB)) 318,318,550
318  IF(NB .EQ. NOB ) GO TO 360
320  READ(NTB)
      IF(IEOF(NTB)) 320,320,310
C
C      READ IN SCATTERING MATRIX B
C
360  IF (ISKIPB .EQ. 0) GO TO 361
      DO 359 I=1, ISKIPB
359  READ (NTB)
361  I = 1
      NUMB = 0
370  READ (NTB) (SMAT(I,J),J=1,6)
      SMAT(I,5) = ABS(SMAT(I,5))
      SMAT(I,6) = ABS(SMAT(I,6))
      LOC=370
      IF(IEOF(NTB)) 375,375,550
375  IF( SMAT(I,1) .LE. ACUT1 .AND. SMAT(I,1) .GE. ACUT2
      1.OR. SMAT(I,1) .LE. ACUT3 .AND. SMAT(I,1) .GE. ACUT4 ) GO TO 377
      GO TO 410
377  IF (ISMVAR .LT. 1) GO TO 400
      DO 390 IJ=1, ISMVAR
389  READ(NTB)
      LOC=389
      IF(IEOF(NTB)) 390,390,550
390  CONTINUE
400  NUMB = NUMB + 1
      I = I + 1
      GO TO 370
C
C      CHECK SMB FOR SYNTHESIZING ADDITIVE NOISE
C
410  IF( ISANB .EQ. 1 ) CALL SANSUB(NUMB, CRSMNB, $420)
C
C      CHECK SMB FOR NOISE SUBTRACTION SUBROUTINE
C
      IF (NSSB .EQ. 2 ) CALL NSSSUB(NUMB, ICCNSB, AVGNB, $420)
C
420  IF( IADJMV .NE. 1 ) GO TO 470
      DO 430 J = 2,6
430  BM(J) =0.
      DNUMB = NUMB
      DO 450 J =2,6
      DO 440 I = 1, NUMB
440  BM(J) =SMAT(I,J) + BM(J)

```



```

450 BM(J) =BM(J)/DNUMB
    DO 460 I=1,NUMB
    DO 460 J=2,6
    SMAT(I,J)=SMAT(I,J)+AM(J)-BM(J)
460 CONTINUE
470 ITDN=0
    DO 473 LL=1,NUMA
475 IND = 0
    DO 480 IJ=1,6
    IF ( M1(IJ) .EQ. 0) GO TO 480
    EE1(IJ) = SMATA(LL,IJ) - E1(IJ)
    EE2(IJ) = SMATA(LL,IJ) + E1(IJ)
480 CONTINUE
    K = 1
4481 I = 1
481 IF(M1(I) .EQ. 0) GO TO 490
    IF(IND .NE. 0) GO TO 488
    IF(EE1(I) .LT. 0.) GO TO 483
    IF(EE2(I) .GT. 360.) GO TO 486
    IF(SMAT(K,1) .LT. 0. .OR. (SMAT(K,I) .LT. EE1(I) .OR. SMAT(K,I)
    1.GT. EE2(I))) GO TO 501
    GO TO 490
483 EE1(I) = EE1(I) + 360.
    IND = 1
    GO TO 488
486 EE2(I) = EE2(I) - 360.
    IND = 1
488 IF(SMAT(K,1) .LT. 0. .or. (SMAT(K,I) .GT. EE2(I) .AND SMAT(K,I)
    1.LT. EE1(I))) GO TO 501
490 IF( I .EQ. 1) GO TO 492
    IF( I .EQ. 5) GO TO 494
    GO TO 495
492 I = 5
    GO TO 481
494 I = 6
    GO TO 481
495 DO 500 I = 2,4
    IF(M1(I) .EQ. 0) GO TO 500
    IF(SMAT(K,1) .LT. 0. .OR. (SMAT(K,I) .LT. EE1(I) .OR. SMAT(K,I)
    1.GT. EE2(I))) GO TO 501
500 CONTINUE
    GO TO 510
501 K = K + 1
    IF( K .GT. NUMB ) ITDN = ITDN + 1
    IF( K .GT. NUMB ) GO TO 473
    GO TO 4481
510 SMAT(K,1) = -SMAT(K,1)
473 CONTINUE
525 DNUMA = NUMA
    DITDN=ITDN
    DOVERN = DITDN/DNUMA
    NTAL = NTA

```



```

NTBL = NTB
NAL = NA
NBL = NB
IF (IADJMV .EQ. 1) WRITE (6,1006) (AM(J),J =2,6)
IF (IADJMV .EQ. 1) WRITE (6,1007) (BM(J),J =2,6)
WRITE(6,1004) DOVERN, NUMA
1000 FORMAT( 1X 25H SMUS - DISSIMILAR RATIO /
1      1X 16H SIGNATURE TYPE      A5 /
2      1X 17H SMA TAPE NUMBER      A5, 15H MODEL NUMBER      A5/
3      1X  6H S/N=      A5 , 3H DB /
4      1X  6H SANA=      A5,5X6HAVGNA=      A5 /
5      1X 21H NOISE SUBTRACTION A=A5,5X6HCCNSA=      A5 /
6      1X 17H SMB TAPE NUMBER      A5, 15H MODEL NUMBER      A5/
7      1X  6H S/N=      A5,  3H DB /
8      1X  6H SANB=      A5,5X6HAVGNB=      A5 /
9      1X 21H NOISE SUBTRACTION B=A5,5X6HCCNSB=      A5 /
A      1X 18H ERROR LIMITS ARE /
B1X6H E(1)=F6.3,6H E(2)=F6.3,6H E(3)=F6.3,6H E(4)=F6.2,6H E(5)=
CF6.2/ 1X 26H ASPECT ANGLE TOLERANCE = F6.2,8H DEGREES /
D1X7H ACUT1= F6.1,7H ACUT2= F6.1,7H ACUT3= F6.1,7H ACUT4= F6.1 /
E      1X  8H ISMVAR=      I2,5X18HADJUST MEAN VALUE      A5 )
1001 FORMAT(1X 31H SCATTERING MATRIX DATA NUMBER      I4,23H DOESN;T EXIST
1 ON TAPE )
1002 FIRNAT*8*A5) / 8(A5) )
1003 FORMAT(I2,2X6(E 8.4),4XI4)
1004 FORMAT(1X 6H D/N = F7.4, 3H B- I4 )
1006 FORMAT(1X24H MEAN VALUES SMA EQUAL      5(F9.4))
1007 FORMAT(1X24H MEAN VALUES SMB EQUAL      5(F9.4))
      CALL EOFMON
      GO TO 20
550 WRITE(6,1005) LOC
1005 FORMAT( 32H END OF FILE ERROR AT STATEMENT      I4 )
      CALL EOFMON
      GO TO 20
      END

```

```

SUBROUTINE SANSUB(NUM,CRSMN,*)

```

C
C
C

```

SUBROUTINE FOR SYNTHESIZING ADDITIVE NOISE

```

```

COMMON /AA1/SMAT(1125,6),IS(7), M1(6), ACUT1,ACUT2,ACUT3,ACUT4
DO 50 I = 1,NUM
DO 50 J = 2,4
IF(M1(J) .EQ. 0 ) GO TO 50
EIJ = 10.*ALOG10(1. + 10.**((CRSMN-SMAT(I,J))/10. ) )
SMAT(I,J) = SMAT(I,J) + EIJ
50 CONTINUE
RETURN 1
END

```



```
      SUBROUTINE NSSSUB(NUM,ICCNS,AVGN,*)  
C  
C      NOISE SUBTRACTION SUBROUTINE  
C  
      COMMON /AA1/SMAT(1125,6),IS(7), M1(6), ACUT1,ACUT2,ACUT3,ACUT4  
      DO 50 I= 1,NUM  
      DO 50 J = 2,4  
      IF(M1(J) .EQ. 0 ) GO TO 50  
      IF(SMAT(I,J) - AVGN .GT. 0.0433 ) GO TO 40  
      SMAT(I,J) = AVGN - 20.0  
      GO TO 50  
40 SMAT(I,J) = AVGN + 10.*ALOG10 ( 10.**((SMAT(I,J) -AVGN)*.1)-1.)  
50 CONTINUE  
      RETURN 1  
      END
```


GENERAL DYNAMICS
FORT WORTH DIVISION

7090 PROCEDURE H64
PROBLEM 064182-002

SMUS - DISSIMILAR RATIO
SIGNATURE TYPE TPP
SMA TAPE NUMBER 62368 MODEL NUMBER C1
S/N = 60 DB
SANA = NO AVGNA = -60 DBSM
NOISE SUBTRACTION A = NO CCNSA = NO
SMB TAPE NUMBER 62367 MODEL NUMBER C2
S/N = 60 DB
SANB = NO AVGNB = -60 DBSM
NOISE SUBTRACTION B = NO CCNSB = NO
ERROR LIMITS ARE
E(1)= 3.010 E(2)= 0. E(3)= 3.010 E(4)= 0. E(5)= 20.01
ASPECT ANGLE TOLERANCE = 180.0 DEGREES
ACUT1 = 180.0 ACUT2 = 0. ACUT3 = 360.0 ACUT4 = 354.4
ISMVAR = 1 ADJUST MEAN VALUE NO

D/N = 0.2515 N = 807

INPUT DATA

TPP	62368	C1	60	NO	NO-60	NO	
62367	C2	60	NO	NO	-60NO	NO	
1	2.	1.	3.	2.			
2	-60.	0.					0
3	0.	1.	0.	1.	0.	1.	
4	180.	3.01	0.	3.01	0.	20.01	
5	180.	0.	360.	354.4	1.		
6	-60.	0.					0
7	0.	56.					
8							

Figure 51. SSDP Sample Problem Output Listing

VITA

George Warfield Gruver

Candidate for the Degree of

Doctor of Philosophy

Thesis: AN APPLICATION OF EQUIVALENCE CLASS TECHNIQUES TO RADAR
SIGNATURE ANALYSIS

Major Field: Electrical Engineering

Biographical:

Personal Data: Born on June 29, 1935, in Oklahoma City, Oklahoma,
the son of Darwin C. and Carmel L. Gruver.

Education: Attended primary and secondary schools in Edmond,
Oklahoma, and graduated from Edmond High School in May, 1953;
attended Milwaukee School of Engineering, Milwaukee, Wisconsin;
received the Bachelor of Science degree in Electrical
Engineering from Oklahoma State University in May, 1961; received
the Master of Science degree in Electrical Engineering from Oklahoma
State University in May, 1962; attended Stanford University, Stanford,
California; completed requirements for the Doctor of Philosophy degree
in May, 1968.

Professional experience: Served in the United States Navy from
October, 1953, to September, 1957, and is now a Lieutenant in the
United States Naval Reserve; employed by the School of Electrical
Engineering of Oklahoma State University as a graduate assistant from
September, 1961, to May, 1962; employed by Sylvania Electronic
Defense Laboratories, Mountain View, California, as a Senior Engineer
from June, 1962, to September, 1965; employed by the Fort Worth
Division of General Dynamics as a Project Aerosystems Engineer since
June, 1966.

Professional Organizations: Member of Eta Kappa Nu and the Society
of the Sigma Xi.